

GEDIZ UNIVERSITY
★ GRADUATE SCHOOL OF NATURAL AND APPLIED SCIENCES

**SONOCHEMICALLY
GROWN ZnO NANORODS
AND THEIR ANTIBACTERIAL PROPERTIES**

M.Sc. THESIS
Rukayya KAWU BALA
(60071204)

Nanotechnology Programme

Thesis Advisor: Asst. Prof. Dr. Yavuz BAYAM

MAY 2014

GEDİZ ÜNİVERSİTESİ ★ FEN BİLİMLERİ ENSTİTÜSÜ

**SONOKİMYASAL YÖNTEMLE
BÜYÜTÜLMÜŞ ZnO NANOYAPILAR VE
ANTİBAKTERİYAL ÖZELLİKLERİNİN İNCELENMESİ**

YÜKSEK LİSANS TEZİ

**Rukayya KAWU BALA
(60071204)**

Nanoteknoloji Programı

Tez Danışmanı: Yard.Doç.Dr. Yavuz BAYAM

MAYIS 2014

Rukayya Kawu Bala a **M.Sc.** student of Gediz University **Graduate School of Natural and Applied Sciences** 60071204, successfully defended the **thesis** entitled “**SONOCHEMICALLY GROWN ZnO NANORODS AND THEIR ANTIBACTERIAL PROPERTIES**”, which she prepared after fulfilling the requirements specified in the associated legislations, before the jury whose signatures are below.

Thesis Advisor : **Asst. Prof. Dr. Yavuz BAYAM**
Gediz University

Jury Members : **Prof. Dr. M. Şengun ÖZSÖZ**
Gediz University

Asst. Prof. Dr. Ramazan ATALAY
Gediz University

Asst.Prof. Dr. Uğur TÜRKAN
Gediz University

Asst. Prof. Dr. Merih PALANDÖKEN
Gediz University

Date of Submission : 09 May 2014

Date of Defense : 27 May 2014

DEDICATION

To the living memory of my Dad

FOREWORD

First and foremost my sincere gratitude and appreciation goes to my advisor in person of Asst. Prof. Dr. Yavuz BAYAM for his tireless effort towards the success of this thesis. His advice, encouragement and motivation stimulated me to work harder not only in my academic carrier but in all aspects of life. I really appreciate working with him because I have gained lot of experience.

My heartfelt gratitude to Dr. Debora Rodrigues and Tugba Onal of Houston University, Texas who helped with the antibacterial study. And also Dr. Ramazan Atalay who assists in the interpretation of the raman data.

The sponsorship of Kano State Government of Nigeria would also not be forgotten without which this work wouldn't have come into existance. I'm very grateful.

To my family I really appreciate their efforts especially my Mum and my sisters for their moral support, prayers and encouragement. I would also like to express my gratitude to my friends especially my group members for their usual cooperation and assistance whenever necessary. Special thanks to Sumeyra Kose who assisted with the turkish part of the thesis.

I thank you all.

May 2014

Rukayya KAWU BALA

TABLE OF CONTENTS

	<u>Page</u>
FOREWORD	v
TABLE OF CONTENTS	vi
ABBREVIATIONS	vii
LIST OF TABLES	viii
LIST OF FIGURES	ix
SUMMARY	x
ÖZET	xii
1. INTRODUCTION	1
1.1 MOTIVATION	3
2. ZnO	5
2.1 Biocompatibility of ZnO	6
2.2 Antimicrobial Properties of ZnO	8
3. SYNTHESIS TECHNIQUES	11
3.1 Vapor-Phase Techniques.....	11
3.1.1 Physical Vapor Deposition(PVD).....	12
3.1.1.1 Pulsed laser deposition(PLD) ..	12
3.1.1.2 Molecular beam epitaxy(MBE)	14
3.1.2 Chemical Vapor Deposition(CVD)	15
3.2 Solution-Based Techniques	17
3.2.1 Hydrothermal	17
3.2.2 Sonochemistry	19
4. GROWTH AND CHARACTERIZATION OF ZnO NANORODS	24
4.1 Synthesis of ZnO Nanorods	24
4.1.1 Seeding Process ...	24
4.1.2 Growth Process	25
4.2 Characterization Techniques.....	29
4.2.1 Optical Microscopy(OM)	30
4.2.2 Scanning Electron Microscopy (SEM)	31
4.2.3 Energy Dispersive X-ray Spectroscopy (EDS).....	32
4.2.4 Raman Spectroscopy (RS).....	33
4.3. Antibacterial Response.....	34
4.3.1 Bacterial Cell Culture.....	35
4.3.2 Toxicity Test	36
4.3.3 Drop plate count.....	38
5. RESULTS AND DISCUSSION	39
5.1 Seedlayer.....	39
5.2 Sample grown for 30 min at 50% amplitude	42
5.3 Sample grown in two-cycle at 50% amplitude	46
5.4 Sample grown for 60 min at 50% amplitude	50
5.5 Sample grown for 60 min at 100% amplitude	53
5.6 Sample grown without seedlayer for 60 min at 50% amplitude.....	57
5.7 Antibacterial response.....	59
6. FUTURE WORK	74
REFERENCES	75
CURRICULUM VITAE	81

ABBREVIATIONS

ZnO	: Zinc Oxide
HMT	: Hexamethylenetetramine
OM	: Optical Microscopy
RS	: Raman Spectroscopy
SEM	: Scanning Electron Microscopy
EDS	: Energy Dispersive X-ray Spectroscopy
PVD	: Physical Vapor Deposition
PLD	: Pulsed Laser Deposition
MBE	: Molecular Beam Epitaxy
CVD	: Chemical Vapor Deposition
TSB	: Tryptic Soy Broth
PBS	: Phosphate Buffered Saline
TSA	: Tryptic Soy Agar
TPU	: Thermoplastic Polyurethane
ROS	: Reactive Oxygen Species
UHV	: Ultra-High Vacuum
RHEED	: Reflection High Energy Electron Diffraction
PEI	: Polyethyleneimine
IPA	: Isopropyl alcohol

LIST OF TABLES

	<u>Page</u>
Table 2.1: Mammalian cells compatible with ZnO nanostructures.....	8
Table 2.2: Recent studies on the synthesis and antibacterial properties of ZnO nanostructures.....	10
Table 3.3: List of ZnO nanostructures synthesis techniques and grown products.....	23
Table 4.4: Chemicals used in the synthesis of ZnO nanorods.....	24
Table 4.5: Synthesis parameters for the sonochemical growth of ZnO nanorods.....	26

LIST OF FIGURE

	<u>Page</u>
Figure 2.1 : Crystal structures of ZnO.....	6
Figure 3.2 : Schematic representation of PLD system.....	14
Figure 3.3 : Schematic representation of MBE growth chamber.....	15
Figure 3.4 : Schematic representation of Horizontal flow chamber.....	17
Figure 3.5 : Frequency range of sound.....	20
Figure 3.6 : Transient acoustic cavitation.....	21
Figure 4.7 : Sonochemical growth set up.....	26
Figure 4.8 : Schematic representation of Sonochemical synthesis of ZnO nanorods...	27
Figure 4.9 : Digital image of ZnO nanorods growth solutions.....	28
Figure 4.10 : Schematic presentation of SEM instrument.....	31
Figure 4.11 : Principle of EDS.....	32
Figure 4.12 : Energy-level diagram showing the states involved in Raman signal.....	33
Figure 4.13 : SEM image of <i>Escherichia coli</i>	34
Figure 4.14 : SEM image of <i>Bacillus subtilis</i>	35
Figure 4.15 : Digital image of Bacterial cell culture.....	36
Figure 5.16 : Optical image of ZnO seed layer.....	40
Figure 5.17 : SEM image of ZnO Seedlayer.....	41
Figure 5.18 : Optical image of sample1.....	42
Figure 5.19 : SEM image of sample1.....	43
Figure 5.20 : EDS spectrum of sample1.....	44
Figure 5.21 : Raman Spectrum of sample1.....	45
Figure 5.22 :Optical Microscope image of sample2.....	46
Figure 5.23 : SEM image of sample2.....	47
Figure 5.24 : EDS spectrum of sample2.....	48
Figure 5.25 : Raman Spectrum of sample2.....	49
Figure 5.26 : Optical Microscope image of sample3.....	50
Figure 5.27 : SEM image of of sample3.....	51
Figure 5.28 : Raman Spectrum of sample3.....	52
Figure 5.29 : Optical Microscope image of of sample4.....	54
Figure 5.30 : SEM image of sample4.....	55
Figure 5.31 : Raman Spectrum of sample4.....	56
Figure 5.32 : Optical Microscope image of sample5.....	57
Figure 5.33 : SEM image of sample5.....	58
Figure 5.34 : Fluorescence image of <i>B.subtilis</i> at 2 h incubation.....	60
Figure 5.35 : Fluorescence image of <i>B.subtilis</i> at 5 h incubation.....	61
Figure 5.36 : Fluorescence image of <i>E.coli</i> at 2 h incubation.....	62
Figure 5.37 : Fluorescence image of <i>E.coli</i> at 5 h incubation.....	63
Figure 5.38 : Percentage toxicity of ZnO nanorods-coated substrate on <i>B.subtilis</i> and <i>E.coli</i>	64
Figure 5.39 : Digital image agar flipping of control sample.....	65
Figure 5.40 : Digital image of agar flipping of <i>B.subtilis</i>	66
Figure 5.41 : Growth zones of <i>B.subtilis</i> and <i>E.coli</i> in the presence of ZnO nanorods measured at different time.....	68
Figure 5.42 : Percentage toxicity of sample4.....	69
Figure 5.43 : SEM image of <i>E.coli</i> on sample4.....	70
Figure 5.44 : Sem image of <i>B.subtilis</i> on sample4.....	71

SONOCHEMICALLY GROWN ZnO NANORODS AND THEIR ANTIBACTERIAL PROPERTIES

SUMMARY

The use of medical devices have significantly increased in the recent decades. However, the success of such devices is being hindered by the implant-associated infections caused mainly by bacterial adhesion to the surface of biomedical devices. Bacteria, when attached to the surface of implant devices, become resistant to any attack by the immune system and conventional antibiotics. In such situation removal of the device become the necessary option. To overcome the problem of the implant-related infections, coating technologies have been developed.

The use of nanomaterials exhibiting antibacterial properties is one of the proposed strategy to tackle the problem of the implant-related infection. Zinc oxide (ZnO) is an inorganic compound which is widely known for its intense antibacterial activity. Various researchers have produced ZnO nanostructures with various techniques and their antibacterial activities were reported.

In this thesis, ZnO nanorods were synthesized on glass substrates by a simple, fast and a cost efficient method, and their antibacterial effect was tested against two different bacteria; *Escherichia coli*, a gram-negative bacterium and *Bacillus subtilis*, a gram-positive bacterium. Before the growth of ZnO nanorods, ZnO seedlayer was first deposited on the substrate by sonicating the substrate in a solution of zinc acetate dihydrate in isopropyle alcohol. Growth of ZnO nanorods was done by sonication of substrate in a solution of zinc nitrate tetrahydrate and hexamethylenetetramine in deionized water. Five different samples were grown by changing the growth condition. The results indicated that the longer reaction time at the maximum amplitude exhibits the best result with the surface been densely coated with nanorods compared to those grown in the short time. It was also observed that the diameter of the ZnO nanorods decreased by refreshing the growth solution, and increased in the continuously grown sample. The size of ZnO nanorods was also found to decrease by increasing the ultrasonic amplitude. In this study, three different samples were used to study antibacterial activity of the sonochemically synthesized ZnO nanorods. Both samples demonstrated some certain level of antibacterial activity against the two different bacteria. It was found that the viability of the bacterial cell was reduced on ZnO nanorods-coated substrates compared to those samples grown on glass. It was also observed that the toxicity tends to increase

by increasing the time of incubation which allows the ZnO nanorods to complete dissolve and also penetrate deeper into the bacterial cell. However, the toxicity of the sonochemically grown ZnO nanorods does not follow similar trend for two different bacteria. while the 30 min continuously grown sample showed higher toxicity towards the gram-negative *E.coli*, the 15+15 min sample demonstrated a greater toxicity against the gram-positive *B. subtilis*. The 60 min sample grown at 100% amplitude showed the highest toxicity towards both *E.coli* with 95% toxicity and *B. subtilis* with 100%. The overall result showed that the the antibacterial action of the ZnO nanorods was more effective on gram-positive *B.subtilis* compared to the gram-negative *E.coli*.

In this thesis, the sonochemical method was found to be a simple, and fast, technique for the synthesis of ZnO nanorods. The results also suggest that further investigation on the mechanism of antibacterial action of ZnO nanorods could serve as a potential candidate for medical devices coating with bactericidal effect.

SONOKİMYASAL YÖNTEMLE BÜYÜTÜLMÜŞ ZnO NANOYAPILAR VE ANTİBAKTERİYAL ÖZELLİKLERİNİN İNCELENMESİ

ÖZET

Tıbbi cihazların kullanımı son çalışmalar neticesinde önemli ölçüde artmıştır. Bununla birlikte, bu tür biyomedikal cihazların başarısı yüzeylerine bakterilerin yapışması sonucu oluşan implant ile ilişkili enfeksiyonları ile düşük seviyede kalmıştır. Yüzeyine bakteri bağlanan implant cihazlar, bağışıklık sistemi ve geleneksel antibiyotiklerin yapacağı herhangi bir saldırıya karşı dirençli hale gelirler. Böyle bir durumda cihazın çıkarılması zorunlu bir seçenek haline gelir. implant ile ilişkili enfeksiyon sorunlarının üstesinden gelmek amacıyla, kaplama stratejileri geliştirilmiştir. Antibakteriyel özelliklere sahip nanomalzemelerin kullanımı, implant ilişkili enfeksiyon sorunlarını çözmek için önerilen stratejilerden biridir.

Çinko oksit (ZnO), yoğun antibakteriyel aktivitesi özelliği olan bir inorganik bileşik olarak bilinir. Farklı araştırmacılar çeşitli tekniklerle ZnO nanoyapıları üretmiş ve bunların antibakteriyel aktivitelerin incelemiştir.

Bu çalışmada, ZnO nanoçubuklar başarılı bir şekilde, basit, hızlı ve düşük maliyetli bir yöntem olan sonokimyasal metot kullanılarak, cam alt-tabakalar üzerinde sentezlendi ve bunların antibakteriyel etkisi iki farklı bakteriye karşı test edildi *Escherichia coli*, bir gram-negatif bakteri ve *Bacillus subtilis*, bir gram-pozitif bakteridir. Deney değişkenleri ayarlanarak, beş farklı örnek üretilmiştir. Daha uzun tutulan reaksiyonlar sonucu üretilen nanoçubuklar, kısa sürede üretilenlere kıyasla daha yoğun bir şekilde yüzeyi kaplamışlardır. Aynı zamanda, büyütme çözeltisini yenilemenin, sürekli aynı çözeltide büyütmeye oranla daha ince ZnO nanoçubuklar üretmeye sebep olduğu görülmüştür. Sonokimyasal metotla sentezlenen ZnO nanoçubukların antibakteriyel aktivitesini incelemek için üç farklı örnek kullanılmıştır. Her üç örnek test edilen uc değişik bakteriye karşı antibakteriyel aktiviteyi belirli düzeyde göstermiştir. Kontrol olarak kullanılan cam alt-tabaka ile karşılaştırıldığında bakteriyel hücrenin ZnO nanoçubuklarla kaplanmış alt-tabakalar üzerinde yaşayabilirliğinin daha düşük olduğu bulunmuştur. Ayrıca, inkübasyon süresi artırılarak ZnO nanoçubukların bakteri hücrelerine daha fazla temas halinde olması sebebiyle toksisitenin artmaya eğilimli olduğu saptanmıştır. Ancak, sonokimyasal metotla büyütülen ZnO nanoçubukların toksisitesi kullanılan iki farklı

bakteriye karşı benzer bir seyir takip etmez. Örnek1 (30 dk, %50 genlik), gram-negatif *E.coli*'ye karşı daha yüksek bir toksisite göstermiştir, örnek2 (15+15 dk, %50 genlik) ise gram-pozitif *B. subtilis*'ye karşı daha yüksek bir toksisite göstermiştir.

Bu tezde, sonokimyasal yöntemin çeşitli uygulamalarda kullanılmak üzere ZnO nanoçubuklar sentezi için basit, hızlı, ölçeklenebilir ve çevreye zararsız bir teknik olduğu tespit edildi. Çıkan sonuçlar neticesinde, bakteri öldürücü etkiye sahip tıbbi cihazları kaplamak için potansiyel bir aday olan ZnO nanoçubukların sonokimyasal yöntemle büyütülebileceği görülmüştür.

1.INTRODUCTION

Materials at the nanometer scale with size ranging from 1-100nm possess an extraordinary physical, chemical and biological properties which is far different from those in the bulk form. This makes nanotechnology an interesting field of research in the recent development with potential to revolutionize the field of electronics, material science and medicine. The size of the nanomaterials is similar to the size ranges of biomolecules and are therefore able to interact with complex biological system. This opens a new window to study, detect and manipulate the biological system for a novel biomedical application including prevention, diagnosis and treatment of many diseases^[1]. Such novel applications include but not limited to the use of nanoparticles in optical and magnetic resonance imaging, the demonstration of potential application of metal nanoshells and carbon nanotubes for the treatment of tumor and cancer cells, and the application of nanowire-based transistors to electrically detect specific biomolecules.

Zinc oxide (ZnO) is a non-toxic, biocompatible inorganic compound that exhibits multiple properties both of semiconductor, piezoelectric and pyroelectric^[2]. It has wide band gap (3.37eV), large exciton binding energy (60 meV)^[3], good transparency and high luminescence at room temperature. Due to their unique physical, chemical and biological properties, nanostructures of ZnO have received tremendous effort from the field of engineering, material science, and medicine for their potential application in electronic, optoelectronic, and biomedical devices such as photo detectors^[4] and drug delivery vehicles for efficient photodynamic therapy for cancer cells^[5]. The high-sensing capability, high electron mobility, and enhanced analytical performance of ZnO nanostructures are widely explored for sensor application such as in biosensors for intracellular measurements^[6], gas sensors^[7], pH and temperature sensors^[8].

ZnO is known to exhibit antimicrobial properties towards both gram-negative and gram-positive bacteria, and even the high temperature and pressure resistant spores. Due to its antimicrobial properties, ZnO nanoparticles are being added to cotton fabrics, food packaging as well as medical device to prevent antimicrobial infection. Recent study also reports the use of ZnO nanorods on paper matrix to prevent deterioration of library materials and could also be used to produce facemasks, tissues, wallpapers and writing paper with antimicrobial property^[27].

Various techniques including both top-down approaches by etching and bottom-up such as Chemical Vapour Deposition, Vapour Liquid Solid, Metal-Organic Chemical Vapour

Deposition, Pulse Laser Deposition and hydrothermal^[9-14] techniques are used to synthesized well- aligned, single crystalline O-D and 1-D nanostructures of ZnO with different morphologies and diameters for different applications. However, the vapor-phase techniques are very expensive and complicated. Because they requiresophisticated experimental set up, high growth temperature up to 1400 °C, low pressure, and suitable substrate selection in MBE and MOCVD^[10, 12].

Solution-based methods are widely used as alternative to the conventional Vapour Phase Techniques to synthesize ZnO nanostructures for various applications. The solution-based methods seem to be relatively simple and require much lower temperature(< 200⁰C) than the vapor-phase methods. One major drawback of the solution base method is that long reaction time is required usually from several hours to even days.

Sonochemical growth method is one of the most simplest and fastest technique which have received a lot of interest from different researchers for the synthesis of ZnO nanostructures at an ambient condition. Using the chemical effect of ultrasound, various morphologies of ZnO nanorods are obtained for various application. However, the chemical effect of ultrasound does not come directly from the interaction of sound waves and the molecular species, rather from cavitation phenomenon. This method is very cost effective, mass-manufacturable and environmentally friendly. Because it does not produce any toxic by-product and does not require any additional heating. This method has been shown to be suitable for any substrate that is stable in alcohol and aqueous solution as well as substrates that do not resist high temperature treatment.

In this thesis, a sonochemical approach was adopted for the synthesis of ZnO nanorods. Scanning electron microscopy (SEM), Energy dispersive X-ray spectroscopy (EDS) and Raman spectroscopy (RS) were used to characterize ZnO nanorods. The antibacterial properties of the ZnO nanorods was tested against two different bacterial strains *Escherichia coli* MG 1655 a gram-negative bacteria and *Bacillus subtilis* 102 a gram-positive bacteria.

1.1 MOTIVATION

Bacterial infection is one of the major problem associated with biomedical devices. Despite all the necessary precautions taken by medical personnel, bacterial cells are still found on the surface of biomedical devices. This is one of the major causes of implant failure. Nosocomial infection which is the fourth leading cause of dead is associated with bacterial infection of medical devices. Bacteria, when attached to the surface of medical devices form a community of what is known as biofilm. The biofilm formation is the strategy by which bacteria resist any attack from the host immune system and conventional antibiotics, and in most cases removal of the device is the only alternative. This causes a significant increases in the cost of health care by additional care and extended antibiotic treatment.

Coating strategy has been the recent approach to eliminating bacteria on medical devices by altering the surface property of the devices such as coating with polyethylene glycol, hydrophilic polyurethanes, polyethylene oxide brushes^[15], positive and negatively charged surfaces^[16]. However, these coatings were found to be effective only against selected types of bacteria and cannot withstand biofilm formation.

Among the varioius strategies proposed for eradication of bacterial infection associated with biomedical devices include modification of the devices' surface by coating with nanostructured materials which exhibit an extraordinary properties than their bulk counterpart. ZnO is among the various metal oxide semiconductor materials nanostructures have received an enormous attention from different research field for various application from electronics to biomedical. Various techniques are being used to produced ZnO nanostructures of various shape and size notably the vapor-phase technique, but this technique is very expensive and require complex experimental set up with high temperature an vacuum environment. One recent approach to the synthesis of ZnO nanostructures is the solution-based methods. However, most of the solution-based techniques require long reaction time for the desired result to be obtained.

Sonochemistry is a very cost effective and fast method to produce nanostructures of ZnO. Different researchers have produced different morphologies of ZnO nanostructures using this inexpensive technique. This technique is based upon the chemical effect of ultrasound on chemical reactions. This process is carried out at an ambient atmosphere without the need for a complex experimental set up and additional heating. This method is of significant importance because of it's vital application in

various fields. Therefore, sonochemistry would serve as an alternative method to produce nanostructures of ZnO at a very low cost rate and within a short period of time.

2. ZINC OXIDE

ZnO is a group II-VI semiconductor, with zinc being a d-block, period 4 metal and oxygen p-block, period 2 non-metal. ZnO is an amphoteric oxide that is nearly insoluble in water but soluble in acids and alkalis. ZnO occurs in abundance on the earth crust. However, most ZnO used today is produced synthetically. ZnO crystallizes in three different structures, hexagonal (wurtzite) fig.1(a), cubic (zincblende) fig.1(b) and the rarely observed cubic (rocksalt).

The wurtzite structure is the most common and the most stable at ambient condition. The zincblende form can be stabilized by growing ZnO on substrates with cubic lattice structure. In both cases, the zinc and oxide centers are tetrahedral. Both hexagonal and cubic crystal structures of ZnO have no inversion symmetry. This and other lattice symmetry properties result in piezoelectricity of the hexagonal and cubic ZnO, and pyroelectricity of hexagonal ZnO. The wurtzite structure has a hexagonal unit cell with two lattice parameters, $a = 3.25 \text{ \AA}$ and $c = 5.2 \text{ \AA}$, belonging to the space group of C_{6v}^4 . The Zn and O are tetrahedrally coordinated and stacked layer-by-layer in alternate planes along the c -axis direction^[17]. The ZnO structure has polar surface (0001), which is either Zn or O terminated and non-polar surfaces (1120) and (1010) possessing an equal number of both atoms. As in most group II-VI materials, the bonding in ZnO is largely ionic (Zn – O) with the corresponding radii of 0.074 nm for Zn and 0.140 nm for O. This property accounts for the preferential formation of wurtzite rather than zinc blende structure, as well as the strong piezoelectricity of ZnO.

ZnO is widely used as an additive material in many industries such as, cement, plastics, ceramics, rubbers, lubricants, glass^[18], paint, sealant, pigments, adhesive, and fire retardants. Zinc oxide is also used in ointments, creams, and lotions to protect against sunburn and other damages to the skin caused by ultraviolet light (UV). It is the highest Ultraviolet A (long wave) and Ultraviolet B (short wave) reflector approved for use as a sunscreen by the Food and Drug Administration in the United States^[19].

ZnO nanostructures are known to be chemically stable, inexpensive, and easily prepared. Nanostructures of ZnO are relatively stable at biological pH and have high binding stability with proteins due to their high isoelectric points (IEP 9.5). These features make ZnO nanostructured surface a good matrix for immobilization of biomolecules^[20] for various application such as biochip, biosensor and drug delivery system. ZnO nanoparticles exhibit antifungal, anticorrosive, UV filtering properties and a good antibacterial effect against both gram-negative and gram-positive bacteria.

Among all synthesized nanomaterials, ZnO is known to have the highest morphology of nanostructures such as nanobelts, nanocombs, nanotubes, nanohelices, nanorings, nanocages, nanoflakes^[2]. Among these various structures, ZnO nanorods are the most commonly studied because of their high aspect ratio and large surface area to volume ratio which ensure high efficiency and sensitivity.

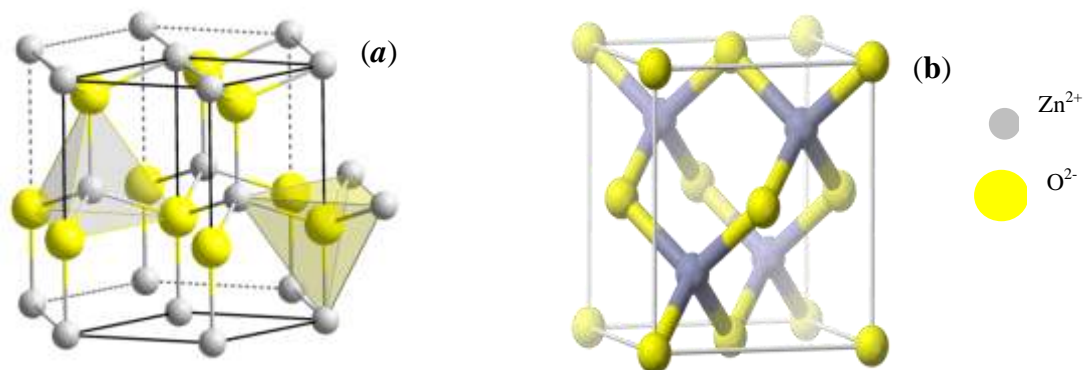


Figure 1. (a) Wurtzite and (b) Zincblende Crystal structures of ZnO^[21].

2.1 BICOMPATIBILITY OF ZnO NANOSTRUCTURES

ZnO nanostructures have been proposed for various biomedical applications such as sensors, drug delivery and antimicrobial agents. Thus, it is very vital to study the biosafety and biocompatibility of ZnO nanostructures for in vivo applications. Numerous researches have been conducted to evaluate the biocompatibility of ZnO nanostructures with the biological system. Zhong *et al.* reported cellular level biocompatibility of ZnO nanowires, they observed continuous growth and reproduction of human Hela cells even at much higher concentration up to 100 μ g/ml for couple of hours. They also reported the non-toxicity of ZnO nanowires towards L929 cell line at a concentration of 10 μ g/ml. However the L929 cell line showed a slight decrease in viability when concentration was higher^[22]. The compatibility of ZnO nanostructures with human SH-SY5Y cells was also reported. The cells were found to be healthy and maintained their normal morphological features after been treated with ZnO nanostructures^[23]. Ramesh *et al.* studied the interaction of ZnO nanorods with the Hela cells. They observed that the ZnO nanorods did not induce any oxidative stress on Hela cells, more than 98% of the cells were reported to be viable at a concentration of 10 μ g/ml^[24].

The biocompatibility of ZnO nanostructures is dependent upon size and concentration, as well as the morphology of the nanostructures. It was reported that, ZnO prism-like and flower-like nanostructures do not induce cytotoxic effect towards RSC96 Schwann cells,

but decrease in cell viability was observed when treated with nanoparticles and microspheres under the same experimental condition ^[25]. Recent study by G. Ciofani *et al.* reports the proliferation and differentiation of two mammalian cell lines; neuronal-like PC12 and myoblastic H9c2 in the presence of ZnO nanowires, Both cells demonstrated high viability and proliferation. Moreover, the presence of ZnO nanowires do not prevent the differentiation of the selected cell lines^[26]. In an experiment to measure the intracellular glucose concentration, ZnO nanosensor was dipped into the human adipocyte and frog oocyte and the penetration of the ZnO sensor was found not to affect the viability of the cell^[6]. Recent study conducted *in vitro* by Akhtar *et al.* suggest ZnO nanoparticles as potential candidate in cancer treatment by selectively killing the cancer cells and causing no harm on normal rat astrocytes and hepatocytes^[27]. ZnO nanoparticles were also reported not to show any cytotoxic effect on human T-cells^[28] and dermal fibroblasts^[29].

Table 1: Mammalian cells compatible with ZnO nanostructures

Cell line	ZnO concentration	ZnO Structure	Reference
Hela cells	100µg/ml	Nanowires	[22]
L9C2	10 µg/ml	Nanowires	
SH-SY5Y	On solid medium	Spherical- rod	[23]
Hela cells	10µg/ml	Nanorods	[24]
RSC96	80µg/ml	Prism/flower-like	[25]
Schwann cells			
H9c2	On substrate	Nanorods	[26]
PC12			
Astrocytes and hepatocytes	15µg/ml	Nanoparticles	[27]
T-Cells	5mM	Nanoparticles	[28]
Dermal fibroblast	410µmol/L	Nanoparticles	[29]

2.2. ANTIMICROBIAL PROPERTIES OF ZnO NANOSTRUCTURES

Antibacterial agents are broadly classified into two categories; organic and inorganic. The inorganic antibacterial agents are more stable due to their ability to withstand harsh processing conditions high temperatures and pressures, whereas organic antibacterial agents that contain antibiotics and humanized antibody are not stable at high temperatures

and pressures. Metal oxides including ZnO, TiO₂, CuO and MgO have been considered as promising inorganic antibacterial agents because they are not only stable under harsh processing conditions but also compatible with the human system^[30].

Among the various metal oxide nanoparticles, ZnO nanoparticles were reported to have the highest toxicity towards bacterial cells with minimum value of lethal dose (LD₅₀)^[31]. Toolabi *et al.* reported that ZnO nanoparticles have the highest toxicity towards four different bacterial strains compared to TiO₂ and CuO, they observed 100 % toxicity towards the tested strains at a concentration of 34.03mmol/L of ZnO nanoparticles^[32]. Laura *et al.* assessed the antibacterial properties of ZnO, TiO₂ and SiO₂. They observed that ZnO exhibited the highest toxicity against the organisms tested with 90% growth reduction^[33]. Antimicrobial power of ZnO nanoparticles is effective against both gram-positive and gram-negative bacteria, fungi, and even the high-temperature and pressure resistance spores.

ZnO nanorods were observed to exhibit antimicrobial effect against *Staphylococcus aureus*, *Escherichia coli*, and a common airborne fungus *Aspergillus niger*. No viable bacterial cell or fungal spore was found in areas treated with ZnO nanorods^[34]. Another study by Chitra and Annudarai reports the antimicrobial activity of ZnO nanoparticles against *Pseudomonas aeruginosa*, *Escherichia coli* and *Aspergillus niger*. They observed damaged cell membrane in a concentration dependent manner^[35].

Although the exact mechanism of antibacterial action of ZnO still remain obscured, several reports attributed the antibacterial effects of ZnO nanoparticles to generation of reactive oxygen species which are known to be toxic to the living cells. It has been reported that ZnO in contact with water catalyses the conversion of dissolved oxygen molecules to super oxide radical anions ($\bullet\text{O}^{-2}$), react with H^{+} to generate ($\text{HO}^{2}\bullet$) radicals, and converted to hydrogen peroxide anions (HO^{2-}), which then react with hydrogen ions to produce hydrogen peroxide molecules (H_2O_2)^[34, 36, 37]. The generated H_2O_2 can bind with the membrane protein on the outer layer of the bacterial cell, penetrate into the cell and eventually kill the cell. The release of hydrogen peroxide make the nanoparticles to remain in contact with the bacterial cell which does not allow further bacterial action by continuous release of hydrogen peroxide^[38]. Zn^{2+} which is also released by the breaking down of ZnO in solution is assume to be another mechanism for the antibacterial effect of ZnO nanostructures. Zn^{2+} penetrates into the cell membrane and interferes with the metal ion homeostasis of the cell^[34].

Another proposed mechanism by which ZnO nanostructures demonstrate bactericidal activity is the direct penetration of bacterial cell wall as observed by Jansson et al., where ZnO nanorods penetrate and damage the cytoplasmic membrane and causes the leakage of its content and subsequently leads to the death of the cell^[37]. The antibacterial effect of ZnO nanostructures has been reported to be both size and concentration dependent. Smaller particles are reported to generate more reactive oxygen species because of their large surface area as such they have higher toxicity^[36]. The antibacterial effect of ZnO nanostructures is also observed not to be only bactericidal but also bacteriostatic by preventing the growth of bacteria in the surrounding area treated with ZnO nanorods^[34]. Bacteria to which ZnO nanostructures exhibit antibacterial effect include *Escherichia coli*, *Staphylococcus aureus*, *Staphylococcus epidermidis*, *Bacillus subtilis*, *Pseudomonas aeruginosa*, *Streptococcus sobrinus*, and *Campylobacter jejuni*^[34, 36-40].

Table 2. Recent studies on the synthesis and antibacterial properties ZnO nanostructures.

Growth technique	Growth temperature/time	ZnO nanostructure	Bacteria Tested	References
Solution-based method	55 °C	Nanoparticles	<i>S. aureus</i> , <i>E. coli</i> ,	[38]
Hydrothermal	90 °C/20 h	Nanorods	<i>S. aureus</i> , <i>E. coli</i> , <i>A. niger</i>	[34]
Hydrothermal	90 °C/6 h	Nanorods	<i>P. aeruginosa</i> , <i>S. epidermidis</i>	[37]
Hydrothermal	120 °C/8 h	Nanorods	<i>S. aureus</i> , <i>E. coli</i>	[36]
Wet Chemical method	80 °C/24 h	Nanoparticles	<i>P. aeruginosa</i> , <i>E. coli</i>	[35]
Wet Chemical method	80 °C/24 h	Nanoparticles	<i>S. aureus</i> , <i>E. coli</i>	[41]
Wet-Chemical method	80 °C/24 h	Nanoparticles	<i>E. coli</i> , <i>B. subtilis</i> , <i>P. aeruginosa</i> , <i>S. pneumoniae</i> .	[42]
Solution-route	60 °C/3 h	Nanorods	<i>S.typhimurium</i> , <i>K.pneumoniae</i> , <i>P. vulgaris</i> <i>S. aureus</i>	[43]
Sonochemical	Room ambient 30-60 min.	Nanorods	<i>B. subtilis</i> , <i>E. coli</i>	This thesis

3. SYNTHESIS TECHNIQUES

ZnO nanostructures can be synthesized by various techniques on different substrate. These methods include the vapor-phase methods such as physical vapor deposition, Chemical Vapor Deposition (CVD), Molecular Beam Epitaxy (MBE), etc and solution-based methods including sol-gel, hydrothermal and sonochemistry. The solution-based method is the most widely used method to synthesize ZnO nanorods for low cost, flexible electronics as well as biological applications because it does not require much higher temperature as the vapor-phase technique and it allows the control of size, morphology, and crystallinity. The ability to control the uniformity, dimension, and morphology of the nanorods by tuning the growth parameters is very important for many applications. This will allow for the desired structure to be obtained depending on the final application. The different techniques are given below.

3.1 VAPOR-PHASE TECHNIQUE

Vapor-phase technique is the most extensively used technique to produce 1D nanostructures. This method relies upon the evaporation of the source material, chemical reduction of the material, and gaseous reaction. The vapor species are subsequently transported and condensed onto the surface of a solid substrate placed in a zone with a temperature lower than that of the source material.

ZnO nanostructures of different morphology have been synthesized through this approach by simple evaporation of Zinc powder under oxygen flow and their subsequent reaction to form ZnO nanostructures or by direct decomposition of commercial ZnO powder.

This process is carried out at high-temperature zone around 1400 °C. The variation of the nanostructures lies upon Zn and oxygen flow ratio. VPT can be done achieved by two growth mechanisms; the catalyst assisted vapor-liquid-solid and the catalyst-free vapor-solid mechanisms. In the vapor-solid process nanostructures are formed by direct condensation of the vapor on the substrate whereas in the vapor-liquid-solid process growth of nanostructures is controlled by a droplet of metal catalyst such as Au, Ni and Cu etc. The liquid droplet serves a preferential site for the adsorption of the reactant Zinc vapor, and as the nucleation site for crystallization. When liquid becomes supersaturated of the reactant material, nanowires begin to grow by precipitation on the substrate. Growth of nanowires stop when the metal catalyst is completely evaporated or by terminating the flow of the reactant vapour^[44].

3.1.1 PHYSICAL VAPOR DEPOSITION (PVD)

This is typically a physical process that is widely used to produce nanostructured materials of various shape and size. Contrary to the chemical vapor deposition, this method does not involve any chemical reaction on the surface of the substrate. This technique is accompanied by three distinct steps: high-temperature evaporation of the material from a solid source or plasma sputter bombardment, transport of the vapor by diffusion to the substrate, and attachment onto the substrate. This process is usually carried out under a vacuum atmosphere. Depending on the energy source, the physical vapor technique can be categorised into 4 different methods:

1. Electron beam physical vapor deposition: In which the material to be deposited is heated to a high vapor pressure by electron bombardment in "high" vacuum and is transported by diffusion to be deposited by condensation on the substrate.
2. Evaporative deposition: In which the material to be deposited is heated to a high vapor pressure by electrically resistive heating in "low" vacuum.
3. Pulsed laser deposition: In which a high-power laser ablates material from the target into a vapor.
4. Sputter deposition: In which a glow plasma discharge(usually localized around the "target" by a magnet) bombards the material sputtering some away as a vapor for subsequent deposition

3.1.1.1 Pulsed Laser Deposition (PLD)

PLD uses a high-power pulsed laser beam focused inside a vacuum chamber to strike the target material. The atoms and ions from the target material vaporize in a plasma plume and deposit on the substrate. This process is usually carried out in an ultra-high vacuum(10^{-9} torr) or in the presence of a carrier gas such as oxygen. In a typical PLD system, the substrate is attached with the substrate holder parallel to the target surface at a target-to-substrate distance of usually 2 – 10 cm. A pulsed-laser is focused onto the target of the material and locally heats and penetrates into the material within a penetration depth, the strong electric field generated by the laser light is sufficiently strong to remove electrons from the bulk material. The free electrons oscillate within the electromagnetic field of the laser light and can collide with the atoms of the bulk material thus transferring some of their energy to the lattice of the target material within the surface region. The

surface of the target is then heated up and the material is vaporized producing an ejected plasma or plume of atoms, ions, and molecules. The plume expands away from the target with a strong forward-directed velocity, distribution of different particles and deposits on the substrate placed opposite to the target^[45].

The various parameters such as laser wavelength, pulse duration and repetition rate, target-to-substrate distance, substrate temperature, background gas and pressure have a great influence on the growth of the nanostructures. By varying the substrate temperature and gas pressure, different size of ZnO nanorods were obtained on sapphire and silicon substrates by ablation of pure ZnO target in an oxygen background. It was found that the diameter of the nanorods decrease significantly with decreasing pressure down to 5 Torr. When the pressure was increased to 20 torr, the diameter of the nanorods increase and started to contact each other. On the other hand, temperature was also observed to play a significant role in the final structure of ZnO nanorods grown under PLD, the diameter of the nanorods was found to increase with increasing temperature from 500-700 °C^[46]. DongQi Y. *et al.* synthesized high density ZnO nanorods on ZnO-buffer-layer coated InP substrate by ablation of ZnO ceramic target in an oxygen background at 5 cm substrate-target distance, and a temperature of 450 °C for 90 min. The nanorods were of good crystalline quality and structural uniformity similar to the wurtzite type of ZnO single crystal^[47]. The nature of the substrate in this method was found to affect the structural quality of the ZnO nanorods as indicated by PL spectra, the ZnO nanorods have preferential growth orientation perpendicular to the substrate surface^[46, 47].

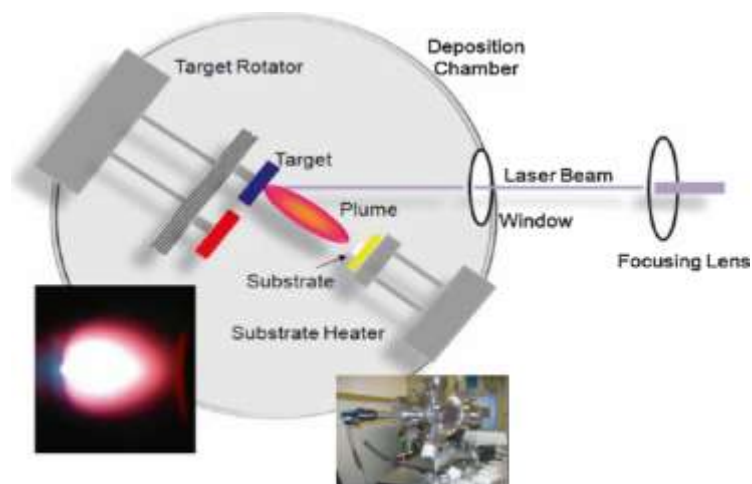


Figure 2. Schematic representation of pulsed laser deposition system. The inset pictures show an actual photographs of the plume (left) and PLD vacuum chamber (right)^[45].

3.1.1.2 Molecular Beam Epitaxy (MBE)

MBE is an ultra-high vacuum (10^{-13} bar) technique used in the synthesis of compound semiconductor materials. MBE is a highly controllable technique with low deposition rate (< 0.01 nm) and high purity ($>99.99999\%$). The low deposition rate allows for the materials to be deposited layer by layer to form a semiconductor device. MBE is mostly used for the of III-V semiconductors such as GaAs. In a typical MBE system, the solid-source material in its pure form is heated in separate quasi-Knudsen effusion cells until it begins to slowly sublimate. The gaseous elements do not interact with each other or with the vacuum chamber gases due to the mean free path which is several orders of magnitude greater than the normal source-sample distance of about 20cm, until they reach the substrate and subsequently condense.

Recently, MBE has been used to deposit oxide materials for advanced electronic, optical, and magnetic applications. Fujita *et al.*, reported the epitaxial growth of crystalline ZnO films on Si substrate using ozone as the source of oxygen^[48]. Heo Y.W *et al.*, prepared ZnO nanorods by catalyst-driven MBE on Ag-coated Si wafers by evaporation of high purity Zn metal from the Knudsen effusion cell using ozone/oxygen, mixture as the oxidizing source. Substrate temperature was varied from 300 °C-500 °C. It was reported that the growth of single crystal ZnO nanorods is site-specific as ZnO deposition was observed only on the Ag-coated regions with no growth on regions of the SiO₂-terminated Si surface that was devoid of Ag^[10]. Because MBE takes place in ultra-high vacuum (UHV) and has relatively low pressure of residual gas at the surface, analysis techniques such as reflection high energy electron diffraction (RHEED) and ellipsometry can be used during growth, both to study and control the growth process. The UHV environment also allows pre or post growth analysis techniques such as Auger spectroscopy^[49].

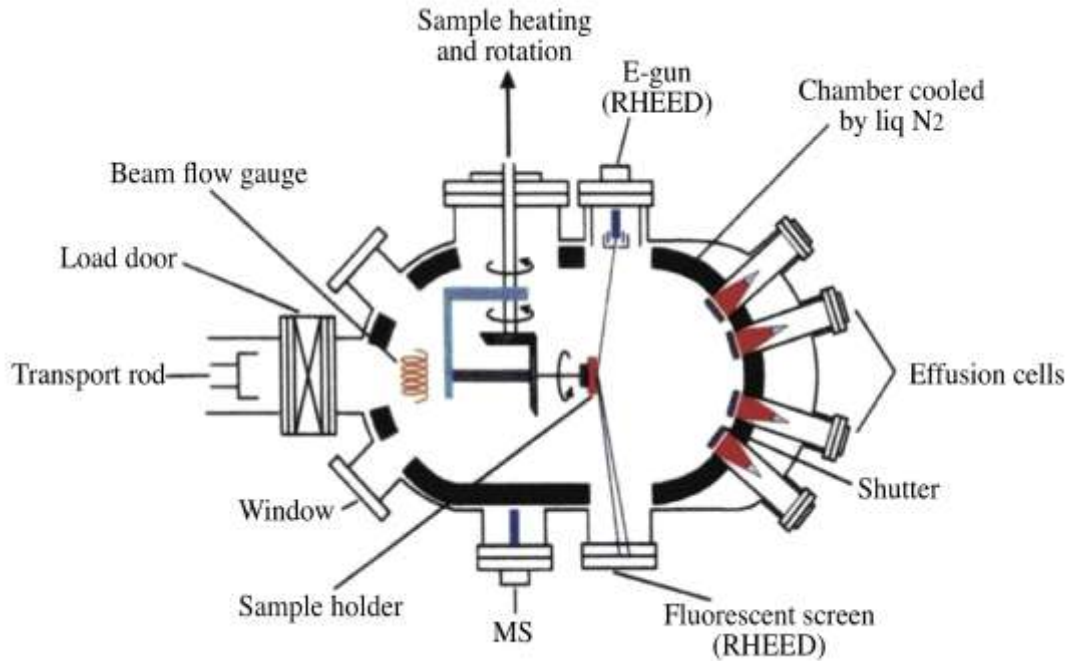


Figure 3. Schematic representation of the MBE growth chamber^[49].

3.1.2 CHEMICAL VAPOR DEPOSITION (CVD)

CVD is a chemical process that is used to produce high purity single crystalline nanomaterials. CVD is often used in the semiconductor industry to produce thin film materials. In typical CVD, the wafer (substrate) is exposed to one or more volatile precursors, which react and/or decompose on the substrate surface to produce the desired nanostructures. Frequently, volatile by-products are also produced, which are removed by gas flow through the reaction chamber. Depending on the manner by which chemical reactions are initiated, CVD is practiced in a variety of formats such as atmospheric pressure CVD, low-pressure CVD, plasma-enhanced CVD and ultra-high vacuum(UHV) CVD.

In this process, Zn source is evaporated in an oxygen atmosphere at a temperature around 1400 °C where they react and/or decompose on the substrate. The growth of ZnO nanostructures depends upon the vapor pressures of Zn and O, and the reaction temperature^[50]. Emelchenco *et al.* synthesized nanowires of ZnO on Si substrate by evaporation of metallic Zn in an oxygen-argon mixture at a temperature of 670 °C. ZnO nanowires of different shapes and size were obtained which were observed to be dependent on the position of the substrate in the growth zone^[51]. Growth of well-aligned ZnO nanorods was reported by Park *et al.* from decomposition of ZnO and graphite in an

Ar atmosphere at a temperature of 500 °C. The presence of graphite was observed to significantly decrease the decomposition temperature^[52]. High purity *c*-axis oriented ZnO nanorods array on Si(110) substrate were synthesized by Bekermann *et al.* by plasma-enhanced CVD process using two volatile bis(ketoiminato) zinc(II) compounds, and Electronic grade argon and oxygen as plasma sources. The effect of deposition temperature was studied by increasing the temperature from 200-300 °C which resulted in increasing lateral growth of the nanorods^[53].

In similar report by Liu *et al.* uniformly oriented ZnO nanorods have been grown on different substrates by plasma-enhanced CVD under helium gas using Diethylzinc (DEZn) and oxygen as precursors. They reported that the percentage of oxygen plays a significant role in the formation of ZnO nanorods under their experimental condition, where no growth was observed when the percentage of oxygen was as low as 5% or 10%^[54]. Adopting the metal-organic CVD technique, ZnO nanorods with average diameter of 50-120 nm were synthesized on bare silicon substrate at a temperature of 500 °C, and the effect of temperature on the as grown ZnO nanorods was investigated^[55]. Liu S-C and Wu J-J synthesized highly-oriented ZnO nanorods on fused silica substrate using zinc acetylacetonate at temperature of 500 °C^[56].

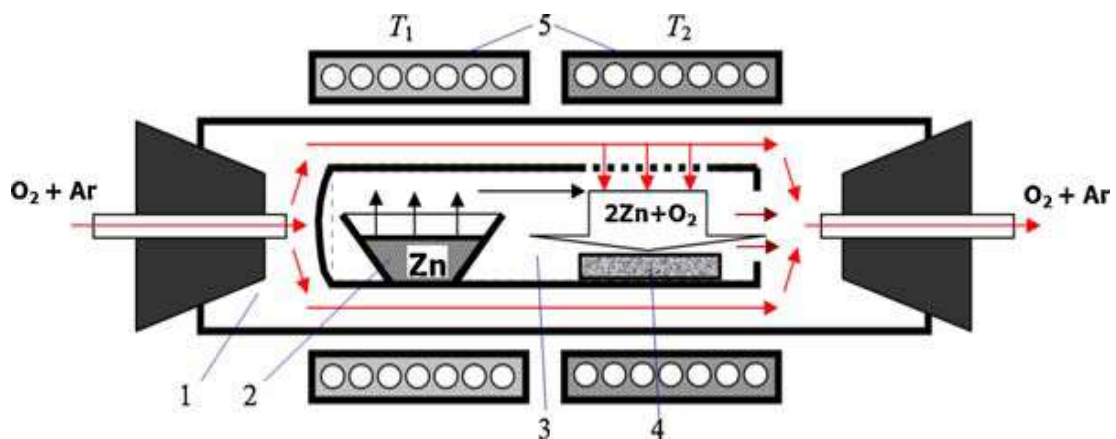


Figure 4. Schematic representation of horizontal flow channel reactor:(1) flowing quartz reactor, (2) Zn source, (3) internal quartz retort, (4)substrates, (5) electric heaters^[51].

3.2 SOLUTION -BASED TECHNIQUES

Solution-based techniques are widely adopted in the synthesis of nanostructures of different morphologies. These techniques present a feasible, low-cost, and environmentally friendly route to the synthesis nanostructured materials. The solution-based techniques usually make use of the soluble salt of the material under study, a

reducing agent and/or a stabilizing agent. Among the various solution -based methods including chemical precipitation, sol-gel, hydrothermal, and sonochemical methods, hydrothermal method is the most widely used method because of its simplicity, high yield and a scalable process^[16,36]. However, it requires long reaction time at relatively low temperature.

Sonochemical method a simple and fast approach which allows for the control of size and morphology under ambient condition happens to be an emerging field of investigation for the synthesis of 1D ZnO nanostructures^[64-67, 76-77]

3.2.1 Hydrothermal Method

Hydrothermal technique is used in the synthesis of single crystal materials that depends on the solubility of minerals in hot solution under high pressure. The crystal growth is performed in an apparatus consisting of a steel pressure vessel called an autoclave, in which a nutrient is supplied along with water. A temperature gradient is maintained between the opposite ends of the growth chamber. At the hotter end the nutrient solute dissolves, while at the cooler end it is deposited on a seed crystal, growing the desired crystal uses the solubility of inorganic substances in water at high temperatures and pressures, and subsequent crystallization of the dissolved material from the fluid.

Hydrothermal method is widely used in the synthesis of nanostructures of ZnO because it is relatively simple compared to the vapor-phase techniques, being a controllable process with high yield. This process relies on the reaction between a solution containing zinc source usually zinc acetate, zinc nitrate, zinc chloride etc and a solution containing reducing agent such as sodium hydroxide and ammonium nitrates.

Typically, hydrothermal synthesis of ZnO nanostructures is carried out in a thermal reactor, mostly Teflon-lined stainless steel sealed chamber. By tuning the experimental variables, this method allows control of size, morphology, and crystallinity of the ZnO nanostructures. Various groups reported the synthesis of ZnO nanorods using this hydrothermally assisted method. Devarami *et al.* synthesized ZnO nanorods by decomposition of zinc acetate and sodium hydroxide, in an aqueous solution at a temperature of 120 °C for 24 h^[57]. In another experiment by Polksongram *et al.* ZnO nanorods were synthesized by decomposition of Zinc nitrate hexahydrate and hexamethylene tetramine (HMT) at various temperature range, and the effect of synthesis condition was studied^[14]. Recent study reports the growth of ZnO nanorods by surfactant

assisted hydrothermal decomposition of zincacetatedihydrate and hexamethyleneteramine at a temperature of 120 °C for 8 h. The surfactant molecule, CTAB serves as the growth director^[36]. Yong *et al.* also reports the synthesis of well aligned ZnO nanowires on a previously ZnO seeded Si substrate by a reaction between Zinc nitrate hexahydrate and HMT, for 1-12 h at 90 °C. The effect of ammonia and polyethyleneimine (PEI) on the morphology of the ZnO nanowires was studied, they observed that introducing both ammonia and PEI at a moderate concentration into the growth solution, results in the increase of the aspect ratio of the ZnO nanowires^[58].

3.2.2. SONOCHEMISTRY

Sonochemistry is the study that focuses on the application of ultrasound to chemical reactions. Ultrasound is the sound pitched above the limit of human hearing. Ultrasound sound ranges from 20 kHz to tens of MHz. Fig. 5 shows the frequency ranges of sound wave. The chemical effect of ultarsound was first observed in 1927 by Alfred L. Loomis, in an experiment about the amount of hertz it took for a sonic wave to penetrate a water barrier. After lots of experiments, it was concluded that the best way to disperse sound through a water medium was to make loud noises. However this field remained untouched until the 1980s with thw advent of inexpensive and reliable high- intensity ultrasound generators.

The chemical effects of ultrasound do not come directly from the interaction of sound waves and the molecular species, rather sonochemistry arises from a phenomenon known as acoustic cavitation; formation, growth and implosive collapse of bubbles in a liquid environment^[59]. Figure 6 shows the steps involve in cavitaion phenomenon from which sonochemistry can be achieved. The chemical effects of ultrasound fall into three areas: homogeneous sonochemistry of liquids, heterogeneous sonochemistry of liquid-liquid or liquid-solid systems, and sonocatalysis (which overlaps the first two). Because cavitation can take place only in liquids, chemical reactions do not generally occur during the ultrasonic irradiation of solids or solid-gas systems. Upon irradiation of liquid with high intensity of sound, the alternate expansion and compression of the acoustic wave create bubbles, these bubbles oscillate and accumulate ultrasonic energy and grow until they reach an unstable size where they eventually collapse and release the concentrated energy stored. The implosive collapse of bubbles generate a localized, short-lived hot spot with very high temperature of ~ 5000 k and pressure of ~ 1000 atm, with high heating and

cooling rate above 10^{10} k/s. This phenomenon causes high energy chemical reactions which are not accessible or difficult to achieve to take place within a short time, often with emission of light, a phenomenon called sonoluminescence^[58]. Sonochemistry has been found to be used in the synthesis of various nanostructures material such as high surface area transition metals, carbides, alloys, colloids, and oxides as well as biomaterials; notably the protein microspheres^[60]. Ultrasonic irradiation of aqueous liquids generates free radicals, and the formation of free radicals by sonolysis of water has been particularly well-studied for many years. Primary sonolysis products in water are $H\cdot$ and $OH\cdot$ radicals. These radicals can recombine to return to their original form or combine to produce H_2 and H_2O_2 . They can also produce $HO_2\cdot$ by combination with O_2 . These strong oxidants and reductants are utilized for various sonochemical reactions in aqueous solutions^[60].

Organic liquids are also known to generate free radicals when irradiated with high intensity of sound. The sonolysis of simple hydrocarbons creates the same kinds of products associated with very high temperature pyrolysis. Most of these products - H_2 , CH_4 (methane), and the smaller 1-alkenes, derive from a well-understood radical chain mechanism. Relatively large amounts of acetylene (C_2H_2) are also produced, which is explained by the stability of this gas at very high temperatures. Suslick and coworkers synthesized nanostructures of inorganic materials by sonochemical decomposition of metal carbonyl compound. They reported that volatile organometallic compounds can fully dissociate their carbonyl ligands inside a bubble during acoustic cavitation, and the resulting metal atoms agglomerate to form a variety of nanostructured materials^[61].

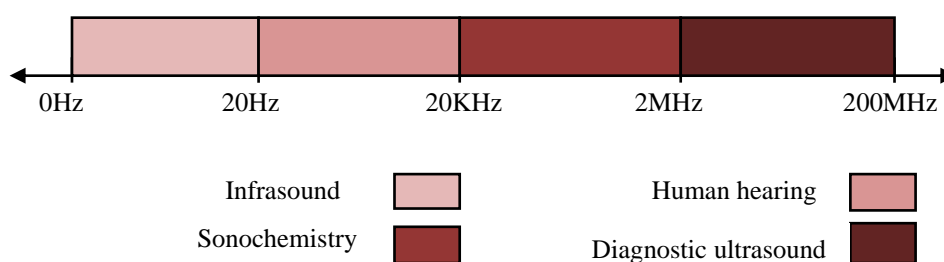


Figure 5. Frequency range of sound.

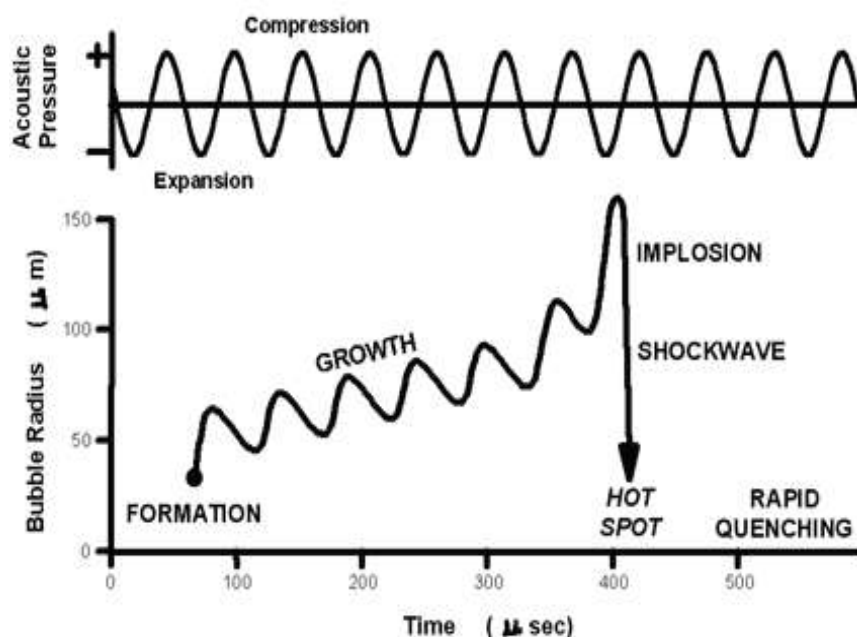


Figure 6. Transient acoustic cavitation; the origin of sonochemistry^[61].

By changing the growth parameters, various sizes and shapes of nanostructured materials were obtained through this simple sonochemical process. For instance, H-Roshan *et al.* synthesized different morphologies of TiO₂ nanoparticles by altering the sonication power. They observed a decrease in the size of the nanoparticles by increasing the sonication power^[62].

Different morphologies of ZnO nanostructures have been recently synthesized by this simple, fast and inexpensive technique at an ambient condition without the use of any growth catalyst or additional heating. Sirisathitkul *et al.* obtained a mixture of zinc compounds consisting of Zn₅(OH)₈(NO₃)₂(H₂O), a mixed phase ZnO/Zn₅(OH)₆(CO₃)₂ and a single phase Zn₅(OH)₆(CO₃)₂ from different concentration of the precursor solutions. They reported that the concentration of the precursors has a great influence on the phase and purity of the Zn product obtained^[63]. Askarinejad *et al.* synthesized nanocrystalline ZnO particles with average diameter between 20 nm to 100nm by sonication of zinc acetate and sodium hydroxide at different growth condition. They also reported that increasing the reaction time and calcination of the particles at 400 °C for 4 hours increases the size of the particle from 25.4 nm to 57.5nm. However, this does not affect the morphology of the obtained nanoparticles^[64].

Several other works have been done in order to produce ZnO nanostructures on various substrates by first depositing seed-layer followed by the growth of the nanostructures by decomposition of Zinc nitrate and Hexamethylenetetramine (HMT) under ultrasonic power.

By adjusting the concentration of the precursor solution, amplitude of ultrasonic wave and the reaction time, various morphologies and diameters of ZnO nanostructures have been obtained such as nanorods, nanowires, nanoflakes and nanowalls^[65-68]. Jung *et al.* synthesized ZnO nanorods of various sizes on Si wafer by first sputtering a thin film of Zn followed by the immersion of the Zn-coated wafer in an equimolar solution of hexamethylenetetramine and zinc nitrate hexahydrate. They observed that increase in concentration of Zn^{2+} and OH^- results in the increase in diameter of the ZnO nanorods from 40 to 200nm^[64]. In a similar report by Syamanta *et al.* average diameter of nanorods increase from 50 nm to 100 nm by increasing the concentration of the precursor solution from 0.01M to 0.1M^[68]. Eugene and coworkers also reported the sonochemical growth of ZnO nanorods on a Pt electrode deposited on alumina substrate. Before the growth, a thin layer of Zn was first deposited using RF sputtering, and ZnO nanorods were successfully grown from a reaction between HMT and Zinc nitrate hexahydrate under the influence of ultrasound, and the obtained ZnO nanorods demonstrated a high sensitivity with low detection limit^[63]. Different size of ZnO nanowires and nanowalls of high quality were synthesized on arbitrary substrates by Vabbina *et al.* they reported a simple seeding process by sonication of Zinc acetate dihydrate which is faster and practicable compared to the aforementioned process, and the structures obtained were of good crystal quality, and have shown enhanced electrical characteristics^[64].

Table 3 summarizes the various techniques used in the synthesis of nanostructures of ZnO on different substrates.

Table 3: List of ZnO nanostructures synthesis techniques and grown products.

Technique	Structure	Substrate/Temperature	Reference
MBE	Nanorods	Silicon 300-500 °C	[10]
Hydrothermal	Nanorods	Glass and Silicon 60-95 °C	[[14]
Soluthermal	Nanorods	TPU 75 °C	[20]
PLD	Nanorods	Sapphire and Silicon 550-700 °C	[46]
CVD	Nanowires	Chip 700 °C	[50]
Sonochemical	Nanorods	Glass and Si wafer Room ambient	[64-67]
Thermal evaporation	Nanorods	Porous Si 600-1000 °C	[69]
MOCVD	Nanowires	Sapphire and Silicon 630 °C	[70]
PECVD	Nanorods	Sapphire and Silicon 700 °C	[71]
Sol-Gel	Nanowires	Silicon 600 °C	[72]

4. GROWTH AND CHARACTERIZATION OF ZnO NANORODS

4.1 Synthesis of ZnO Nanorods

The samples investigated in this thesis were grown by sonochemical technique, at ambient condition. Fig.7 shows the experimental setup used in the sonochemical growth of ZnO nanorods. A continuous ZnO seed-layer was first deposited over the substrate followed by the growth of ZnO nanorods. This method has been reported to be feasible as it does not require complex setup, it does not produce any hazardous by-product, therefore not harmful to the environment^[55-60]. Different samples were synthesized by changing the growth condition and the antibacterial properties were assessed.

All chemicals used in this thesis were used directly without any further purification, and all preparations were done at room temperature. Table 4 shows the chemicals used in the deposition of ZnO seedlayer and growth of ZnO nanorods.

Table 4. Chemicals used in the synthesis of ZnO nanorods.

Chemicals	Molar Mass	Supplier
Zinc acetate dihydrate	219.51g/mol	Tekkim
Zinc nitrate tetrahydrate	261.44g/mol	Sigma Aldrich
Hexamethylenetetramine	140.19g/mol	Sigma Aldrich
Isopropyl alcohol	60.1g/mol	Sigma Aldrich

4.1.1 Seeding Process

Deposition of seed layer is very crucial in the sonochemical growth of ZnO nanorods on substrate. Several reports have shown that for ZnO nanorods to be obtained from a reaction between Zinc nitrate and HMT, a catalytic thin layer of metallic Zn is required^[62-64]. However, this process seems to prolong the process and makes it more difficult because Zn deposition is not available in most clean rooms. To mitigate these problems, a simple, one-step seeding process was developed using Zinc acetate dihydrate, which has been shown to form a suitable seed layer for the growth of ZnO nanorods on both polar and non-polar substrates^[73].

To seed the surface of the glass substrate, a 0.005M solution of Zinc acetate dihydrate in isopropyl alcohol was prepared by dissolving 0.55g Zinc acetate dihydrate($C_4H_{10}O_6Zn$) in a beaker containing 0.5L Isopropyl alcohol (IPA) at room temperature. The solution was stirred with a magnetic stirrer at 750rpm for 15 min. A clear solution was obtained and the glass substrate was then immersed into the solution and sonicated for 30 min at 50% of the maximum amplitude of the 24KHz ultrasonic probe working at 400 W.

4.1.2 Growth Process

Growth of ZnO nanorods on a previously ZnO-seeded substrate was shown to be possible from a reaction between HMT and zinc nitrate under the effect of ultrasound. An aqueous solution of 0.04M Zinc nitrate tetrahydrate ($Zn(NO_3)_2 \cdot 4H_2O$), and 0.04M Hexamethylenetetramine ($C_6H_{12}N_4$) was prepared. First, 2.8038g of HMT was dissolved in a beaker containing 0.5L deionised water and stirred with a magnetic stirrer at 750 rpm for 5 min. In a separate beaker containing another 0.5L deionised water, 5.2288g of $Zn(NO_3)_2 \cdot 4H_2O$ was dissolved and the solution was also stirred at 750 rpm for 5 min. Equal volume of the two solutions was mixed by stirring. The substrate was then immersed into the solution and sonicated at 50% of the maximum amplitude of the 24 kHz ultrasonic probe working at 400W for 30 min.

The same experiment was conducted for the second sample, but in this case the solution was refreshed after 15 min. Due to the fact that growth of ZnO nanowires tend to slow down as time increases because of the depletion of Zn^{2+} ions, introducing a fresh solution has been reported to improve the aspect ratio^[73].

In order to study the time effect on the growth of the ZnO nanorods, sonication time was further increased to 1 hour keeping other parameters constant. The role of the seed layer was also studied by conducting another experiment without seeding the substrate keeping all parameters constant.

The effect of the ultrasonic frequency was also studied by conducting another experiment at 100% amplitude of the ultrasonic probe for 60 min.

Table 5. shows the different growth parameters involve in the sonochemical growth of ZnO nanorods.

Table 5. Growth parameters for the sonochemical growth of ZnO nanorods.

Samples	Solution Concentration	Seeding time	Growth time	Ultrasonic power
1	0.04M	30 min	30 min	50%
2	0.04M	30 min	15 min + 15 min	50%
3	0.04M	30 min	1 hour	50%
4	0.04M	30	60 min	100%
5	0.04M	No seeding	60 min	50%

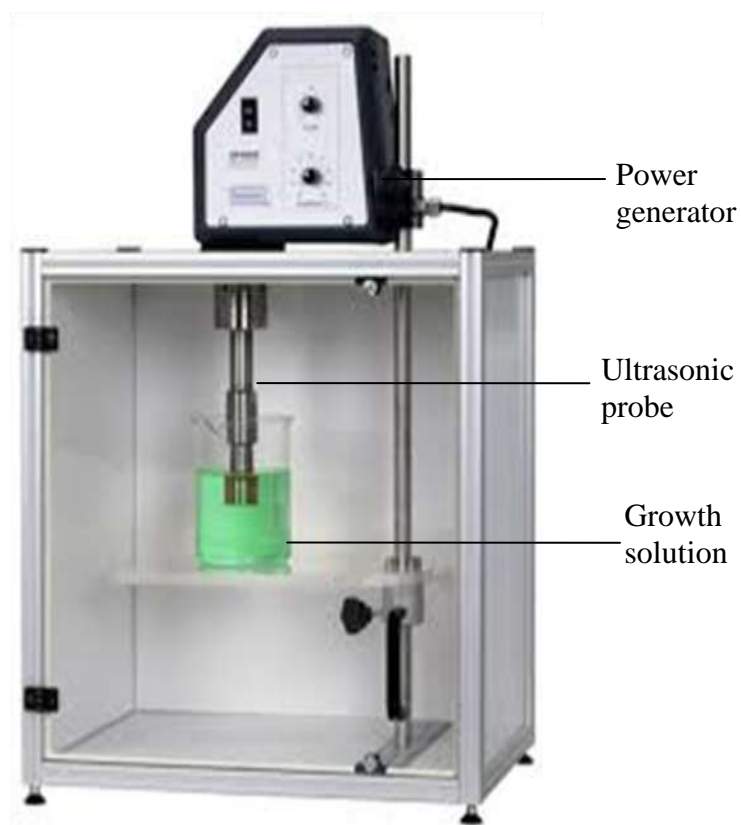
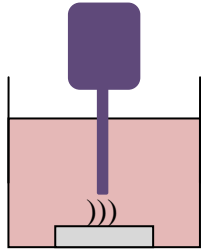


Figure 7: Sonochemical growth set up.



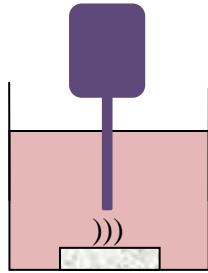
Bare glass substrate



Seeding process; Zinc acetate dihydrate in IPA + ultrasound

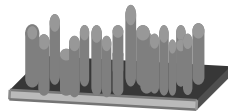


Seeded substrate



Growth process; Zinc nitrate tetrahydrate + HMT in DI water + ultrasound

))) denotes ultrasound



ZnO nanorods on seeded substrate

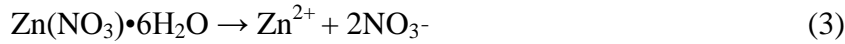
Figure 8. Schematic representation of sonochemical synthesis of ZnO nanorods.



Figure 9: Digital image of ZnO nanorods growth solutions.

Fig. 9 shows the solution containing equal volume of 0.04M zinc nitrate tetrahydrate and HMT prepared at room temperature. The solution was clear before the growth. After being irradiated with high intensity of sound, the solution was found to be cloudy with white precipitate. This indicated that the ultrasonic energy alone is strong enough to allow for the dissolution of the molecular species without being subjected to further treatment. The temperature was found to increase from the average room temperature (22- 25 °C) to 65-80 °C depending on the time of sonication.

Possible chemical reactions involve in the formation of ZnO nanorods by sonication of zinc nitrate and HMT [65, 73, 74].



Both HMT and zinc nitrate participate in the formation of $\text{Zn}(\text{OH})_4^{2-}$ crystal which is produce from the sonochemical reaction of Zn^{2+} and 4OH^- . NH_4^+ cations and OH^- anions are release from the hydrolysis of HMT as shown in equation (1) and (2) above, and Zn^{2+} cations are release from the dissolution of zinc nitrate as in equation (3).

Growth of the ZnO nanorods is initiated by the negatively charged ZnO seed layer with O_2^- ionization, this attract the Zn^{2+} by coulomb force of attraction and subsequently bound to the ZnO seed surface. By incorporating OH^- available in the solution, $\text{Zn}(\text{OH})_4^{2-}$ crystals are produced. $\text{Zn}(\text{OH})_4^{2-}$ are known to be unstable under sonication, therefore phase transition from $\text{Zn}(\text{OH})_4^{2-}$ to ZnO nanorods is said to occur at this stage^[75].

Alternatively, ZnO nanorods can also be grown from a reaction between Zn^{2+} and $\bullet\text{O}_2^-$ during sonication. Radicals $\bullet\text{OH}$, $\bullet\text{H}$, $\bullet\text{HO}_2$ and $\bullet\text{O}_2^-$ are generated through the sonolysis of water in air atmosphere^[60], and the reaction proceed as follows^[65, 74].



4.2. CHARACTERIZATION TECHNIQUES

In order to analyse the ZnO nanorods grown by sonochemical technique, different techniques have been used in this thesis both for surface characterization and elemental analysis of the sonochemically synthesized ZnO nanorods. These include optical microscopy, scanning electron microscopy(SEM), raman spectroscopy, and energy dispersive X-ray spectroscopy(EDS). Details of the characterization techniques are given below.

4.2.1 Optical Microscopy

Optical Microscopy is the oldest technique that is used to view smaller samples which are otherwise invisible with the naked eye. This technique uses visible light and a system of lenses to magnify images of small samples, often referred to as light microscopy. The image from an optical microscope can be captured by normal light-sensitive cameras to generate a micrograph. Originally images were captured by photographic film but modern developments in CMOS and charge-coupled device (CCD) cameras allow the capture of digital images.

The optical microscope is of two basic configuration: the simple microscope which uses a lens to magnify image of an object through angular magnification alone, giving an erect magnified virtual image. Simple microscopes are not able to achieve higher magnification. The compound microscope on the other hand uses a lens (the objective lens) close to the object being viewed to collect light which focuses a real image of the object inside the microscope. That image is then magnified by a second lens or group of lenses (the eyepiece) that gives the viewer an enlarged inverted virtual image of the object. The use of a compound objective/eyepiece combination allows for much higher magnification, reduced chromatic aberration and exchangeable objective lenses to adjust the magnification. A compound microscope also makes more advanced illumination setups, such as phase contrast possible. The compound microscope is the most widely used in the current research field. The compound microscope has several parts which play together to generate the image of the sample being studied. When the beam of light from the microscope lamp passes through the condenser and then through the object to the convex lense of objective, it forms a real inverted and enlarged image of the object in the focal plane of eyepiece (by adjustment). This image now acts as object for the eyepiece. Eyepiece lense finally forms a further enlarged virtual image of the object. Thus,

magnifying power of a compound microscope is the multiplication product of magnifying powers of objective and eyepiece.

In this thesis, Nikon H6001 optical microscope equipped with digital camera fitted with clemex captiva digital image analysis software was used to view the surface of the sonochemically synthesized ZnO nanorods.

4.2.2. Scanning Electron Microscopy (SEM)

SEM is one of the most widely used technique for the surface characterization of nanostructured materials. It provides detail topographic feature of the samples including shape and size of particles making up the sample. It uses highly focused electron beams which can be raster scanned on the surface of the sample. In a typical scanning electron microscopy, sample is scan in a raster pattern with a focused beam of electrons produced by an electron gun. The condenser and objective lenses located below the electron gun adjust the diameter of the electron beam and produce a small electron probe. These electrons interact with the atoms in the sample. The interaction between electrons and atoms of the sample produce a variety of signals including X-rays, backscattered electrons, and secondary electrons which can be detected. These signals give information about the surface topography and composition of the sample. Scanning electron microscopy is a non-destructive technique and produce very high resolution image less than 1nm. SEM can achieve a magnification from 10X to approximately 30,000X.

Scanning electron microscope FEI Quanta 250 -FEG equipped with EDS was used for the structural characterization of the sonochemically synthesized ZnO nanorods.

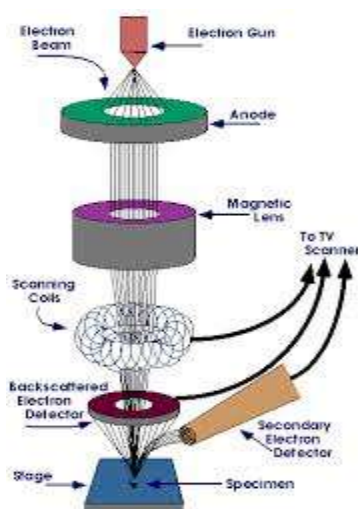


Figure 10. Schematic presentation of SEM instrument^[76].

4.2.3. Energy Dispersive X-ray Spectroscopy(EDS)

EDS is an analytical technique that is used for the elemental analysis or chemical characterization of samples. EDS makes use of the X-ray spectrum emitted by a solid sample bombarded with a focused beam of electrons to obtain a localized chemical analysis. At rest, an atom within the sample contains ground state (or unexcited) electrons in discrete energy levels or electron shells bound to the nucleus. The incident beam may excite an electron in an inner shell, ejecting it from the shell while creating an electron hole where the electron was. An electron from an outer, higher-energy shell then fills the hole, and the difference in energy between the higher-energy shell and the lower energy shell may be released in the form of an X-ray. The number and energy of the X-rays emitted from a specimen can be measured by an energy-dispersive spectrometer. As the energy of the X-rays are characteristic of the difference in energy between the two shells, and of the atomic structure of the element from which they were emitted, this allows the elemental composition of the specimen to be measured. EDS characterization capabilities are due in large part to the fundamental principle that each element has a unique atomic structure allowing unique set of peaks on its X-ray spectrum. EDS analysis is usually done in connection to SEM, thereby using electron beam as the excitation source. A detector is used to convert X-ray energy into voltage signals; this information is sent to a pulse processor, which measures the signals and passes them onto an analyzer for data display and analysis.

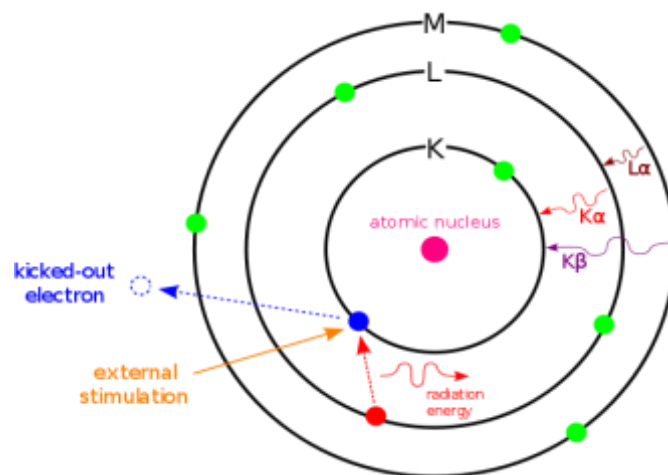


Figure 11. Principle of EDS^[77].

4.2.4. Raman Spectroscopy

RS is a spectroscopic technique that is used to observe vibrational modes in a system. In a typical raman spectroscopy, sample is illuminated with a laser beam. Light scattered from the illuminated spot is collected with a lens and sent through a monochromator. Due to elastic Rayleigh scattering, wavelengths close to the laser line are filtered out while the rest of the collected light is dispersed onto a detector. Raman spectroscopy relies upon inelastic or raman scattering of monochromatic light usually from a laser in the visible, near IR or near UV range. Photons of the laser light are absorbed, interact with the molecular vibrations, phonons or other excitations in the system, and then re-emitted. Frequency of the re-emitted photons is shifted towards higher or lower frequencies in comparison with original monochromatic frequency, which is called the Raman effect. This shift provides information about vibrational properties in the system. Every material has a specific raman spectrum which is considered to be a finger-prints, therefore the information acquired from raman spectroscopy is very crucial.

In this study, a confocal Raman microstage with an excitation wavelength of 488 nm was used to determine the optical and structural properties of ZnO nanostructure synthesized at room temperature.

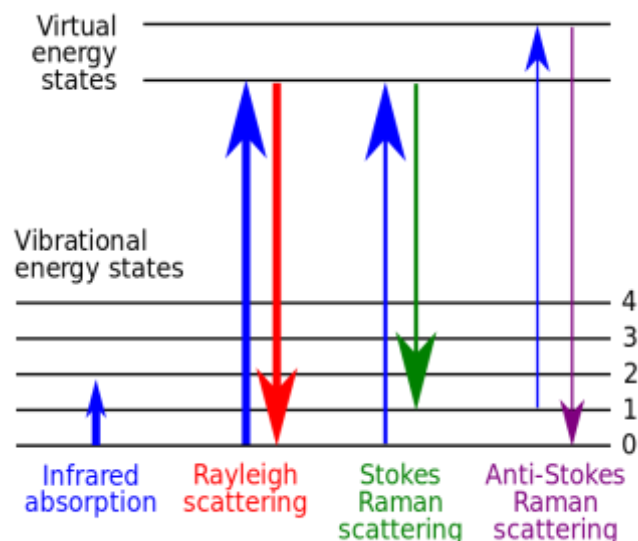


Figure 12. Energy-level diagram showing the states involved in Raman signal^[78].

4.3. ANTIBACTERIAL RESPONSE

Two different bacterial strains were used to test the antibacterial properties of the sonochemically grown ZnO nanorods.

Escherichia coli a Gram-negative, facultative anaerobic, rod-shaped bacterium that is commonly found in the lower intestine of warm-blooded organisms. Most strains of *E.coli* are harmless but there are a number of strains that causes intestinal and extra-intestinal diseases including bacteremia and urinary tract infection by means of virulence factors that affect a wide range of cellular processes^[79]. *E.coli* is one the four most common gram-negative pathogens that account for 32% of nosocomial infection^[80].

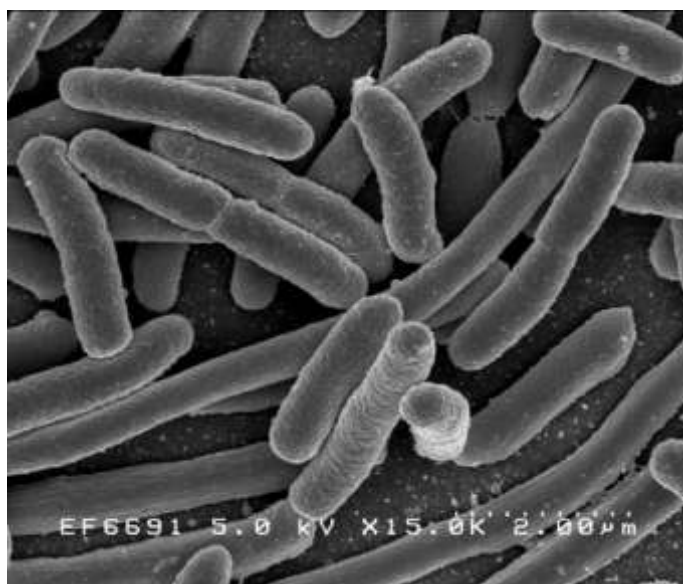


Figure 13. SEM image of *Escherichia coli*^[81].

Bacillus subtilis a gram-positive, rod-shaped bacterium that has the ability to form a tough, protective endospore, allowing the organism to tolerate extreme environmental conditions. Although *B.subtilis* is commonly found in soil, water, air and decomposing plant residue, but it is also reported to inhabit the gut and considered as a normal gut commensal. Although the pathogenicity of *B.subtilis* is very rare, it can to cause diseases in immunocompromised patient^[82].

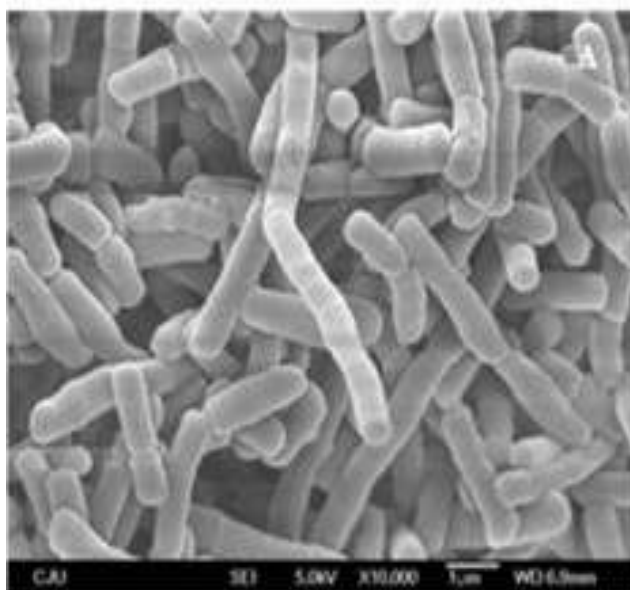


Figure 14. SEM image of *Bacillus subtilis*^[83].

4.3.1. Bacterial cell culture

Bacterial cells were cultured in Tryptic soy broth (TSB) containing 17.0 g Enzymatic Digest of Casein, 3.0 g Enzymatic Digest of Soybean Meal, 5.0 g Sodium Chloride, 2.5 g Dipotassium Phosphate, and 2.5 g Dextrose per litre of purified water. Enzymatic digest of casein and enzymatic digest of soybean meal are nitrogen sources in TSB, dextrose is the carbon energy source that facilitates organism growth, sodium Chloride maintains osmotic balance and dipotassium phosphate is a buffering agent. Using a sterile wire loop a small amount of bacteria was transferred into Erlenmeyer flask containing TSB and incubated at 37 °C for 24 h in an orbital shaker incubator and agitated at 150 rpm. This aerate the medium and provide dissolved oxygen for homogeneous growth of the cells and also prevent precipitation. Cells were washed with phosphate buffered saline (PBS) to remove any traces of the culture media. The bacterial optical density (OD) was adjusted to 0.2 at 600nm using a spectrophotometer.



Figure 15. Digital image of Bacterial cell culture media.

4.3.2 Toxicity test

In order to test the toxicity of the sonochemically grown ZnO nanorods towards bacterial cells, the two different glass substrates coated with ZnO nanorods and a bare glass slide without ZnO which was used as control were first washed with ethanol and then rinsed with phosphate buffered saline to eliminate any contaminant on the surface of the substrates. Substrates were then placed in a multi-well cell culture dish and bacterial suspension was seeded and incubated. The incubation time was varied between 2 h and 5 h. after the incubation, substrates were washed with PBS to remove non adherent cells, and viability was studied using live/dead assay.

4.3.2.1 Live/Dead assay

Live/Dead baclight bacterial viability kit (Invitrogen) was used to distinguish metabolically active cells from injured and dead cells. The Live/Dead bacLight bacterial viability kits utilize mixtures of SYTO-9 green-fluorescent nucleic acid stain and the red-fluorescent nucleic acid stain, propidium iodide. These stains differ both in their spectral characteristics and in their ability to penetrate healthy bacterial cells. When used alone, the SYTO 9 stain generally labels all bacteria in a population; those with intact mem-

branes and those with damaged membranes. In contrast, propidium iodide penetrates only bacteria with damaged membranes, causing a reduction in the SYTO-9 stain fluorescence when both dyes are present. Thus, with an appropriate mixture of the SYTO- 9 and propidium iodide stains, bacteria with intact cell membranes stain fluorescent green, whereas bacteria with damaged membranes stain fluorescent red. The excitation/emission maxima for these dyes are about 480/500 nm for SYTO- 9 stain and 490/635 nm for propidium iodide. The background remains virtually nonfluorescent. The percentage of inactive cells was determined from the ratio of the number of cells stained with PI divided by the number of cells stained with SYTO-9. The results were averaged out and the standard deviations were calculated. The kits are well suited for use in fluorescence microscopy or for use in quantitative analysis with a fluorometer, fluorescence microplate reader, flow cytometer or other instrumentation.

4.3.2.2 Fluorescence microscopy

Fluorescence microscopy is an essential tool in the field of biology and the biomedical sciences, as well as in materials science due to attributes that are not readily available in other contrast modes with traditional optical microscope. It uses fluorescence or phosphorescence to generate an image by the absorption and subsequent re-emission of light by organic or inorganic specimen. The specimen is first labelled with fluorescent stains and then illuminated with light of a specific wavelength which is absorbed by the fluorophores, causing them to emit light of longer wavelengths (i.e., of a different color than the absorbed light). The illuminated light is separated from the much weaker emitted fluorescence through the use of a spectral emission filter.

In this study, the stained cells were analyzed with BX 51 Olympus Fluorescence Microscope (Leeds Instrument Inc.) equipped with a DP72 digital camera under a 40x objective and a Fluorescein isothiocyanate (FITC) filter. All images were acquired and analyzed using Cell Sens Dimension digital imaging software (Olympus). Image-Pro Plus 6.1 (Media Cybernetics, Inc.) software was used to count the cells. The toxicity or the percentage of inactive cells was expressed as the percentage ratio of the total number of inactive cells (red) to the total number of cells (green). Average and standard deviation values were calculated on the percentages based on that cell count.

Agar flipping test was further conducted to study the continuous growth of cells in the presence of the ZnO nanorods. This was done by incubating the cells together with ZnO nanorods in tryptic soy agar (TSA) at 37 °C for 48 h. Growth was measured after 24 h and 48 h of incubation.

4.3.3 Drop plate method

This is a method used to determine the number of colony in a bacterial suspension. ZnO nanorods-coated substrates were incubated together with bacterial cell for 2 and 5 h. After the incubation period, substrate were taken and washed with PBS to remove the attached cells. 1ml of the obtained bacterial suspension was dispensed into a dilution tube containing 9ml of sterile buffered solution. Four serial dilutions were made. 3 drops of 25µl of each dilution was placed onto agar plate. Drops were allowed to soak into the media before turning, and plates were incubated overnight at 37 °C. Viable cells were counted after the incubation period.

5. RESULTS AND DISCUSSION

In this thesis, growth ZnO nanorods and their antibacterial properties against two different bacterial strains was reported. ZnO nanorods of different size were obtained from sonochemical reaction of zinc nitrate tetrahydrate and HMT. Growth was carried out within 30-60 min, subsequent to a 30 min seeding process as stated in the experimental section. The sonochemically grown ZnO nanorods were analysed by different techniques. Details are given below.

5.1. Seedlayer

Figure 16 shows the optical microscope image of the ZnO seed layer deposited on glass substrate, prior to growth ZnO nanorods. Images were taken from different spots at 50x and 100x magnification respectively. It can be seen that higher magnification give a better resolution. These images also shows that the particles are widely dispersed on the substrate.

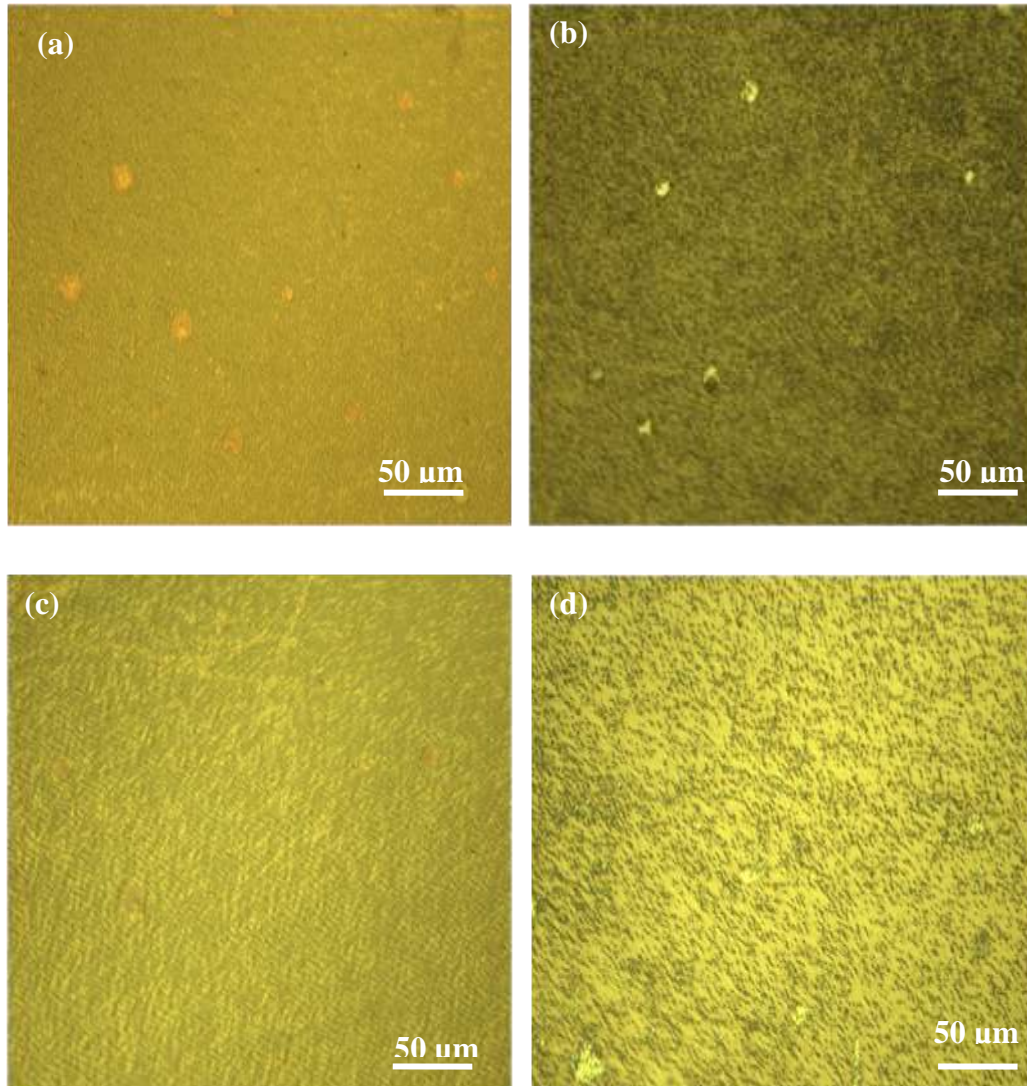


Figure 16: Optical image of ZnO seed layer taken with 50x magnification, (a) spot 1, (b) spot 2 and 100x magnification (c) spot 1, (d) spot 2.

Figure 17 shows the SEM images of the ZnO seed layer. The images agree well with the optical microscope image showing the surface covered with ZnO seed layer, with few areas devoid of the growth as observed in fig17(a). It can be seen that nanoparticles of

similar shape and size were formed fig17(b). This would serve as the nucleation site for the growth of ZnO nanorods on the substrate.

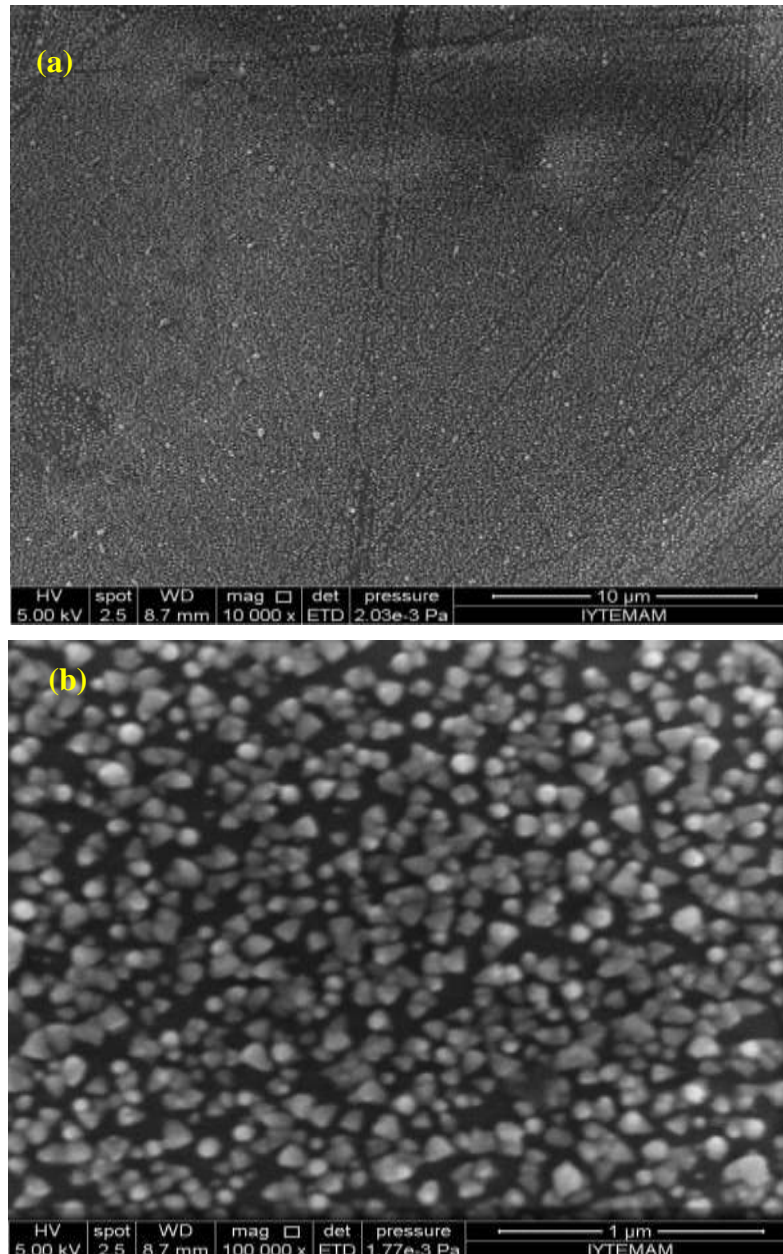


Figure 17: SEM image of ZnO seed layer deposited on glass substrate (a) 10 000x magnification and (b) 100 000x magnification.

5.2. Sample grown for 30 min at 50% amplitude

Optical Microscopy

Figure 18 shows the optical images of different spots of the 30 min continuously grown sample. Images were first taken at 50x magnification (a) and (b), and again taken at 100x magnification (c) and (d). It can be seen that growth of ZnO nanorods was not homogeneous with some spots having dense growth as in fig.18 (a) and (c) while low growth was observed in other spots (b) and (d).

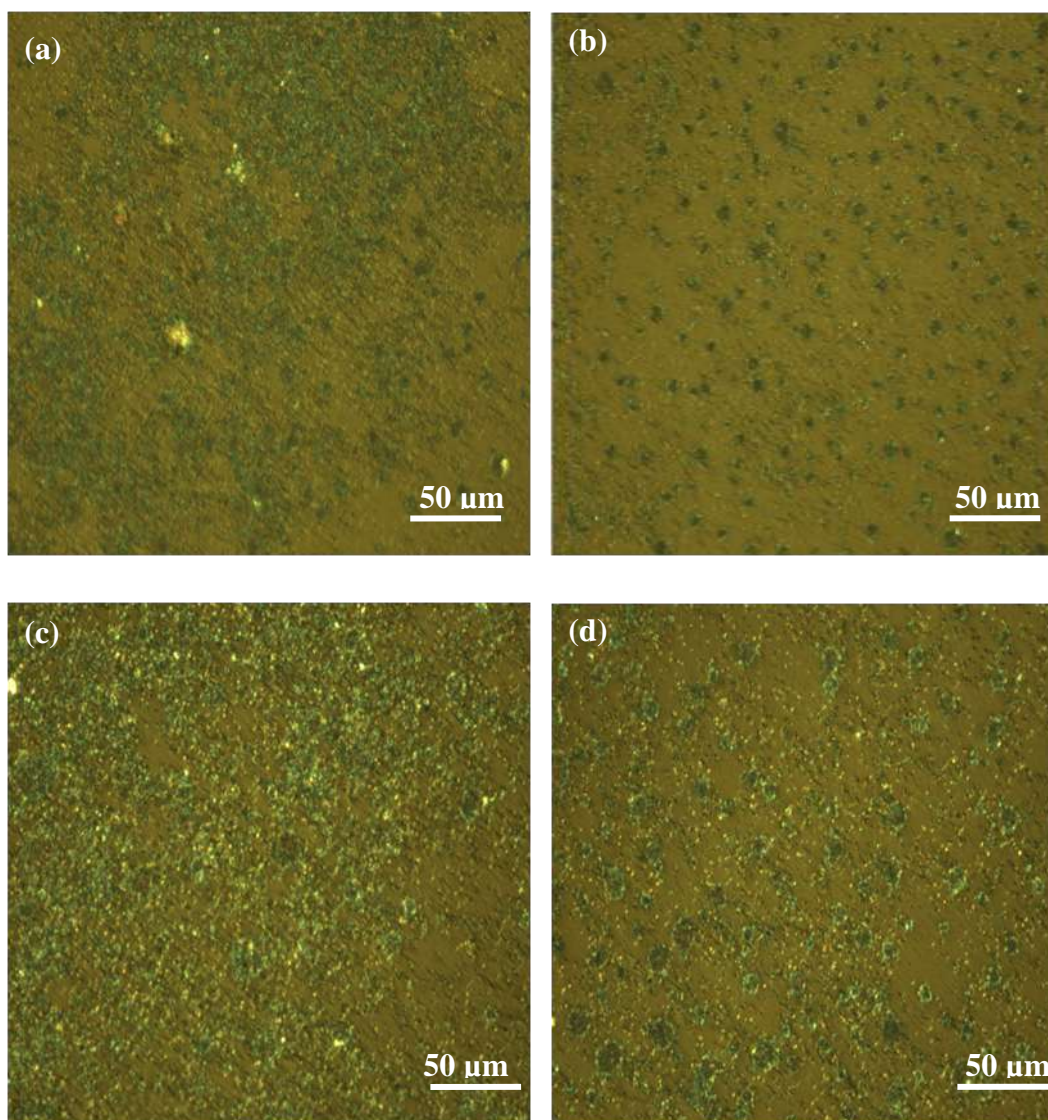


Figure 18: Optical image of ZnO nanorods grown for 30 min, at 50% amplitude, taken with 50x magnification, (a) spot 1, (b) spot 2 and 100x magnification (c) spot 1, (d) spot 2.

SEM

Figure 19 shows the SEM image of 30 min continuously grown sample. The images show a non-homogeneous growth of ZnO nanorods fig 19(a). The images also show ZnO nanorods of uniform shape and size fig 19(b) were obtained in this sample. The average diameter was found to be $\sim 78\text{nm}$ as estimated using clemex image analysis software.

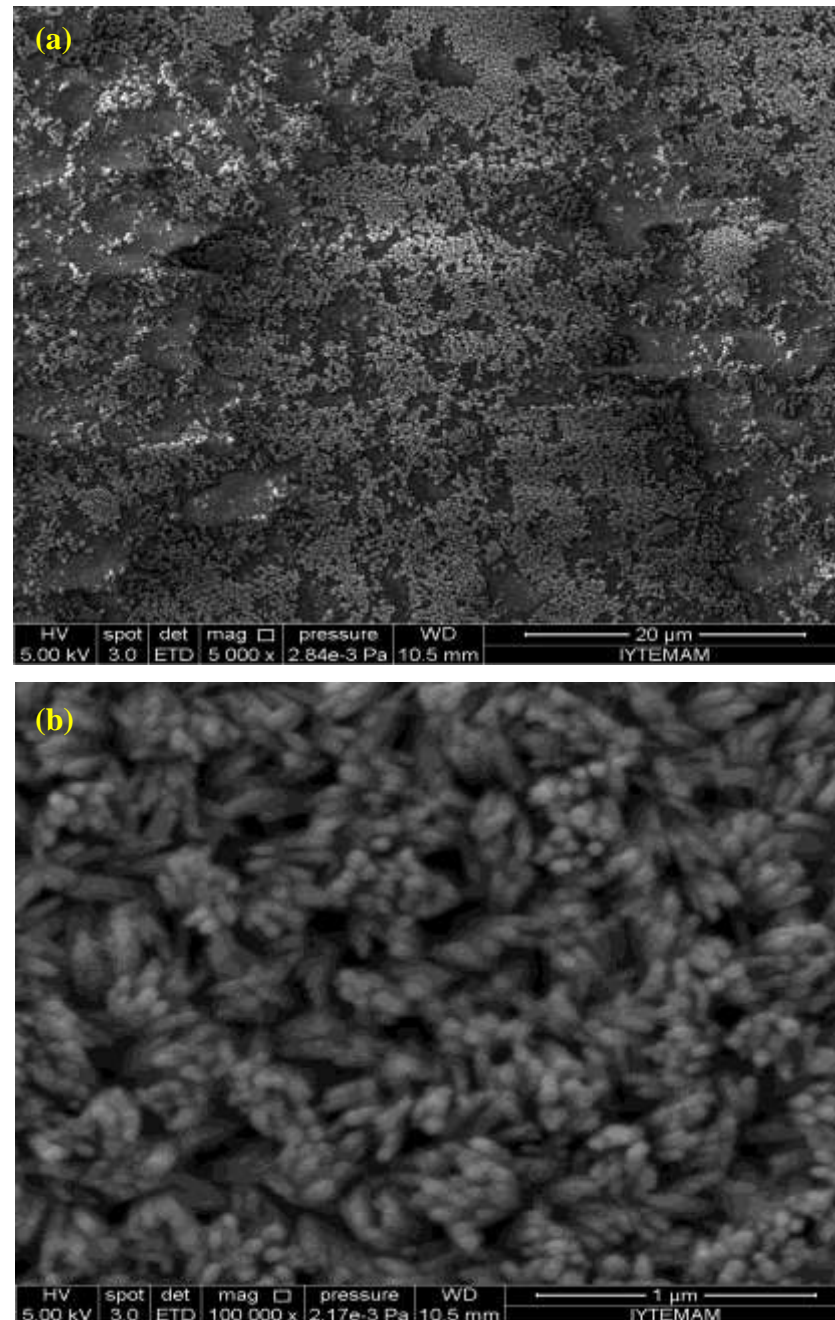


Figure 19: SEM images of ZnO nanorods grown for 30 min, at 50% amplitude sample. (a) 10 000x magnification and (b) 100 000x magnification.

EDS

Figure 20 show the EDS spectrum of ZnO nanorods grown for 30 min, at 50% amplitude. The chemical analysis shows the presence of Zn and O which indicated that the nanorods are composed purely of Zn and O. However, Si was also identified but this could be nowhere but from the glass substrate.

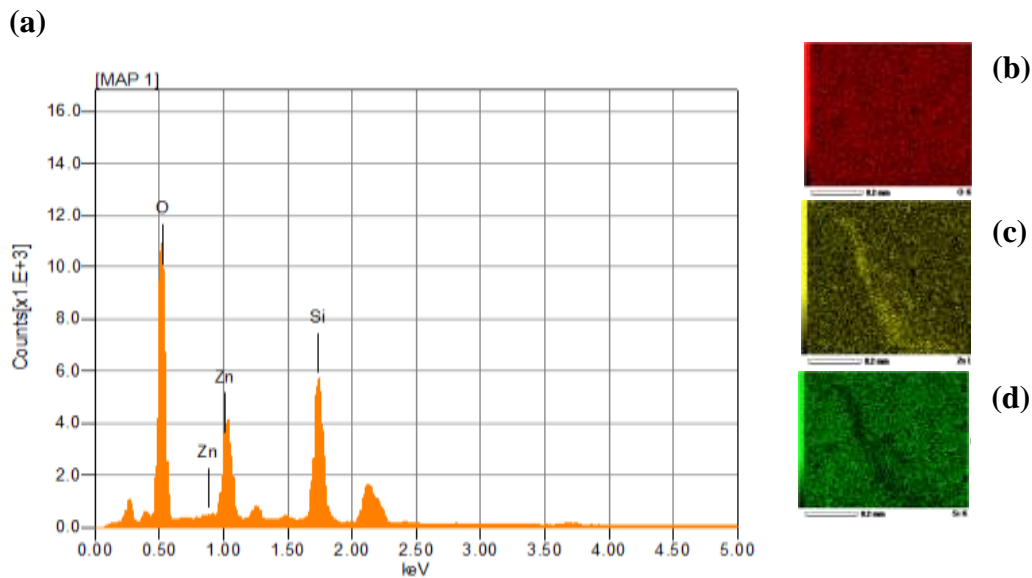


Figure 20: EDS spectrum of ZnO nanorods grown for 30 min, 50% amplitude sample. (a) graphical presentation, (b) oxygen mapping, (c) zinc mapping and (d) silicon mapping.

Raman Spectroscopy

Every material exhibits a characteristic Raman spectrum which is considered to be a fingerprint. Raman spectra are very sensitive to crystal quality, structural defects, and the disorder of grown structures. Therefore, Raman spectroscopy provides distinct information about the structure of the material.

ZnO has a hexagonal wurtzite structure which belongs to the C_{6v}^{4-} with two formulae units per primitive cell. $A_1 + 2E_2 + E_1$ are the Raman active optical phonon modes predicted by group theory, among which A_1 and E_1 are the polar phonons which can split into transverse optical (TO) and longitudinal optical (LO) modes. E_2 is the non-polar mode

which is composed of two modes frequency $E_2(\text{High})$ associated with oxygen atoms and $E_2(\text{Low})$ associated with Zn sub-lattice^[84, 85].

Figure 21 shows the Raman spectrum of ZnO nanorods grown for 30 min, at 50% amplitude. $E_2(\text{Low})$ and $E_2(\text{High})$ are observed in this sample which are vibrational mode of ZnO crystal. Additional peak can be seen at 325cm^{-1} . This could be assigned to the second order Raman spectrum arising from the zone boundary phonon $E_2(\text{Low})$ and $E_2(\text{High})$ ^[85].

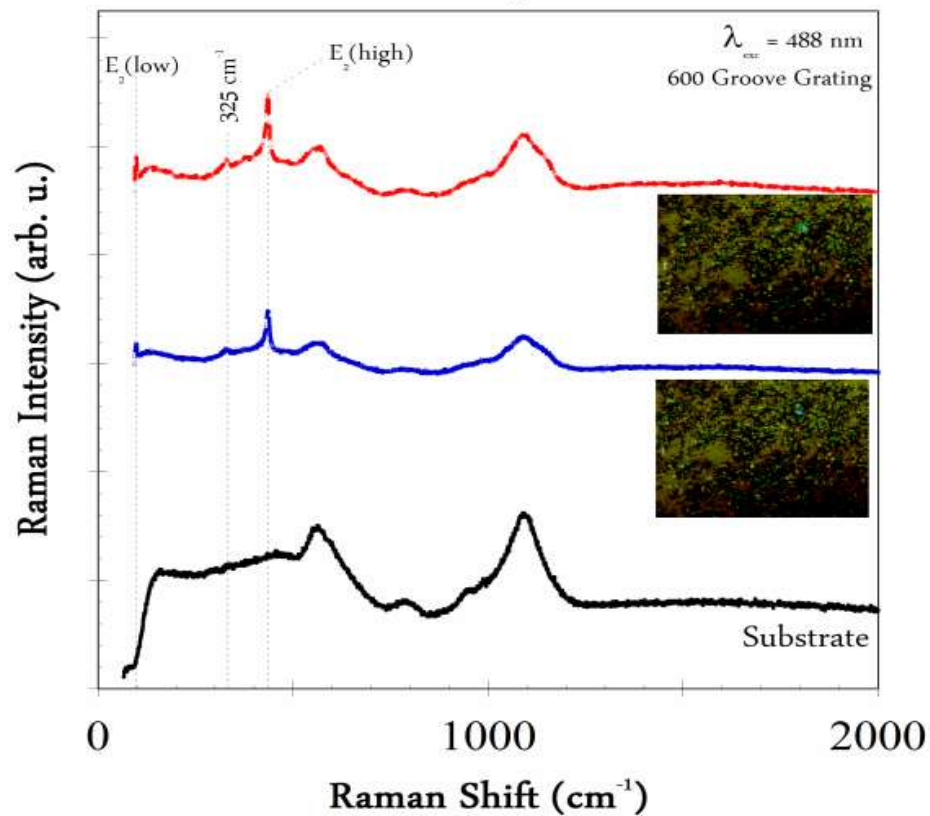


Figure 21: Raman spectrum ZnO nanorods grown for 30 min, at 50% amplitude sample. (black) substrate, (red) and (blue) ZnO at different spots. inset confocal raman image.

ZnO nanorods of uniform size were obtained in this sample. However, growth of ZnO nanorods was observed to be non-homogeneous. This indicates that during the 30 min sonication period, $\text{Zn}(\text{NO}_3)_2$ and HMT do not completely decompose. This results in decrease in the amount of Zn^{2+} and OH^- in the solution. Therefore, the formation of $\text{Zn}(\text{OH})_2$ complexes from the dehydration of which ZnO nanorods are formed is decreased. Nucleation was also reported to be difficult when the concentration of Zn^{2+} and OH^- is low in the solution, this decreases the growth rate and resulted in the non-homogeneity of the growth.

5.3. Sample grown in two-cycle at 50% amplitude

Optical Microscopy

Figure 22 shows the optical images of ZnO nanorods grown in two-cycle, at 50% amplitude. The images were taken from different spots, and at 50x and 100x magnification. It can be seen that growth of ZnO nanorods in the sample was similar to the continuously grown sample with some points having dense growth while some points have few growth of ZnO nanorods.

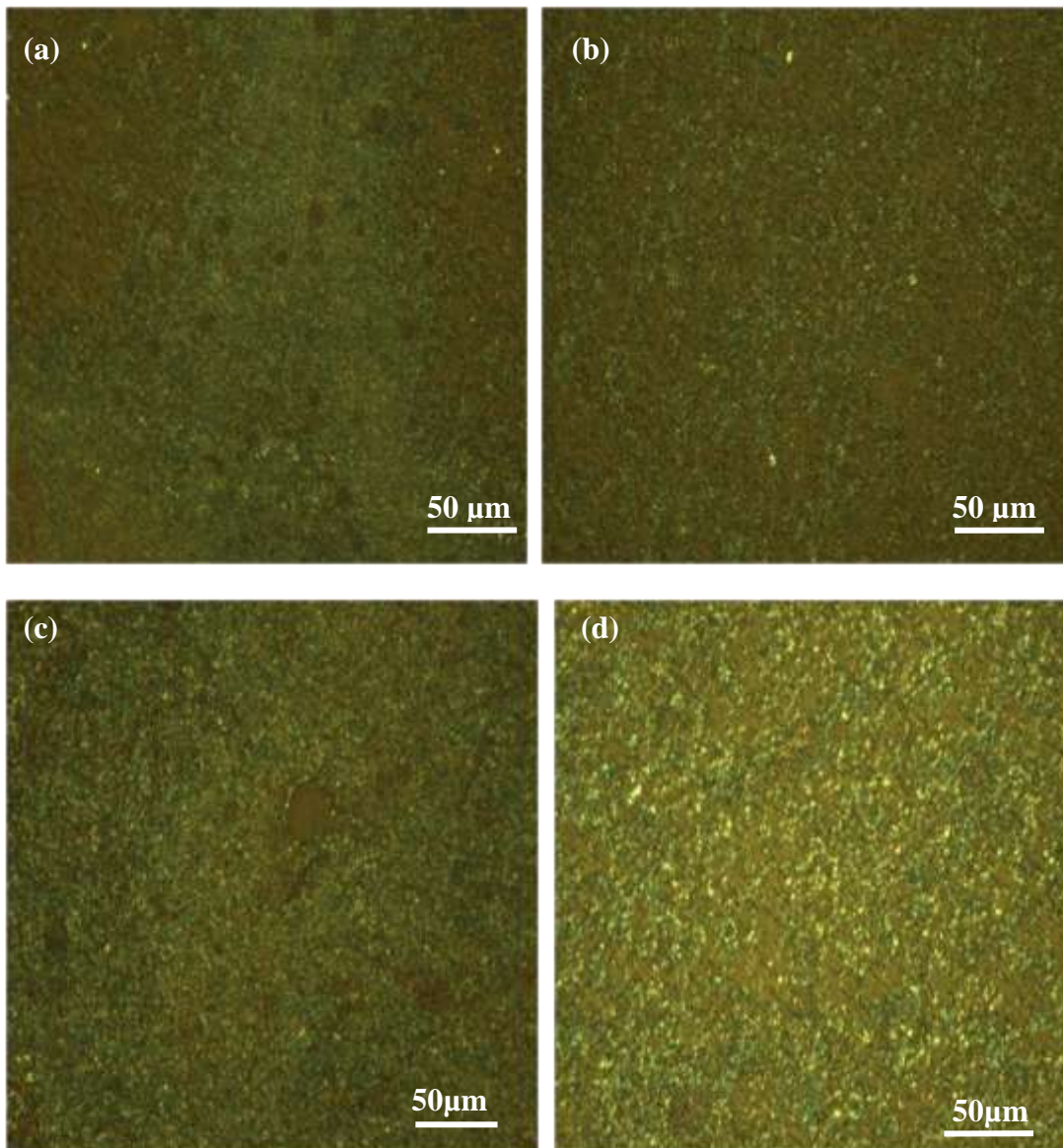


Figure 22: Optical image of ZnO nanorods grown in two-cycle, at 50% amplitude, taken with 50x magnification, (a) spot 1, (b) spot 2 and 100x magnification (c) spot 1, (d) spot 2.

SEM

Figure 23 shows the SEM image of ZnO nanorods grown in two-cycle, at 50% amplitude. The images show a non-homogeneous growth of ZnO nanorods fig 23(a). The images also show ZnO nanorods of uniform shape and size fig 23(b) were obtained in this sample. The average diameter was found to be ~65nm.

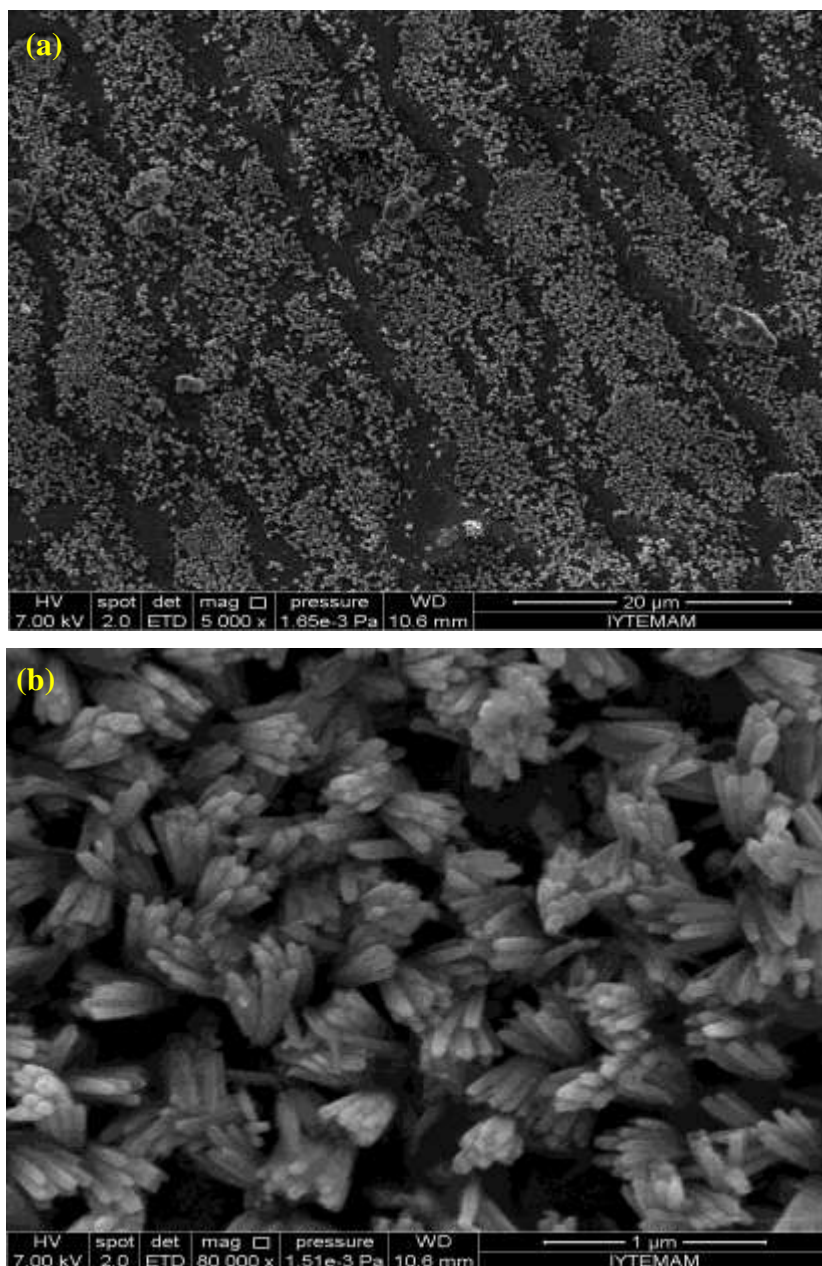


Figure 23: SEM images of ZnO nanorods grown in two-cycle, at 50% amplitude. (a) 10 000x magnification and (b) 100 000x magnification.

EDS

Figure 24 shows the EDS spectrum of ZnO nanorods grown in two-cycle, at 50% amplitude. The chemical analysis shows the presence of Zn and O which indicated that the nanorods are composed purely of Zn and O. However, Si was also identified but this could be nowhere but from the glass substrate.

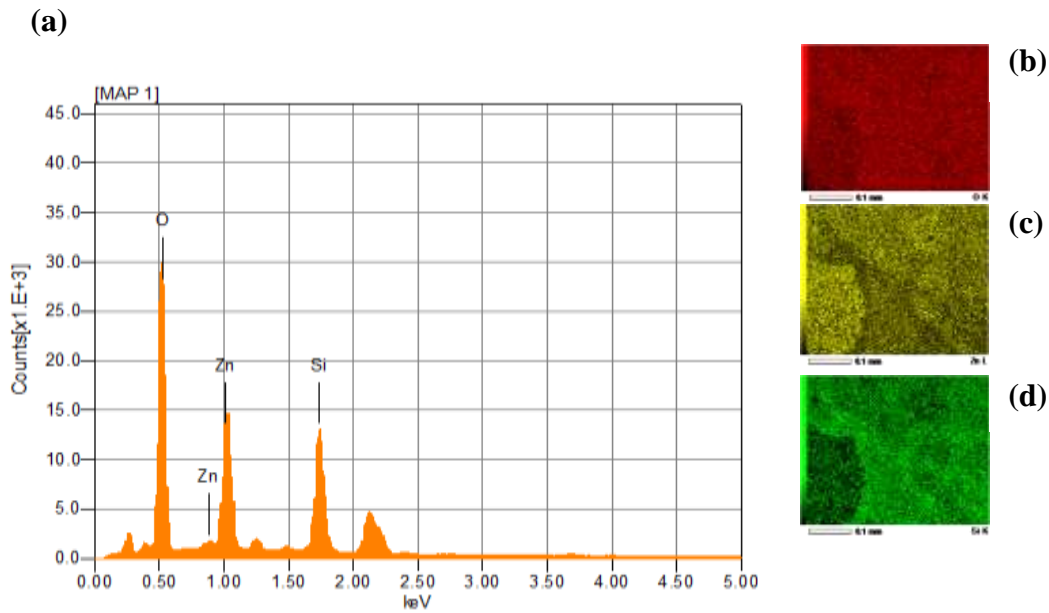


Figure 24: EDS spectrum ZnO nanorods grown in two-cycle, at 50% amplitude. (a) graphical presentation, (b) oxygen mapping, (c) zinc mapping and (d) silicon mapping.

Raman Spectroscopy

Figure 25 shows the Raman spectrum of ZnO nanorods grown in two-cycle, at 50% amplitude. Because of the non-homogeneity of the growth observed in this sample, as indicated by both optical microscopy and SEM, measurements were taken from two different spots. However, $E_2(\text{High})$ can be observed in all the spots which is a finger print of ZnO wurtzite structure. Black is the substrate while blue and red are the two different points, and the insets are the confocal Raman images. The peak at 97cm^{-1} is assigned as the $E_2(\text{Low})$. The peak shifted from the bulk value by $\sim 5\text{cm}^{-1}$. The peak at 453cm^{-1} is assigned as the $E_2(\text{High})$ which is shifted by a value of $\sim 16\text{cm}^{-1}$. The shift in the peak is due to the optical phonon confinement effect observed in nanostructures [86]. The

differences observed in the peak intensity of the two different spots can be attributed to the difference in amount of ZnO and crystal quality in the specific point which agrees with previous findings^[85]. Additional prominent peaks were also observed which are characteristics of nanostructures.

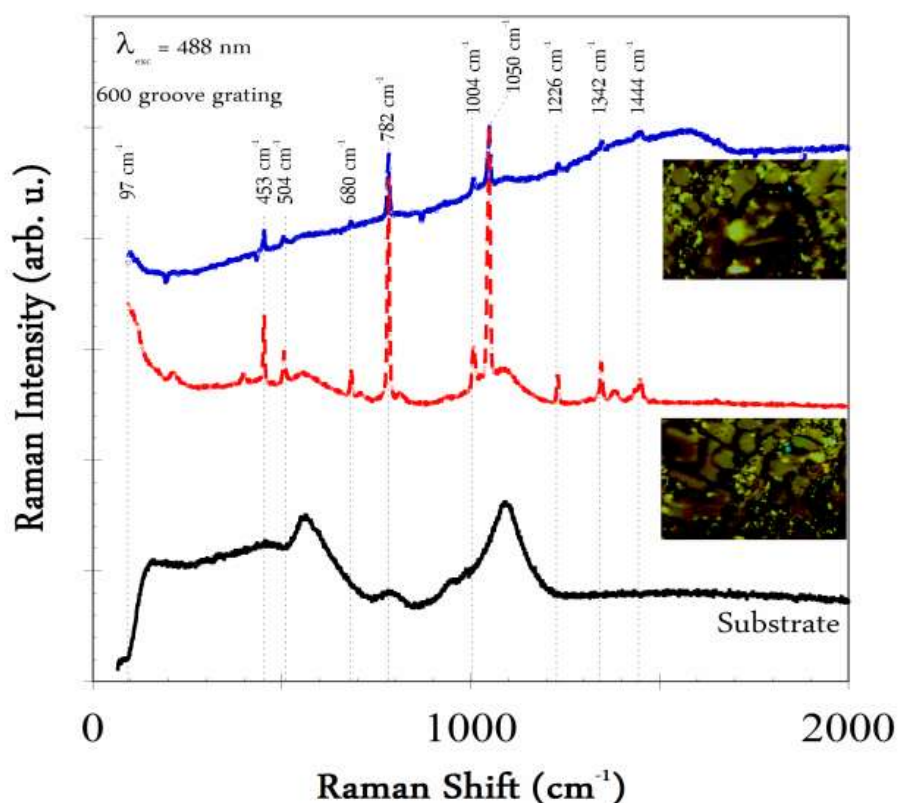


Figure 25: Raman spectrum of ZnO nanorods grown in two-cycle at 50% amplitude. (black) substrate, (red) and (blue) ZnO at different spots. inset confocal raman image.

Growth of ZnO nanorods was found to be non-homogeneous with ZnO nanorods of uniform shape and size as in the previous sample. However, the diameter was found to decrease from ~78 nm in the continuously grown sample to ~65 nm in this sample. This indicates that refreshing the growth solution during the first half of the growth period allows the growth of ZnO nanorods to continue along 0001 direction, thereby decreasing the diameter and also increases the aspect ratio^[67].

5.4. Sample grown for 60 min at 50% amplitude

Optical Microscopy

Figure 26 shows the optical images of ZnO nanorods grown for 60 min, 50% amplitude. Growth of ZnO nanrods was found to be more dense and homogeneous. It can be seen that the glass substrate was almost entirely covered with ZnO nanorods. The images also show that ZnO nanorods clustered at some points giving a different optical property.

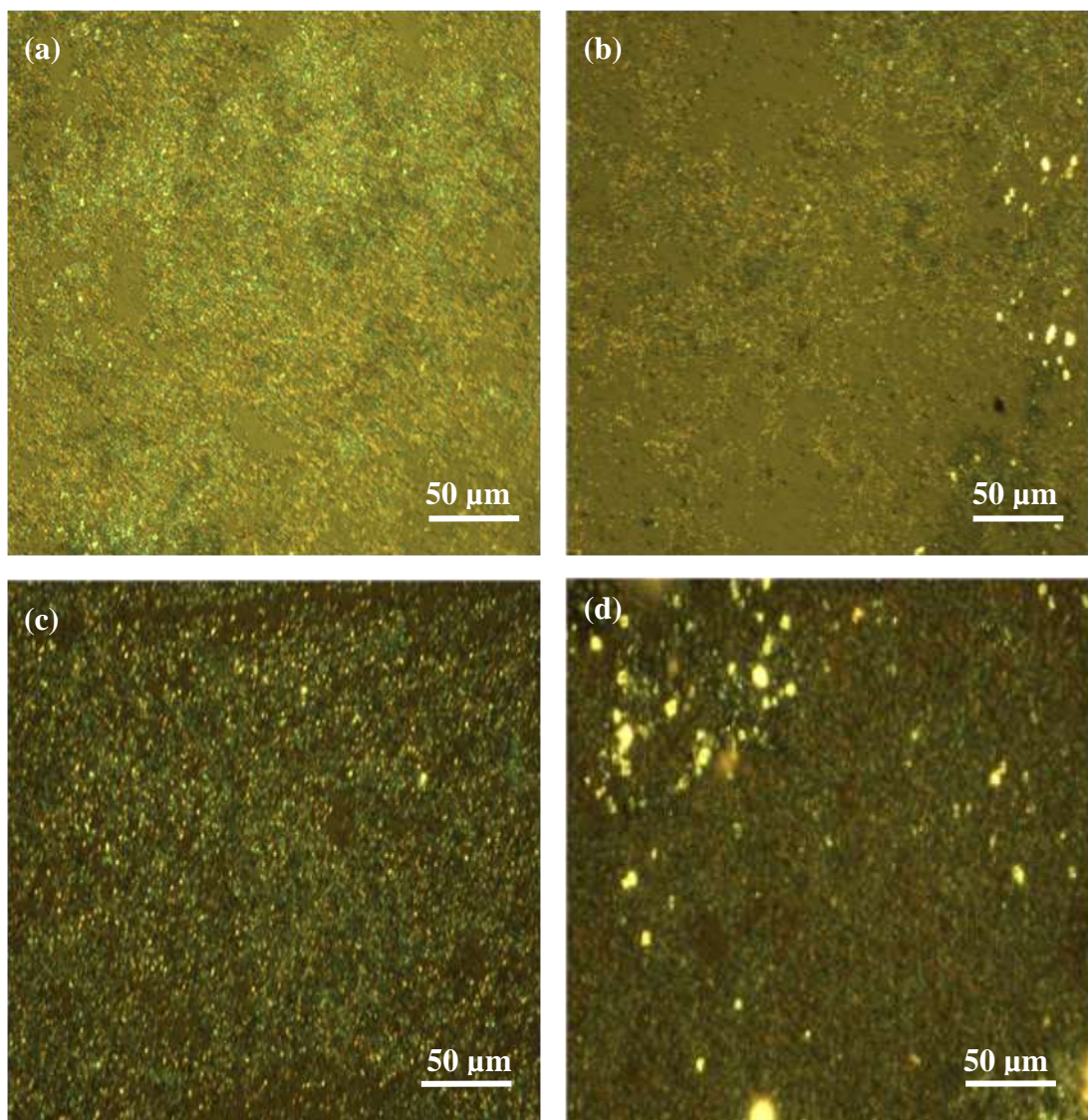


Figure 26: Optical image of ZnO nanorods grown for 60 min, at 50% amplitude, taken with 50x magnification, (a) spot 1, (b) spot 2 and 100x magnification (c) spot 1, (d) spot 2.

SEM

Figure 27 shows the SEM image of ZnO nanorods grown for 60 min, at 50% amplitude. A dense growth of ZnO nanorods was observed in this sample fig. 27(a). The ZnO nanorods were found to be of variable size in this sample as seen in fig. 27(b), with the average diameter been ~ 107 nm.

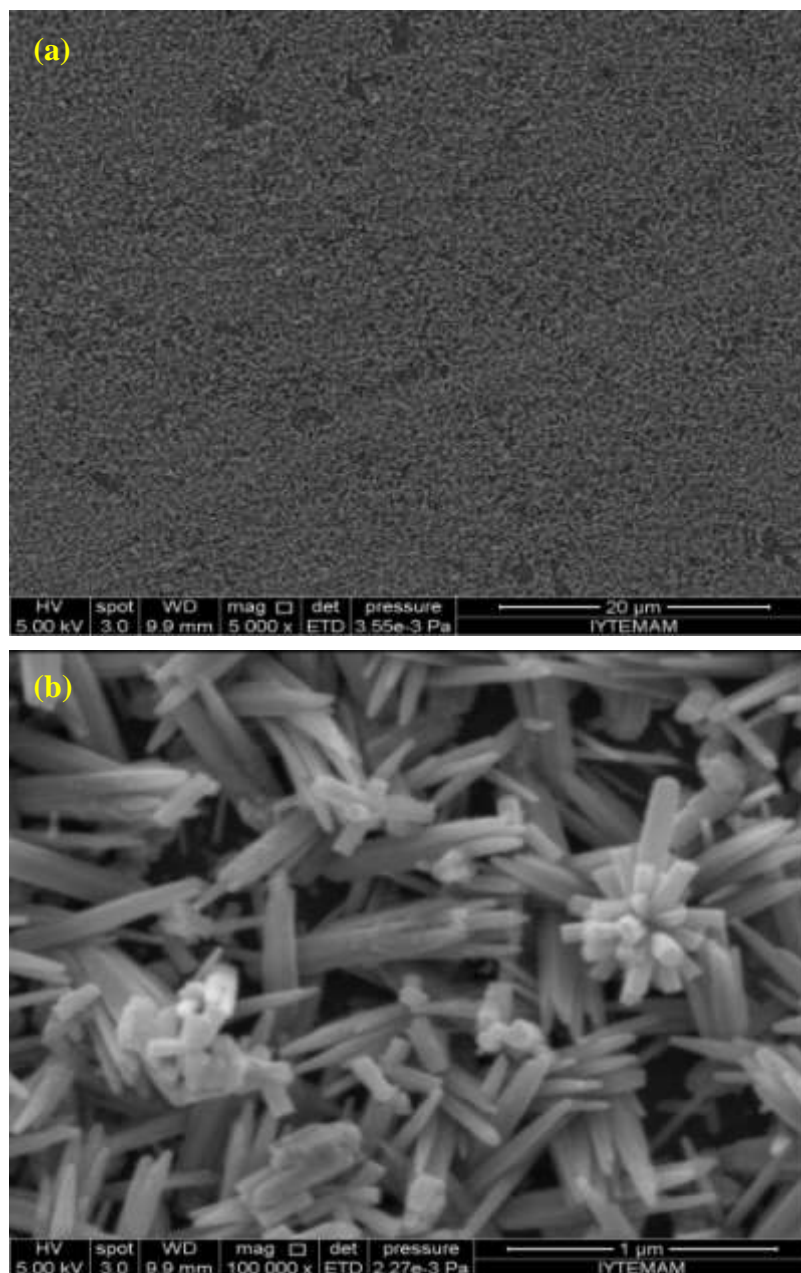


Figure 27: SEM images of ZnO nanorods grown for 60 min, at 50% amplitude.(a) 10 000x magnification and (b) 100 000x magnification.

Raman Spectroscopy

Figure 28 shows the Raman spectrum of sample 3. $E_2(\text{High})$ was observed in this sample which is a vibrational mode of ZnO wurtzite crystal associated with motion of oxygen. $A_1(\text{LO})$ which usually arises due to oxygen deficiency and/or increase in the lateral grain size of the structures^[87], was also observed in this sample. This corresponds to the growth condition, in which the sample was sonicated for the longer period of time. Increase in sonication time results in the increase number of oxygen vacancies and also leads to crystal lattice deformation^[88]. And the peak at 1045cm^{-1} is assigned as the second order Raman phonon.

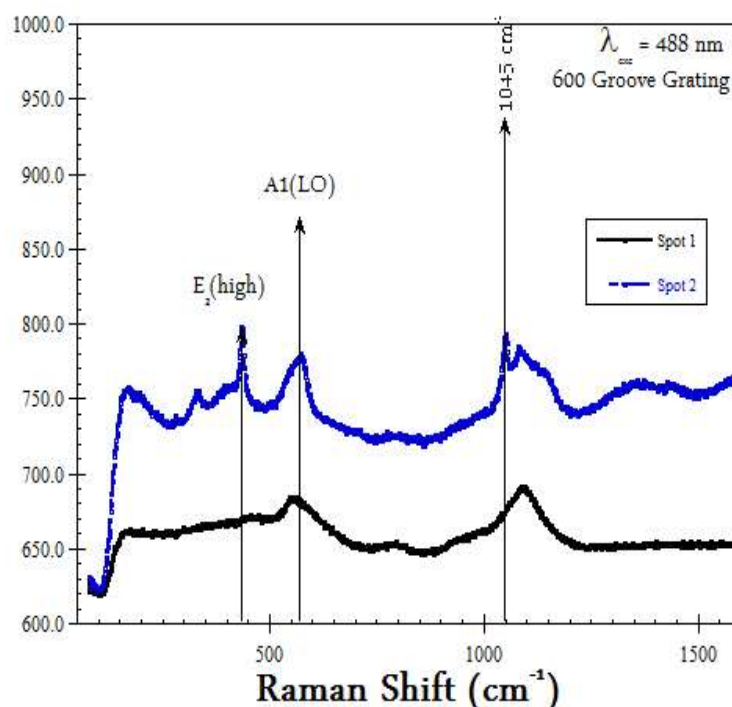


Figure 28: Raman spectrum of ZnO nanorods grown for 60 min, at 50% amplitude. (black) glass substrate, and (blue) ZnO.

Growth of ZnO nanorods was found to be dense and homogeneous. This indicates that the long sonication period allows for the complete decomposition of $\text{Zn}(\text{NO}_3)_2$ and HMT, which provides sufficient Zn^{2+} and OH^- , therefore nucleation can be easily achieved and the growth rate increases^[89]. However, the average diameter was found to be $\sim 107\text{nm}$ as the sonication time increases, this is in comparison with previous work^[63, 88]. The increased diameter is due to the long sonication period in which the increase in nucleation rate

results in shortage of Zn^{2+} ions in the solution, thereby hindering the growth of the nanorods along the 0001 direction, while favouring the 2110 direction growth which increase the diameter of the nanorods. It was also observed that, while some of the nanorods are of typical hexagonal shape, some are observed to have tapering and sharp end. Furthermore, some ZnO nanorods tend to cluster and form a flower-like structure during the long sonication period as depicted in fig. 27(b). This correlate with previous studies which indicates that when ZnO nanorods are growing, the amount of Zn^{2+} is decreasing in the solution and the density of charge at the end of the ZnO nanorods is increased, and each Zn^{2+} ion is attracted by some nanorods. Therefore, ZnO nanorods are connected to each other by Zn^{2+} ions, forming a flower-like structure^[75]. This shows that sonication can have a great influence on the orientation of the ZnO nanorods. The decrease in concentration of Zn^{2+} in the solution also accounted for the appearance of ZnO nanorods withsharp tip. In a similarly findings, decrease in the amount of Zn vapor source results in the formation of needle-like structures^[65].

5.5. Sample grown for 60 min at 100% amplitude.

Optical Microscopy

Figure 29 shows the optical microscopy of the ZnO nanorods grown for 60 min, at 100% amplitude. Images were taken from different spots at 50x and 100x magnification. The images show that a dense and homogeneous was growth obtained.

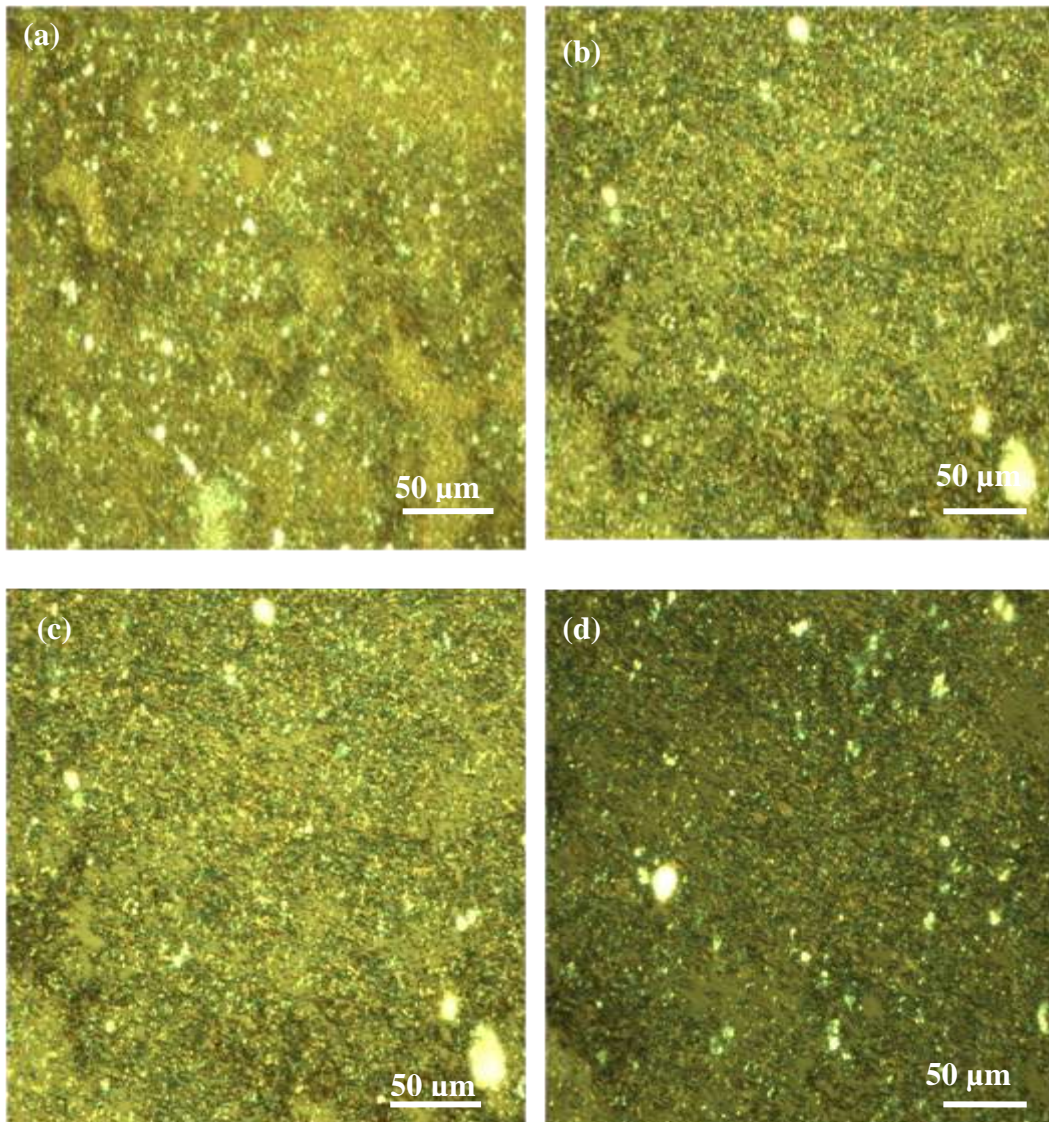


Figure 29: Optical images of ZnO nanorods grown for 60 min, at 100% amplitude taken with 50x magnification, (a) spot 1, (b) spot 2 and 100x magnification (c) spot 1, (d) spot 2.

The growth of ZnO nanorods was found to be dense and homogeneous as in previous sample. However, ZnO nanorods in this sample were found to be of uniform shape and size as observed in fig. 30(b), and the average diameter was found to be $\sim 50\text{nm}$ which is less than half of the 50% amplitude grown sample with $\sim 107\text{nm}$. The decrease in diameter could result from the high intensity of ultrasound. The increase in ultrasound

intensity increase the cavitation phenomenon, therefore collapse cavity in the solution creates shockwave which decrease the size of the nanorods^[62].

SEM

Figure30 shows the SEM image of ZnO nanorods grown for 60 min, at 100% amplitude of the ultrasonic probe. Dense and homogeneous growth of ZnO nanorods can be seen in this sample.

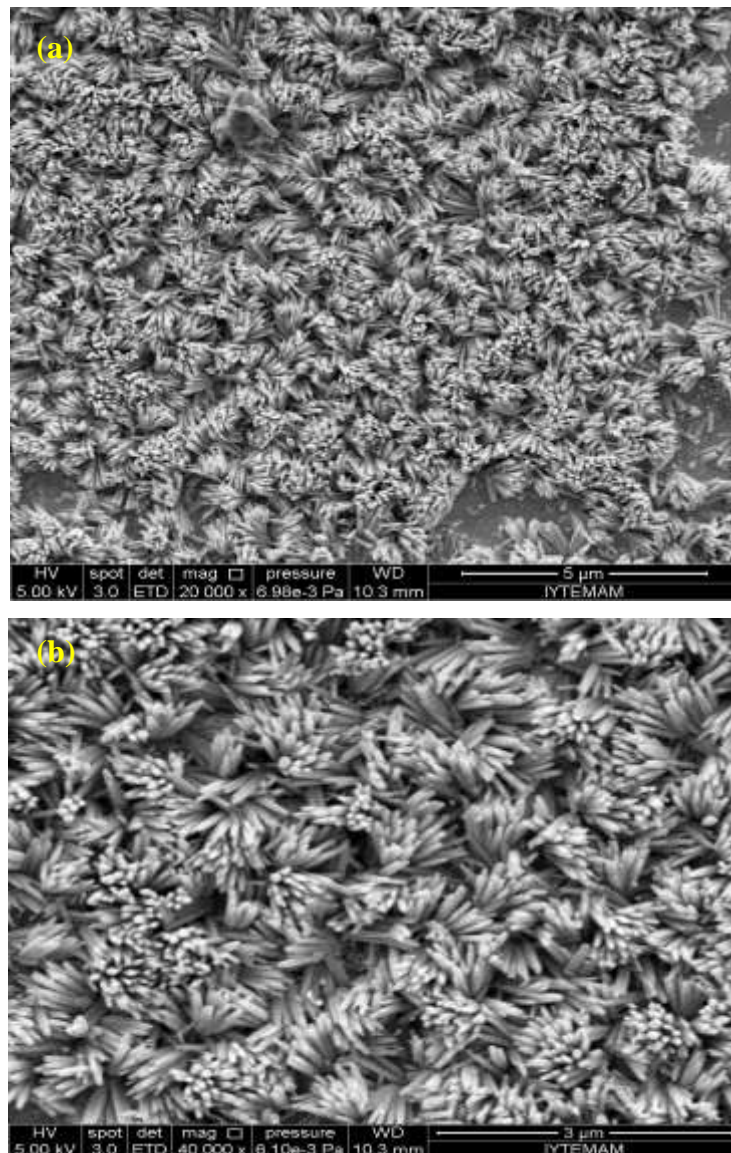


Figure 30: SEM images ZnO nanorods grown for 60 min, 100% amplitude. (a) 10 000x magnification and (b) 100 000x magnification.

Raman Spectroscopy

Figure 31 shows the Raman spectrum of sample 4. $E_2(\text{High})$ was identified in this sample which is a vibrational mode of ZnO wurtzite crystal associated with motion of oxygen. $A_1(\text{LO})$ can also be seen in this sample which arises due to oxygen deficiency and/or increase in the lateral grain size of the structures^[87]. This is similar to the previous sample which was also grown for 60 min, but unlike the previous sample grown at 50% of the maximum amplitude, this sample was grown at 100% amplitude which indicated that the high frequency does not have much effect on the crystal quality as does the time. However, additional characteristics of nanostructures are seen in this sample. And the peak at 1040cm^{-1} is assigned as the second order Raman phonon.

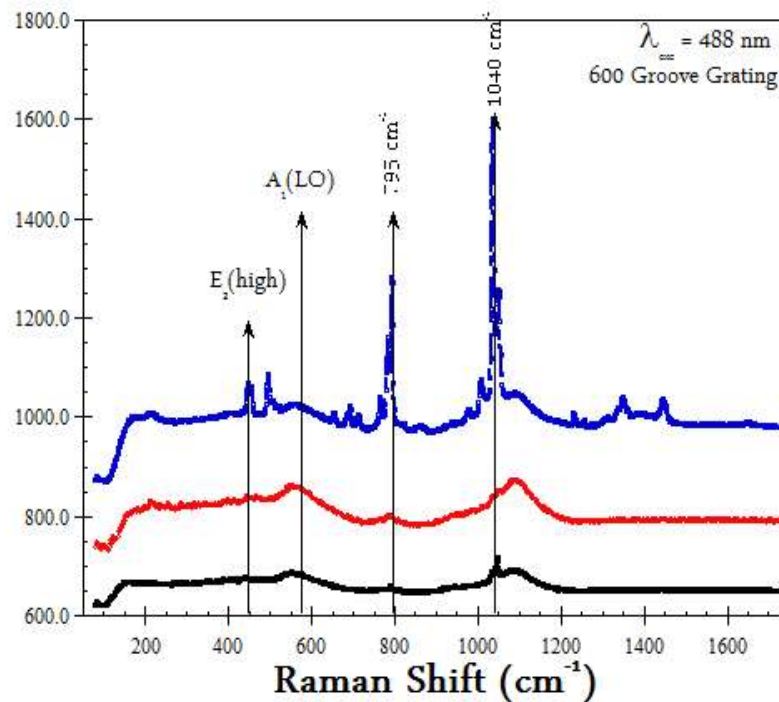


Figure 31: Raman spectrum of ZnO nanorods grown for 60 min, at 50% amplitude (black) glass substrate, (red) and (blue) ZnO at different spots.

5.6. Sample grown without seedlayer

Optical Microscopy

Figure 32 shows the optical image of ZnO nanorods grown in absence of the seedlayer. It can be seen that ZnO nanorods were randomly oriented on substrate due to the absence of the seedlayer.

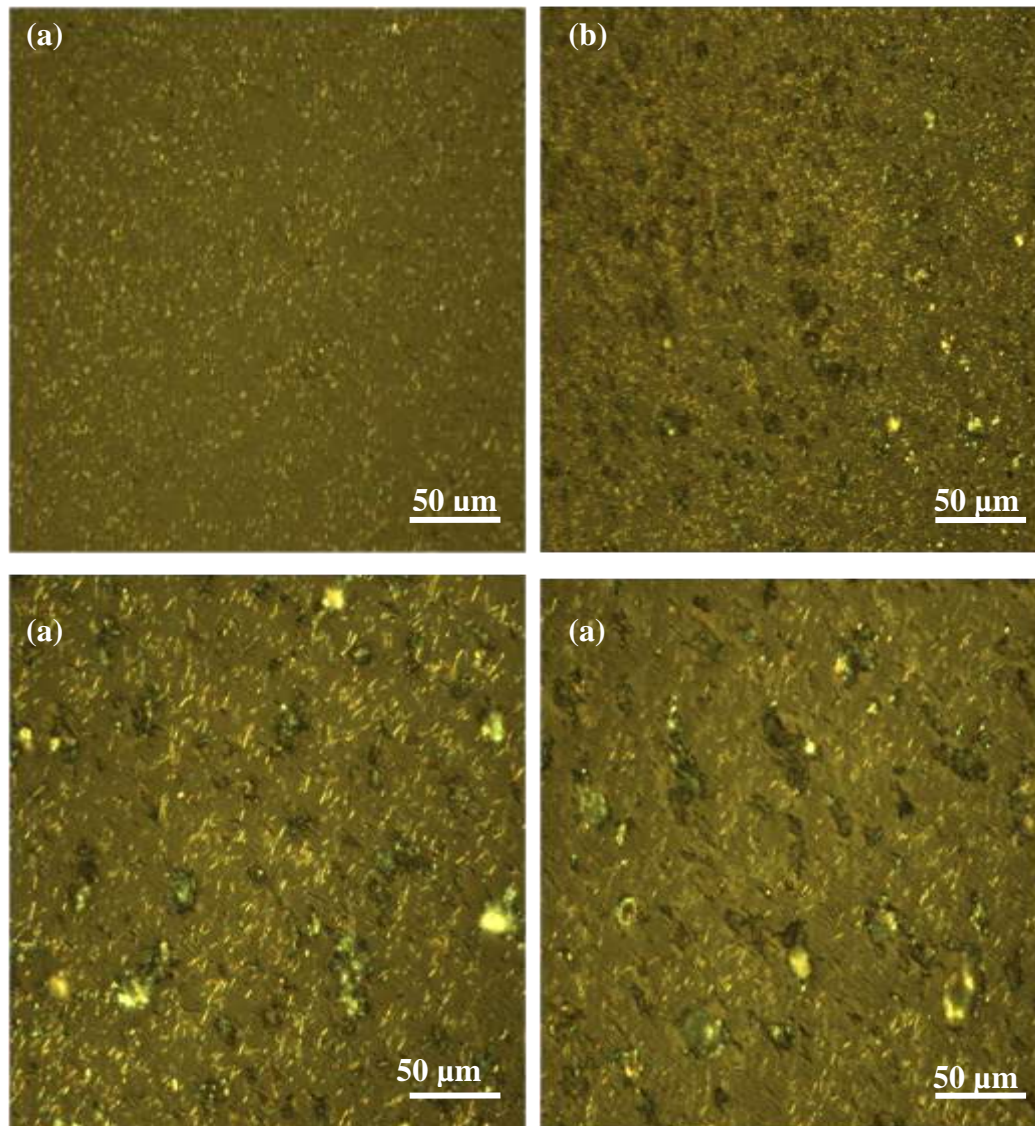


Figure 32: Optical image of ZnO nanorods grown without seedlayer for 60 min, at 50% amplitude taken with 50x magnification, (a) spot 1, (b) spot 2 and 100x magnification (c) spot 1, (d) spot 2.

SEM

Figure 33 shows the SEM image of ZnO nanorods grown directly on the substrate without the seedlayer. Randomly oriented ZnO nanorods were obtained in this sample fig.33(a). The ZnO nanorods were also found to be of irregular shape and size fig 33(b).

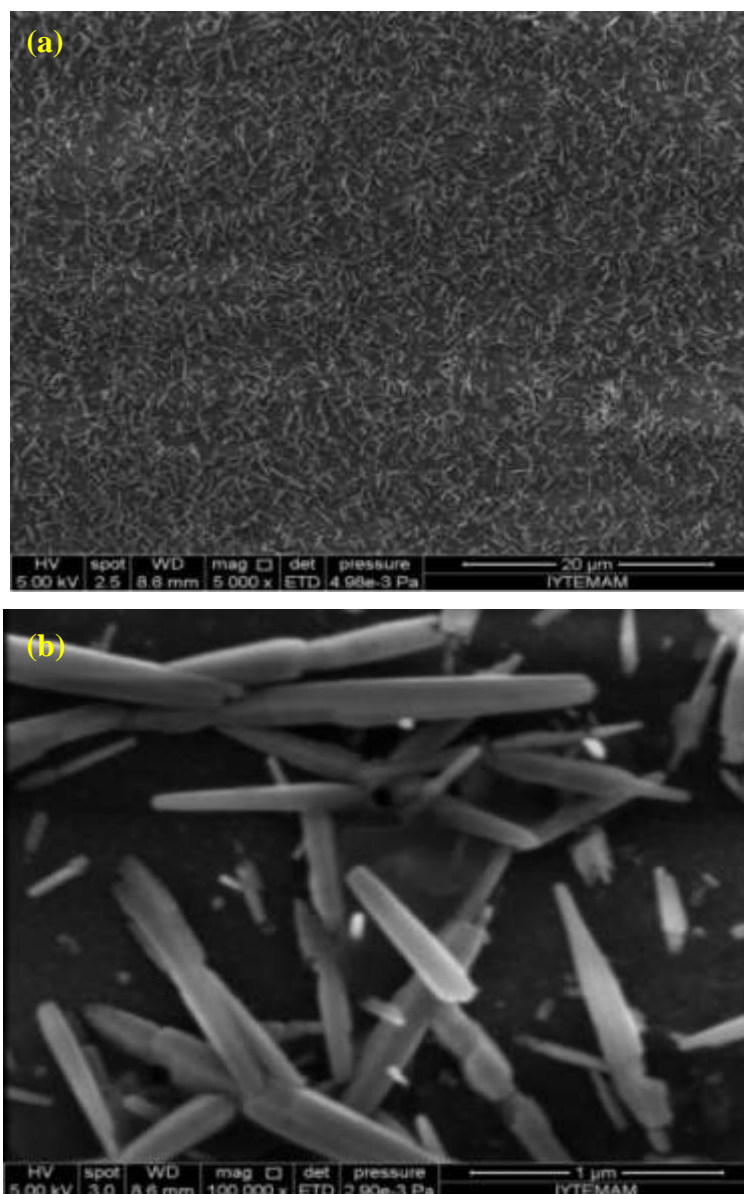


Figure 33: SEM images of ZnO nanorods grown in absence of seedlayer.(a) low resolution and (b) high resolution.

In this sample it can be concluded that the seedlayer plays a significant role in the formation of ZnO nanorods on substrate. Because of the lattice mismatch between the nanorods and the substrate, it is not easy for the ZnO nanorods to grow directly on the surface of

the substrate^[90]. Therefore, the seedlayer serves as the nucleation site for the ZnO nanorods.

It was also observed that the seedlayer directs the orientation and morphology of the ZnO nanorods as seen in fig. 33(b), the ZnO nanorods grown in the absence of seedlayer were of irregular shape and size.

5.7 Antibacterial Response

The two different bacterial strain; *Escherichia coli* MG 1655 a gram-negative bacterium and *Bacillus subtilis* 102 a gram-positive bacterium, showed different response to the three ZnO nanorods samples. This is indicated by the three different methods used to assessed the toxicity of the ZnO nanorods. However, in all the three methods, the ZnO nanorods-coated glass substrates showed greater toxicity compared to glass substrate which was used as a control sample.

5.7.1 Live/Dead assay

Figure 34 shows the fluorescence image of *B. subtilis* on the two ZnO nanorods samples, and the control sample. Images were taken after 2 h of incubation. Green fluorescence show the total number of bacterial cells on the substrate, while the red fluorescence show the number of damaged/dead bacterial cells. The results indicated that the number of bacteria on the two ZnO nanorods surfaces is higher than on the control sample. This could be due to nanotopographic surface generated by the nanorods, which might have allow the bacterial cells to adhere more to the surface. However, the numbers of dead cells are higher on the ZnO nanorods samples than the glass samples. The results also showed that the number of dead cells on ZnO nanorods grown continuously for 30 min was higher than on ZnO nanorods grown in two-cycle.

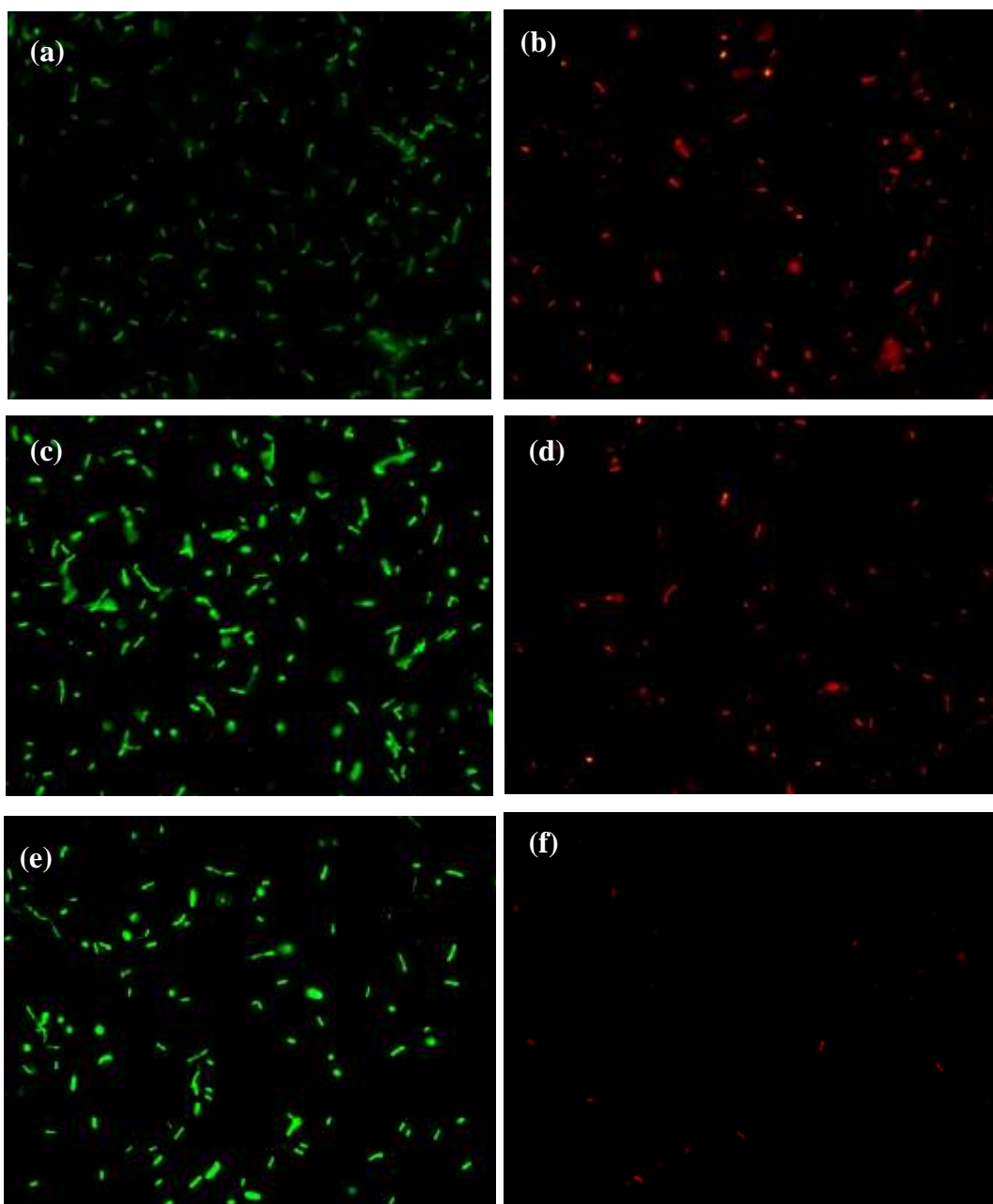


Figure 34: Fluorescence image of *B. subtilis* after 2 h of incubation. (a) total cells, (b) dead cells on ZnO nanorods grown for 30 min, at 50% amplitude, (c) total cells, (d) dead cells on ZnO nanorods grown in two-cycle at 50% amplitude, and (e) total cells, (f) dead cells on glass control.

Figure 35 shows the fluorescence images of *B. subtilis* on the two ZnO nanorods samples, and the control sample after 5 h incubation. This results also showed that the number of dead cells on the ZnO nanorods samples were higher than on control sample (fig.35f). It was observed that ZnO nanorods grown in two-cycle at 50% amplitude (fig.35d) has higher number of dead cells than on ZnO nanorods grown for 30 min at 50% amplitude (fig.35b).

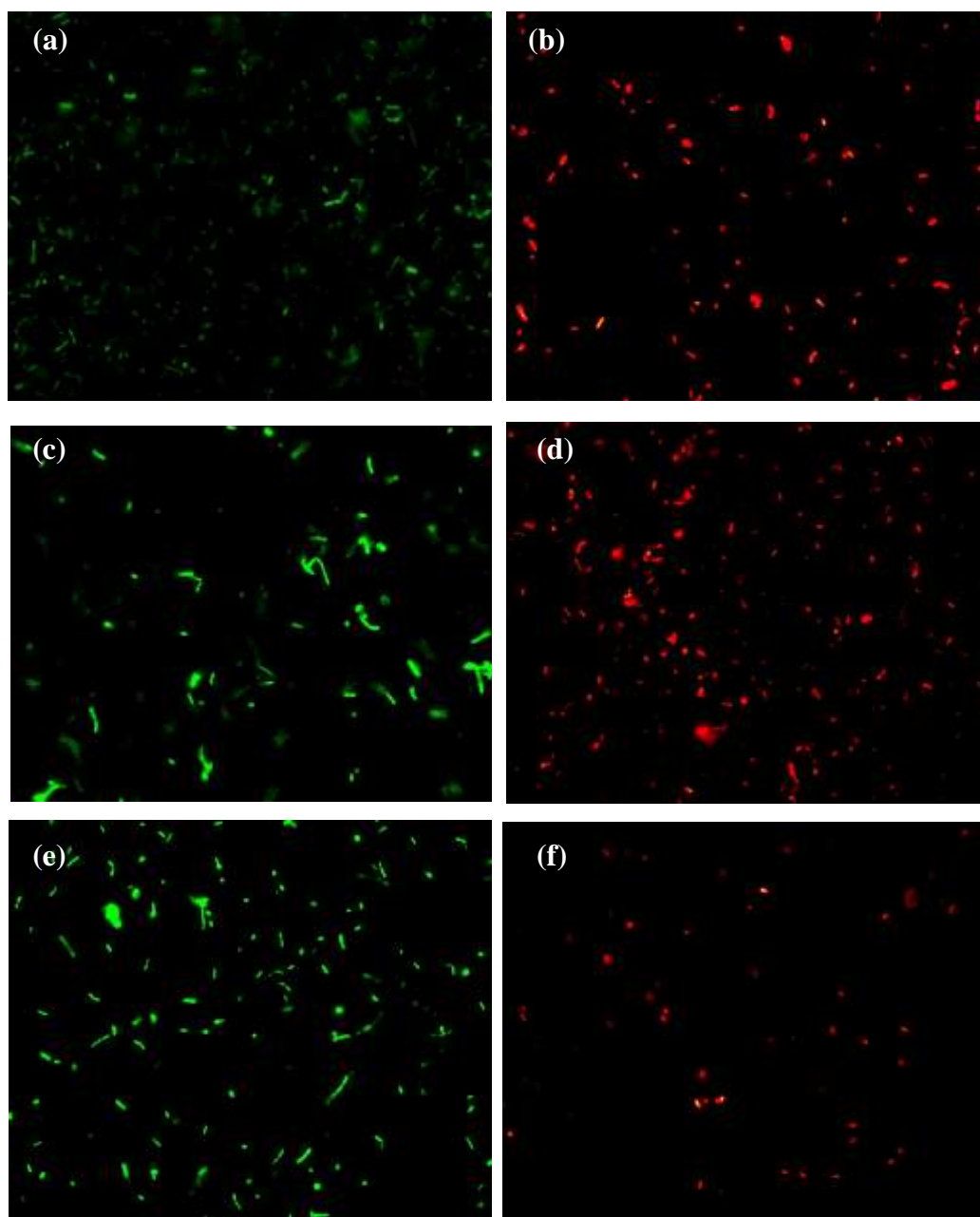


Figure 35: Fluorescence image of *B. subtilis* after 5 h of incubation. (a) total cells, (b) dead cells on ZnO nanorods grown for 30 min, at 50% amplitude, (c) total cells, (d) dead cells on ZnO nanorods grown in two-cycle at 50% amplitude, and (e) total cells, (f) dead cells on glass control.

Figure 36 shows the fluorescence images of *E. coli* on two ZnO nanorods coated samples, and glass substrate; the control sample. Images were taken after 2 h of incubation. It was observed that the number of dead cells on ZnO nanorods grown for 30 min at 50% amplitude fig.36(b) was higher than on ZnO nanorods grown in two-cycle at 50% amplitude fig.36(d), and the control sample fig.36(f) has least number of dead cells.

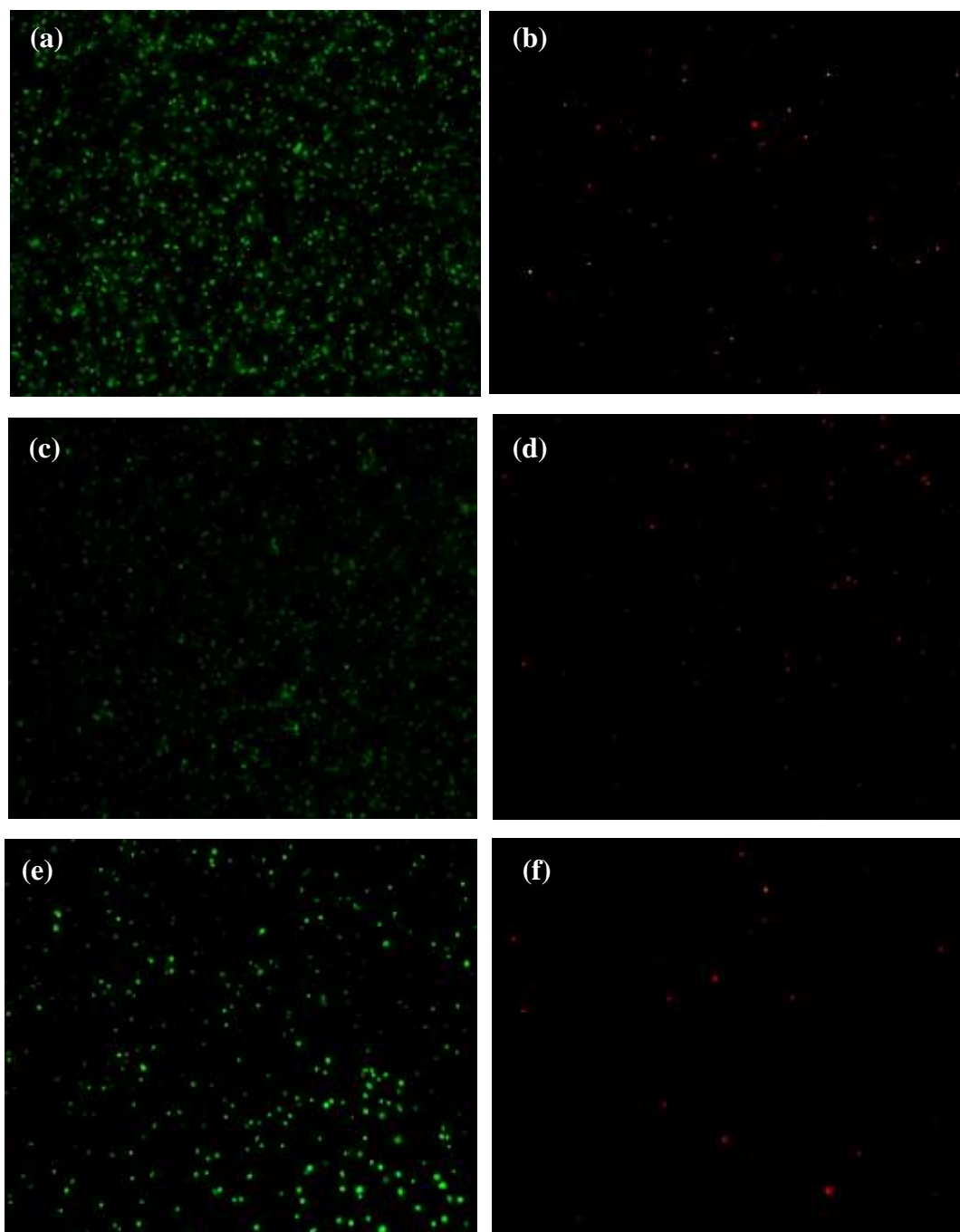


Figure 36: Fluorescence image of *E. coli* after 2 h of incubation. (a) total cells, (b) dead cells on ZnO nanorods grown for 30 min, at 50% amplitude, (c) total cells, (d) dead cells on ZnO nanorods grown in two-cycle at 50% amplitude, and (e) total cells, (f) dead cells on glass control.

Figure 37 shows the fluorescence images of *E. coli* on two ZnO nanorods samples, and control sample after 5 h incubation. This results also showed that the numbers of dead cells on the ZnO nanorods samples were higher than on control sample fig.37(f). It was also observed that ZnO nanorods grown for 30 min at 50% amplitude fig.37(b) has higher number of dead cells than on ZnO nanorods grown in two-cycle at 50% amplitude fig.37(d).

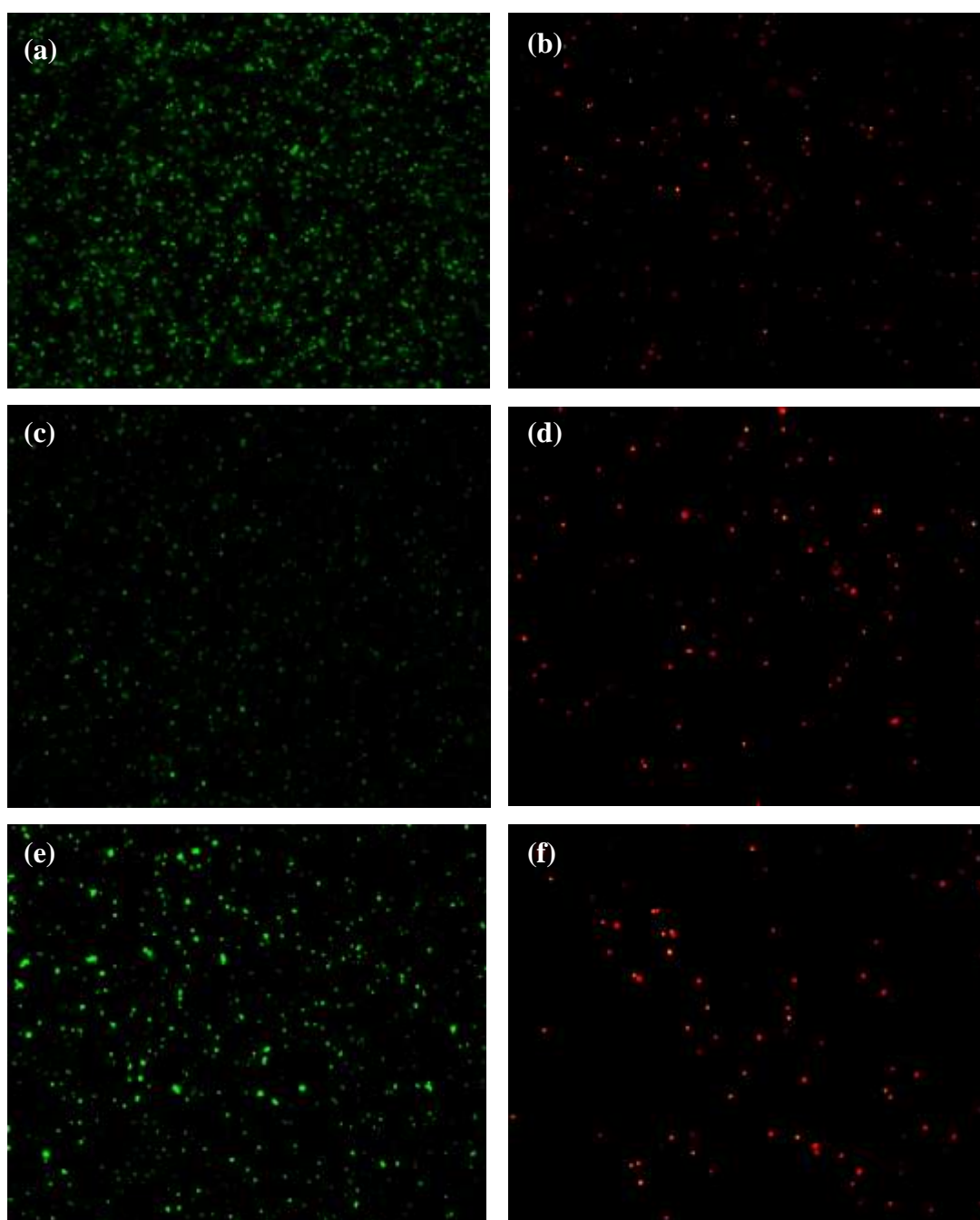


Figure 37: Fluorescence image of *E. coli* after 5 h of incubation. (a) total cells, (b) dead cells on ZnO nanorods grown for 30 min, at 50% amplitude, (c) total cells, (d) dead cells on ZnO nanorods grown in two-cycle at 50% amplitude, and (e) total cells, (f) dead cells on glass control.

Figure 38 shows the percentage of dead cells as a function of the two ZnO nanorods samples, for different time of incubation.

For *B. subtilis* it can be seen that over 50% of the cells were dead within the first 2h of incubation on sample1, which was a bit higher than sample2 with about 48% dead cells. However, the percentage of dead cells on both samples were higher than the glass substrate with only about 37% dead cells. As the incubation period increases from 2 h to 5 h, the reverse case was observed with sample2 showing greater toxicity having 80% of the cells dead. Nevertheless, the toxicity of sample1 increases as well with about 65% of the cells dead. This is more than the glass with about 57% of the cells dead. This indicated that the toxicity increases with increasing time of incubation in both the samples.

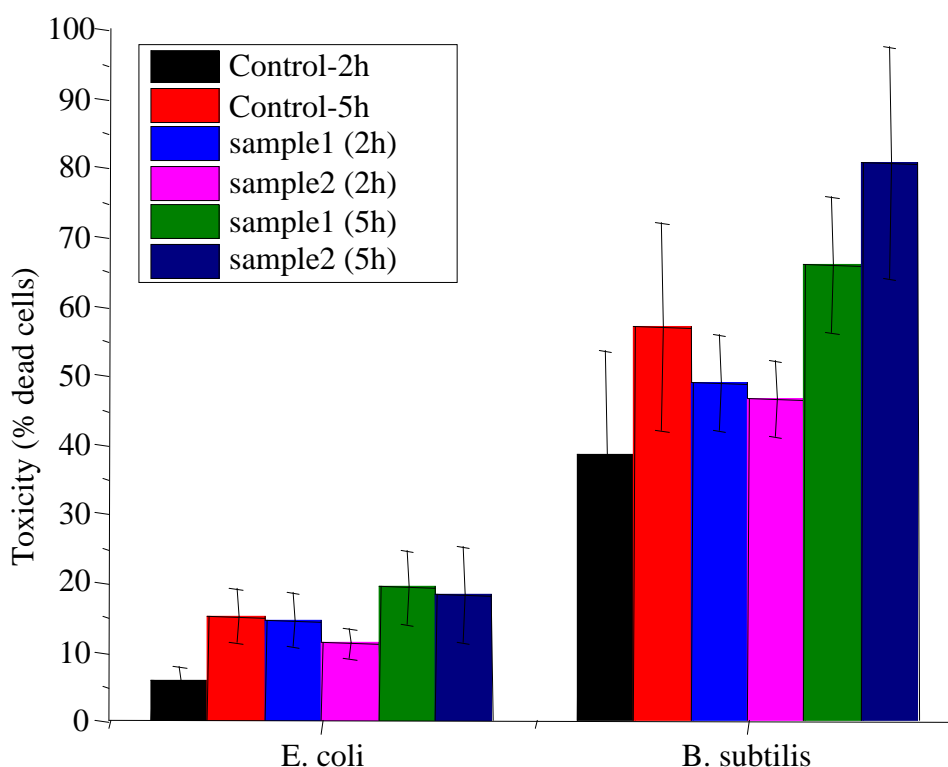


Figure 38: Toxicity of ZnO nanorods samples on *E. coli* and *B. subtilis* after 2 and 5 h of incubation.

For gram negative *E. coli*, level at which ZnO nanorods exhibited toxicity was not as profound as in the gram-positive *B. subtilis* in both 2 h and 5 h (fig.38). About 11% of the cells were found dead in the first 2 h of incubation on sample2, and the percentage was found to increase to about 20% after 5 h. The results indicated that sample1 was more toxic with about 15% dead cells at the first 2 h and 22% at 5 h of incubation. In contrast to both sample1 and sample2, the percentage of dead cells on glass was found to be 8% and 17% after 2 and 5 h incubation respectively. This indicates that the ZnO nanorods have shown antibacterial action on the bacterial cells.

5.7.2. Agar flipping test

Agar flipping test was further conducted to monitor the continuous growth of the bacterial cells in the presence of ZnO nanorods for a long period of time. Growth of cells was measured at both 24 and 48 h. It is worthy of note that ZnO nanorods-coated substrates greatly reduced the growth of bacterial cell compared to glass substrate(fig. 39). The continuous growth of bacterial cells follows the same trend as the toxicity test. The growth of *E. coli* in the 30 min continuously grown sample is less than the 15+15 min sample in both 24 and 48 h. The same with *B. subtilis* the 30 min continuously grown sample has less growth than the two-cycle 15+15 min sample during the 24 h incubation, but as the incubation period was extended to 48 h, two-cycle 15+15 sample has less growth. This indicated that there are other possible mechanism by which ZnO nanorods exhibited the antibacterial action.

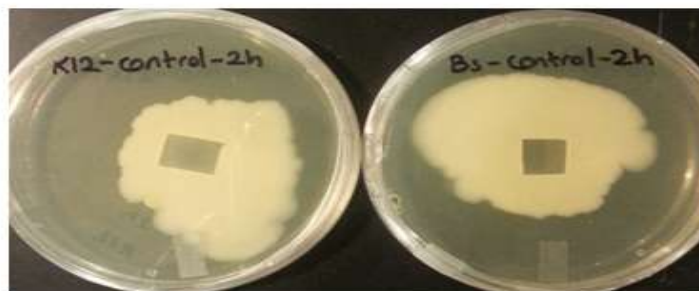
Figure 39 shows the growth of *B. subtilis* on agar plate with the control sample. Growth of cells was found to increase as the incubation period increases. The growth was observed to be higher in the control plates compared to the ZnO nanorods samples. This indicated that the ZnO nanorods have to a certain extent suppressed the growth of cells.



a) Control plates (2h) at time 0h



b) Control plates (2h) at time 24h



c) Control plates (2h) at time 48h

Figure 39: Digital image of agar flipping test of glass substrate. (a) 0 h, (b) 24 h, and (c) 48 h.

Figure 40 shows the growth of *B. subtilis* on agar plate in the presence of ZnO coated substrates. It can be seen that the growth of cells was less than that of the control which shows that the ZnO nanorods coated substrate have some cytotoxic effect on the bacterial cells by preventing cellular growth compared to the glass substrate.

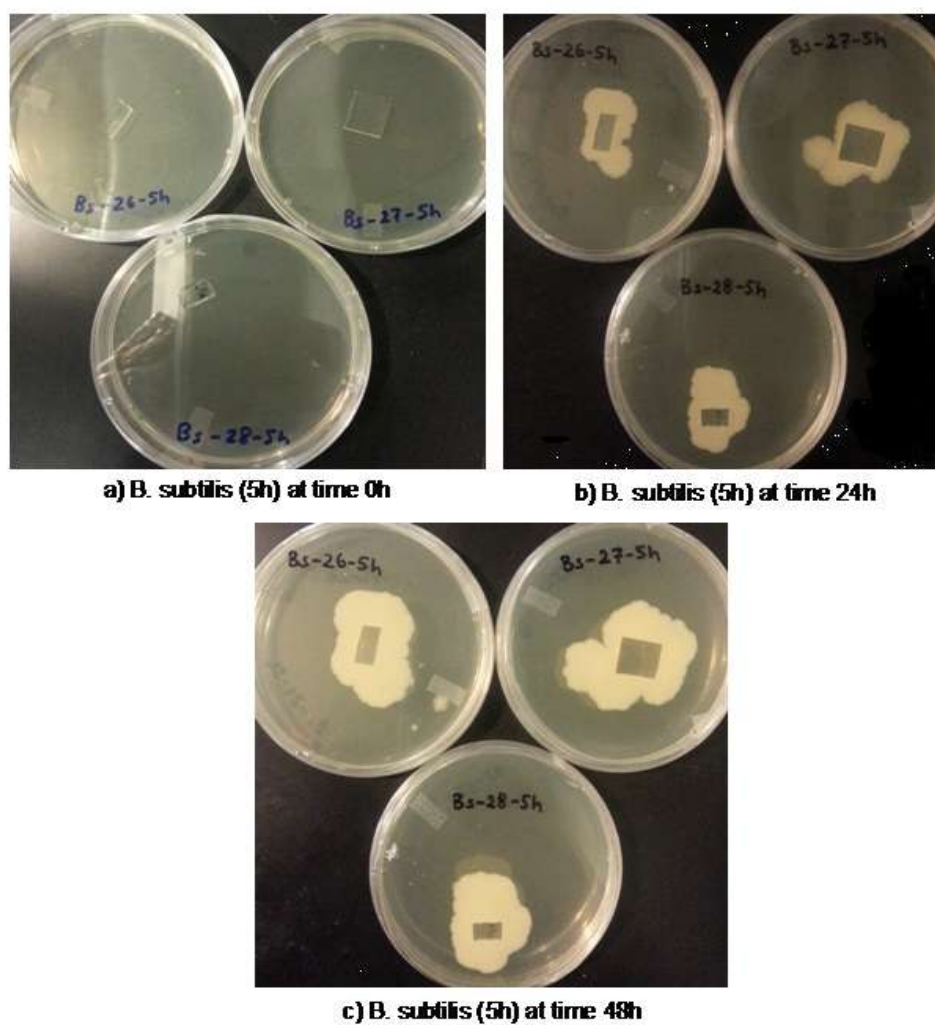


Figure 40: Digital image of agar flipping test of *B. subtilis* on ZnO nanorods substrate. (a) 0 h, (b) 24 h, and (c) 48 h.

Figure 41 shows the overall growth of cells on agar plate in the presence of ZnO nanorods. The growth of bacterial cells was found to be in correlation with the toxicity of the ZnO nanorods; the higher the toxicity, the less growth of cells observed.

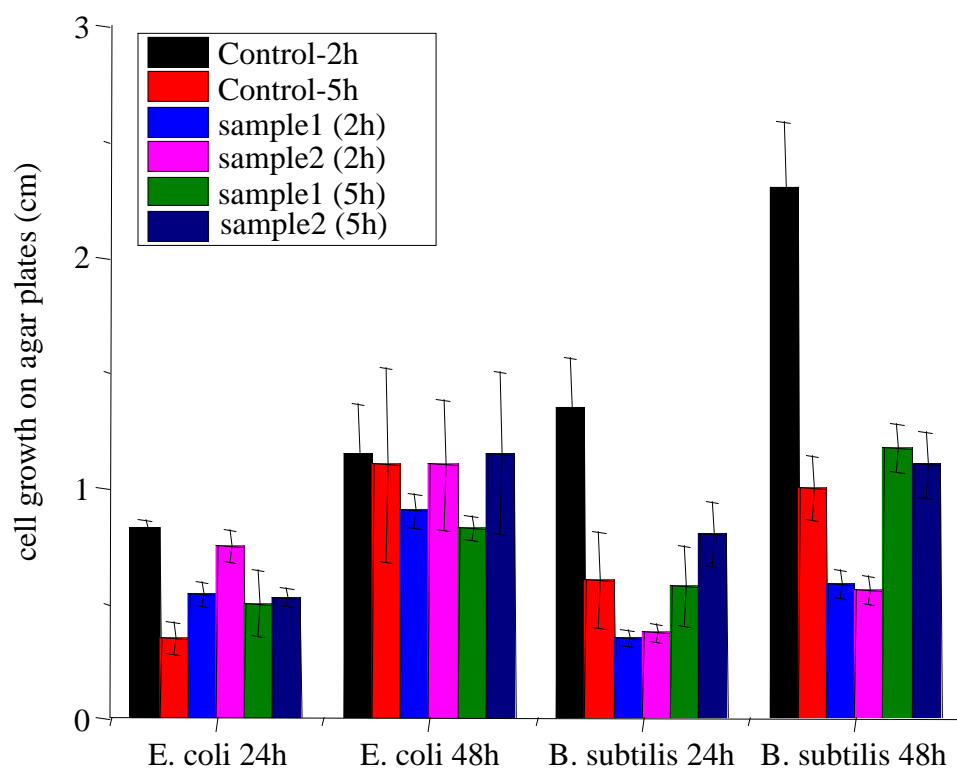


Figure 41: Growth zones of *E. coli* and *B. subtilis* measured on agar plate at different time intervals, for the two different ZnO nanorods samples.

5.7.3 Drop plate count

Figure 42 shows the percentage toxicity of sample sonicated for 60 min at 100% amplitude, using the drop plate count method. This sample was observed to exhibit the maximum antibacterial properties towards both *E.coli* and *B.subtilis* compared to other two samples. Over 90% of the bacterial cells were found dead even at 2 h incubation period. However, the highest antibacterial action was observed on *B.subtilis* at 5 h incubation period with no viable cell observed. The substrate grown under this condition was found to be densely coated with ZnO nanorods, this might have resulted in more ZnO nanorods penetrating bacterial cell, and/or release of more Zn^{2+} ions, thereby killing more bacterial cells.

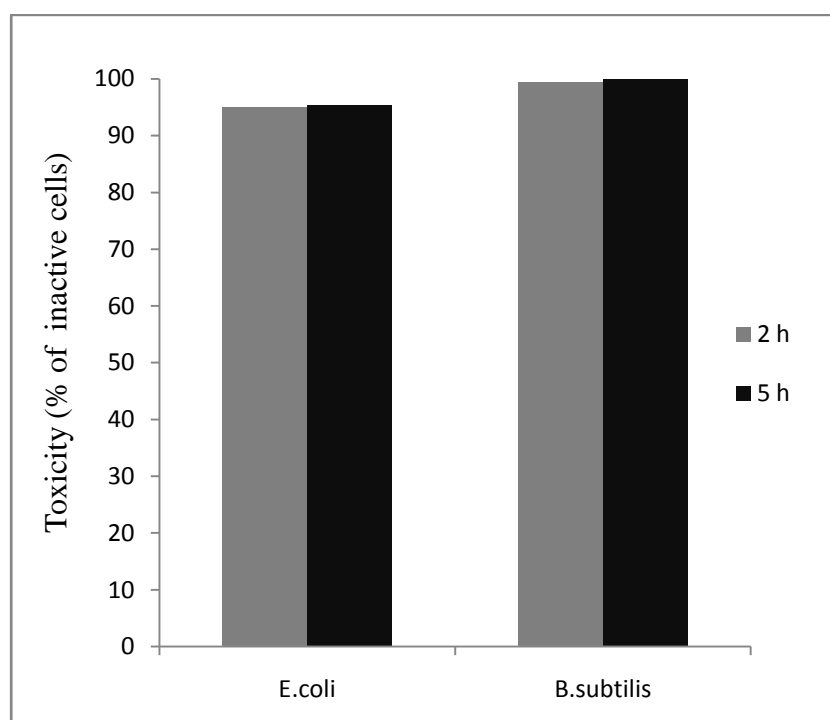


Figure 42: Percentage toxicity of sample 4 on *E.coli* and *B.subtilis* after 2 and 5 h incubation.

Figure 43 shows the SEM image of *E.coli* on glass and ZnO nanorods substrates after 48 h incubation. Damage of bacterial cells was observed on the ZnO nanorods (b), which indicates the toxicity of the ZnO nanorods towards the bacterial cells compared to the glass substrate(a).

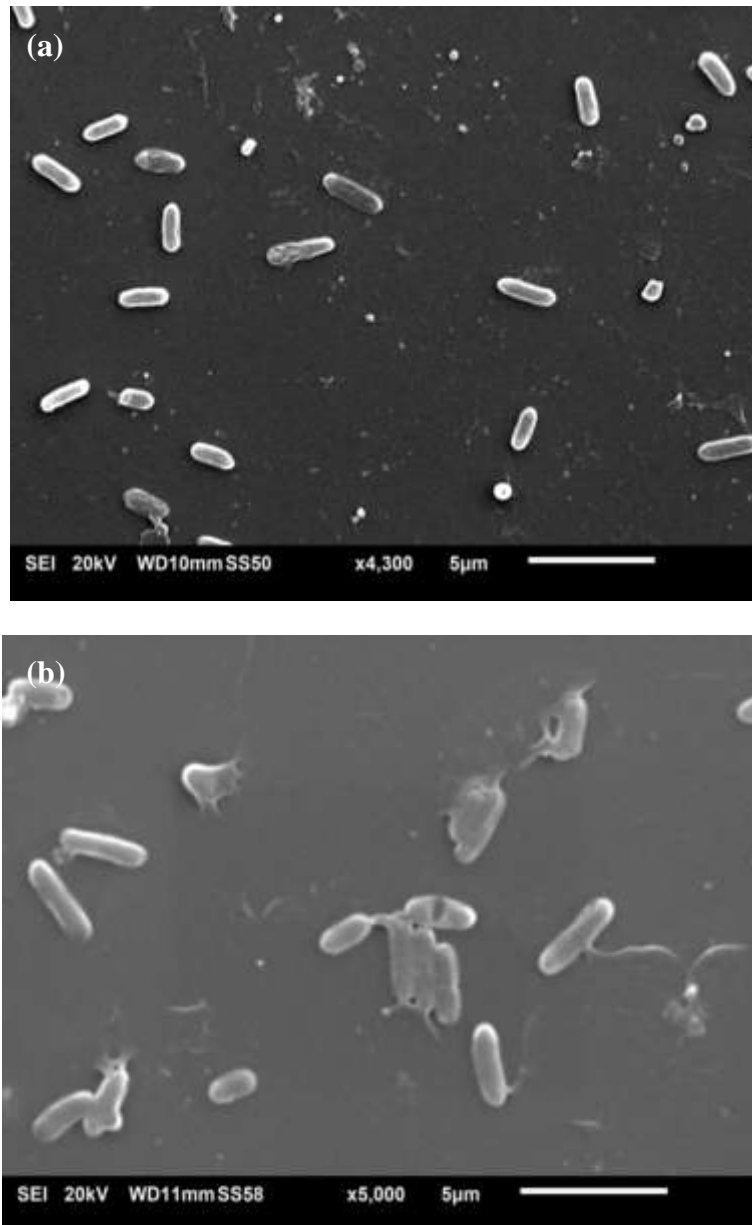


Figure 43: SEM image of *E.coli* after 48 h incubation on (a) glass control (b) ZnO nanorods.

Figure 44 shows the SEM image of *B.subtilis* on (a) glass and (b) ZnO nanorods substrates. It can be seen that bacterial cells on the ZnO nanorods substrate were damaged compared to those on glass substrate. This indicates the toxicity of the ZnO nanorods towards the bacterial cells.

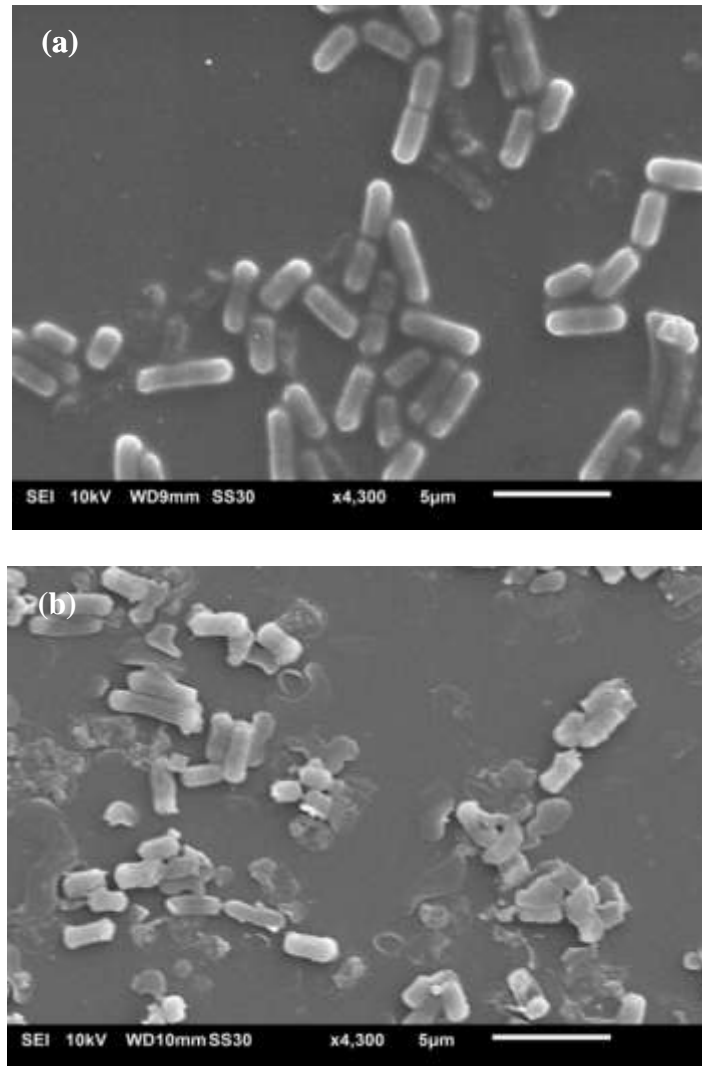


Figure 44: SEM image of *B.subtilis* after 48 h incubation (a) glass control (b) ZnO nanorods

CONCLUSION

ZnO nanorods of various size were synthesized by sonochemical method. It was found that the sonication period and the amplitude play an essential role in the growth of ZnO nanorods on substrate. The long sonication period at the maximum amplitude produced the best result, with ZnO nanorods densely grown on the substrate.

The antibacterial properties of the sonochemically synthesized ZnO nanorods toward *E.coli* and *B.subtilis* was investigated. It was found that the sample sonicated for long period at the maximum amplitude exhibited the highest antibacterial properties, compared to the two other samples that were grown for 30 min at 50% amplitude. The number of dead cells was found to be over 90% for the gram-negative *E.coli* cells at both 2 and 5 h of incubation, this is ~4.5-fold more than the 30 min continuously grown sample, and ~5-fold more than the 15 min two-cycle grown sample. The gram-positive *B.subtilis* showed the maximum susceptibility with 100% death of cells. However, this is just ~1.5-fold more than the 30 min continuously grown sample, and 1.2-fold more than the 15 min two-cycle grown sample.

The exact mechanism of antibacterial activity of ZnO nanostructures still remain a debating topic among researchers. Many believed the generation of reactive oxygen species by ZnO nanostructures to be one of the major mechanism by which ZnO can induce the death of the cell, other proposed mechanisms include release of Zn^{2+} from the dissolution of ZnO in moist environment which damage the bacterial cell wall, penetration of the bacterial cell wall is also considered to be another mechanism by which ZnO damage the bacterial cell and causes its death^[34, 36, 37, 91].

In this thesis, It can be concluded that the antibacterial mechanism of the sonochemically grown ZnO nanorods could be due disruption of bacterial cell wall by the ZnO nanorods as indicated by the SEM images (fig.43, 44) Possible release of Zn^{2+} ions from the slow dissolution of ZnO which penetrate the cell membrane and interfere with the homeostasis of the cell or cause a prolonged lag phase of the growth cycle can also be considered another factor for the antibacterial activity of the prepared ZnO nanorods^[92]. It was also found that the antibacterial properties of the ZnO nanorods increase with increasing time of incubation (fig.40-42).

The overall results show that the ZnO nanorods exhibited higher toxicity towards *B. subtilis* than *E.coli*. This is not different with results obtained in previous findings, with gram-positive bacteria being more susceptible than the gram-negative bacteria. This is

attributed to their cell wall structural differences, so may have interact differently with the ZnO nanorods through Van der Waals and electrostatic interaction^[34, 36, 37]. Moreover, gram-negative bacteria are more resistant to antibiotic than gram-positive bacteria. This might have allow *E.coli* to resist attack by the ZnO nanorods under this experimental condition. The results also indicated that the antibacterial effect of ZnO nanorods was bactericidal; killing the bacteria, rather than bacteriostatic, as it does not prevent the adherence of bacteria.

6. FUTURE WORK

Based on the findings from this study, for wide range of potential application of ZnO nanostructures in the biomedical field, the following future work could be done:

- ❖ Synthesis of ZnO nanorods on different substrates including polymers for various biological application.
- ❖ Investigation of the antibacterial effect of ZnO nanorods against other bacterial strains, especially the pathogenic strains.
- ❖ Investigation of the detail mechanism of antibacterial action of ZnO nanorods.
- ❖ Investigation of the interaction of ZnO nanorods with human cells
- ❖ Investigation of the possible toxicity of ZnO nanorods towards cancer cells.
- ❖ Explore the possibility of sonochemical method in the synthesis of nanostructures of other metal oxide semiconductores .

REFERENCES

1. McNeil, S.E., *Nanotechnology for the biologist*. Journal of Leukocyte Biology, 2005. **78**: p. 585.
2. Wang, Z.L., *Zinc oxide nanostructures growth, properties, and applications*. . Journal of Phy. Condensed matt., 2004. **16**, : p. 829-858.
3. Hou, T.-N., Yamada, T., Nguyen, P., Chen, Y. and Meyappan, M.. . , *Single crystal nanowire vertical surround gate field effect transistor*. Nano letters. , 2004. **4**(2): p. 1247-1252.
4. Lupan, O., Chow, L., Chai, G., Chernyak L., Tirpak, O. L., and Heinrich, H. , *Focused- ion beam fabrication of ZnO nanorod-based UV photo detector using in-situ lift- out technique*. Physica Status, Solidi(a) 2008. **205**(11): p. 2673-2678.
5. Chang, S.J., Hsueh, T. J., Chen, I. C., and Huang, B. R. , *Highly sensitive ZnO nanowire CO sensor with adsorption of Au nanoparticle*. . Nanotechnology,, 2008. **19**: p. 175502.
6. Fulati, A., Ali, S. U., Asif, M. H., Alvi, N. H., Willander, M., Brannmark, C., Stralfors, P., Borjesson, S. I., Elinder, F. and Danielsson, B. , *An intracellular glucose biosensor based on nanoflakes ZnO*. Sensors and Actuators B, 2010. **150**: p. 673-680.
7. Liao, L., Lu, H. B., Shuai, M., Li, J. C., Liu, Y. L., Liu, Z., Shen, Z. X., and Yu, T., *A novel gas sensor based on field ionization from ZnO nanowires; moderate working voltage and high stability*. Nanotechnology, 2008. **19**: p. 1775501.
8. Menzel, A., et al., *Multifunctional ZnO-Nanowire-Based Sensor*. Advanced Functional Materials, 2011. **21**(22): p. 4342-4348.
9. Wu, J.J., Wen, H. I., Tseng, C. H., Liu, S. C. , *Well-aligned ZnO nanorods via hydrogen treatment of ZnO films*. Adv. Funct. Mater, 2004. **14**: p. 806–810.
10. Heo, Y.W., Varadarajan, V., Kaufman, M., Kim, K., Norton, D. P., Ren, F., Fleming, P. H., *Site-specific growth of ZnO nanorods using catalysis-driven molecular-beam epitaxy*. Appl.Phys. Lett. , 2002. **81**: p. 3046–3048.
11. Wang, Z.L., *Nanobelts, Nanowires and Nanodiskettes of semiconducting oxides; From materials to nanodevices*. Advance materials, 2003. **15**: p. 5.
12. Yuan, H., Zhang, Y. and *Preparation of well-aligned ZnO whiskers on glass substrate by atmospheric MOCVD*. . J. Cryst. Growth, 2004. **263**: p. 119–124.
13. Sun, Y., Fuge, G. M., Ashfold, M. N. R., *Growth of aligned ZnO nanorod arrays by catalyst-free pulsed laser deposition methods*. Chem. Phys. Lett, 2004. **396**: p. 21–26.
14. D. Polsongkram, P. Chamninok S. Pukird L. Chow, O. Lupan and H.K. G. Chai , S. Park , A. Schulte *Effect of synthesis conditions on the growth of ZnO nanorods via hydrothermal method*. physica B, 2008. **403**: p. 3713-3717.
15. Roosjen, A., Hans J. K., Henny C. V., Willem N., and Henk J. B., *Inhibition of yeast and bacteria by poly(ethylene oxide)-brushes on glass in parallel plate flow chamber*. microbiology, 2003. **149**: p. 3229-3246.
16. Gottenbos, B., Dirk, W. G., Henny C. V., Jan, F., and Henk J. B, *Antimicrobial effects of positively charged surfaces on adhering gram-positive and gram-negative bacteria*. Journal of antimicrobial chemotherapy, 2011. **48**: p. 7-13.
17. Vaseem, M., Umar, A. and Hahn, Y-B., *ZnO Nanoparticles: Growth, Properties, and Applications*, in *Metal Oxide Nanostructures and Their Applications*, A.a.H. Umar, Y-B., Editor. 2010, American Scientific Publishers. p. 1–36.

18. Hernandezbattez, A.G., Viesca, R., Fernandez, J., Diazfernandez, J., MacHado, J., Chou, A., Riba, R., *CuO, ZrO₂ and ZnO nanoparticles as anti wear additive in oil lubricants*. *Wear* 2008. **265**(422): p. 3–4.
19. Mitchnick, M.A., Fairhurst, D., Pinnell, S.R., *Microfine zinc oxide (Z-cote) as a photostable UVA/UVB sunblock agent*. *Journal of the American Academy of Dermatology*, 1999. **40**(1): p. 85–90.
20. Liu, T.-Y., Liao, H-C., Ling, C-C., Hu, S-S. and Chen, S-Y., *Immobilization of protein on arrayed ZnO nanorods grown on thermoplastic polyurethane(TPU) substrate for biomedical application*. *Langmuir*, 2006. **22**: p. 5804-5809. .
21. wikipedia. *zinc_oxide*. [cited 2013 23 Sept].
22. Zhou L., R., Y., Min, Y., Fan, B., Cheng, L. and Wang, Z. L., *Cellular Level Biocompatibility and Biosafety of ZnO Nanowires*. *J. Phys. Chem. C*, 2008. **112**: p. 51.
23. Jan, T., Iqbal, J., Ismail, M., Zakaullah, M., Naqvi, S. H. and Badshah, N., *Sn doping induced enhancement in the activity of ZnO nanostructures against antibiotic resistant S. aureus bacteria*. *International Journal of Nanomedicine*, 2013. **8**: p. 3679-3687.
24. Gopikrishnan, R., Zhang, K., Ravichandran,P., Baluchamy, S., Ramesh, V., Biradar, S., Ramesh, P., Pradhan,J., Hall, J. C., Pradhan, A. K. and Ramesh, G. T. , *Synthesis, characterization and biocompatibility of ZnO nanorods for biomedical application*. . *Nano-Micro letters* 2010. **2**(1): p. 31-36.
25. Yin, Y., Lin, Q., Sun, H., Chen, D., Wu, Q., Chen, X. and Li, S., *Cytotoxic effects of ZnO hierarchical architectures on RSC96 Schwann cells*. *Nanoscale Research Letters*, 2012. **7**: p. 439.
26. Ciofani, G., Genchi, G.G., and Mattoli, V. , *ZnO nanowire arrays as a substrate for cell proliferation and differentiation*. *Mater. Science and Engineering C* 2012. **32**: p. 431-347.
27. Akhtar, M.J., Ahamed, M., Kumar, S., Khan, M. M., Ahmad, J. and Alrokayan, S. A., *Zinc oxide nanoparticles selectively induce apoptosis in human cancer cells through reactive oxygen species*. *International Journal of Nanomedicine*, 2012. **7**: p. 845-857.
28. Reddy, K.M., Feris, K., Bell, J., Wingett, D. G., Hanley, C. and Punnoose, A., *Selective toxicity of zinc oxide nanoparticles to prokaryotic and eukaryotic systems*. *Appl. Phys. Lett.*, 2007. **90**: p. 213902.
29. Agren, M.S.a.M., U. , *The release of zinc ions from and cytocompatibility of two zinc oxide dressings*. *Journal of Wound Care*, 2004. **13**(9): p. 367-369.
30. Zhang, L., Jiang, Y., Ding, Y., Povey, M., York, D., *Investigation into the antibacterial behaviour of suspensions of ZnO nanoparticles (ZnO nanofluids)*. *J. of Nanoparticle Research*, 2007. **9**(3): p. 479-489.
31. Hu, X., Cook, S., Wang, P. and Hwang, H-M. , *Invitro evaluation of cytotoxicity of engineered metal oxide nanoparticles*. . *Sci. total Environ.* , 2009. **407**: p. 3070-3072. .
32. Toolabi, A., Zare, M. R., Rahmani, A., Hoseinzadeh, E., Sarkhosh, M. and Zare, M., *Investigating Toxicity and Antibacterial Aspects of Nano ZnO, TiO₂ and CuO with Four Bacterial Species*. *J. Basic. Appl. Sci. Res.*, 2013. **3**(2): p. 221-226.
33. Adams, K.L., Lyon, Y. D. and Alvarez, P. J., *Comparative eco-toxicity of nanoscale TiO₂, SiO₂, and ZnO water suspensions*. *Water Research*, 2006. **40**: p. 3527-3532.
34. Jaisai, M., Baruah, S., and Dutta, J. , *Paper modified with ZnO nanorods – antimicrobial studies*. *Journal of Nanotechnol.*, 2012. **3**: p. 684–691.

35. Chitra, K.a.A., G., *Antimicrobial activity of wet chemically engineered spherical shaped ZnO nanoparticles on food borne pathogen*. International Food Research Journal, 2013. **20**(1): p. 59-64.
36. Subhasree, R.S., Selvakumar, D., Kumar, N. S. , *Hydrothermally mediated synthesis of ZnO nanorods and their antibacterial properties*. Letters in Applied Nano-bio science, 2012. **1**(1).
37. Jansson, T., Clare-Salzler, Z.J., Zaveri, T. D., Mehta, S., Dolgova, N. V., Chu, B., Ren, F., and Kesolowsky, B. G. , *Antibacterial effect of Zinc oxide nanorods surfaces*. . Journal of nanoscience and nanotech, 2012. **12**: p. 7132-7138.
38. Singh, G., Joyce, E. M., Beddow, J., and Mason, T. J. , *evaluation of antibacterial activity of zno nanoparticles coated sonochemically onto textile fabrics*. . Journal of Microbio. Biotech. and Food Sciences. , 2012. **2**(1): p. 106-120.
39. Servinc, B.A.a.H., L. , *Antibacterial activity of dental composites containing ZnO nanoparticles*. Wiley inter sci. , 2010.
40. Xie, Y., He, Y., Irwin, P. L., Jin,T. and Shi, X., *Antibacterial Activity and Mechanism of Action of Zinc Oxide Nanoparticles against Campylobacter jejuni*. . Applied and Environmental Microbiology., 2011. **77**(7): p. 2325-2331.
41. Rajendran, R., Balakumar, C., Ahammed, A.H., Jayakumar, S., Vaideki, K. and E.M. and Rajesh, *Use of zinc oxide nano particles for production of antimicrobial textiles*. International Journal of Engineering, Science and Technology, 2010. **2**(1): p. 202-208
42. ASHE, B., *A Detail investigation to observe the effect of zinc oxide and Silver nanoparticles in biological system.*, in *Biotechnology and Medical Engineering2011*, National Institute Of Technology Rourkela-769008, Orissa, India. p. 110.
43. Ramani, M., Ponnusamy, S., Muthamizchelvan, C., Cullen, J., Krishnamurthy, S. and Marsili, E., *Morphology-directed synthesis of ZnO nanostructures and their antibacterial activity*. Colloids and Surfaces B: Biointerfaces, 2013. **105**: p. 24– 30.
44. Li, S.Y., Lee, C. Y. and Tseng, Y. T.(2003). , *Copper-catalyzed ZnO nanowires on silicon (1 0 0) grown by vapor–liquid–solid process*. . Journal of Crystal Growth, 2003(247): p. 357–362. .
45. Fan, J.C., Sreekanth, K.M., Xie, Z., Chang, S.L. and Rao, K.V., *p-Type ZnO materials: Theory, growth, properties and devices*. Progress in Materials Science., 2013. **58**: p. 874–985.
46. Liua, Z.W., Ong, C. K., Yu, T. and Shen, Z. X. , *Catalyst-free pulsed-laser-deposited ZnO nanorods and their room temperature photoluminescence properties*. Applied Physics letters, 2006. **88**: p. 053110.
47. DongQi, Y., Zhong, H. L., Jiao, L., Hao, H. Qiu, Z. H., Andy, S. L., Xi, C., Qiang, F., and ShuangShuang, Q., *Self-catalyst synthesis of aligned ZnO nanorods by pulsed laser deposition*. Science in China Series G : Physics, Mechanics & Astronomy, 2009. **52**(2): p. 207-211.
48. Fujita, M., Kawamoto, N., Tatsumi, T., Yamagishi, K. and Horikoshi, Y., *Molecular Beam Epitaxial Growth of ZnO on Si Substrate Using Ozone as an Oxygen Source*. Jpn. J. Appl. Phys. , 2003. **42**: p. 67-70.
49. Andrew, R.B., *Molecular Beam Epitaxy*. Connexions module:, 2009. **m25712**.

50. Chang, P., Fan, Z., Tseng, W., Wang, D., Chiou, W., Hong, J. and Lu, J. G. . , *ZnO Nanowires Synthesized by Vapor Trapping CVD Method*. Chemistry of Materials, 2004. **16**: p. 5133.
51. O. Lupan, G.A.E., V.V. Ursaki, G. Chai, A.N. Redkin, A.N. Gruzintsev, I.M. Tiginyanu, L. Chow, L.K. Ono, B. Roldan Cuenya, H. Heinrich, E.E. Yakimov. , *Synthesis and characterization of ZnO nanowires for nanosensor applications*. Materials Research Bulletin 2010. **45**: p. 1026–1032.
52. Park, S.-S., Lee, J.-M., Kim, S.-J., and Kim S.-W. , *Catalyst-free synthesis of ZnO nanorods by CVD*. Journal of the Korean physical society., 2008. **53**(1): p. 183-187.
53. Bekermann, D., Gasparotto, A., Barreca, D., Bovo, L., Devi, A., Fischer, R. A., Lebedev, O. I., Maccato, C., Tondello, E. and Tendeloo, G. V., *Highly Oriented ZnO Nanorod Arrays by a Novel Plasma Chemical Vapor Deposition Process*. Crystal Growth & Design., 2010. **10**(4): p. 2011-2018.
54. Liu, X., Wu, X., Cao, H. and Chang, R. P. H., *Growth mechanism and properties of ZnO nanorods synthesized by plasma-enhanced chemical vapor deposition*. Journal of applied physics, 2004. **9**(6): p. 3141-3147.
55. Kim, K.S.a.K., H. W., *Synthesis of ZnO nanorod on bare Si substrate using metal organic chemical vapor deposition*. Physica B: Condensed Matter, 2003. **328**(3-4): p. 368-371.
56. Liu, S.-C.a.W., J.-J., *Growth of Highly Oriented ZnO Nanorods by Chemical Vapor Deposition*. Material Research Society 2002. **703**.
57. Devaramani, B.S., Ramaswamy, Y. S., Manjasetty, B. A. and Gopalakrishin-Nair, T. R. , *The novelty of synthesis and varied applications of ZnO nanosystems*. Int. Conf. on frontiers in chemical research (ICFCR). 2008.
58. Zhitao, H., Sisi, L., Jinkui, C. and Yong, C., *Controlled growth of well-aligned ZnO nanowire arrays using the improved hydrothermal method*. Journal of Semiconductors, 2013. **34**(6): p. 063002-1-6.
59. Suslick, K.S., *Sonochemistry*. Science 1990. **247**: p. 1439-1445.
60. Suslick, K.S., *Sonochemistry*. Kirk-Othmer Encyclopaedia of Chemical Technology, 1998. **26**: p. 517-541.
61. Bang, J.H. and K.S. Suslick, *Applications of ultrasound to the synthesis of nanostructured materials*. Adv Mater, 2010. **22**(10): p. 1039-59.
62. Roshan, A.H., Kazemzadeh, S. M., Vaezi M. R. and Shokuhfar, A., *The effect of sonication power on the sonochemical synthesis of titania nanoparticles*. Journal of Ceramic Processing Research., 2011. **12**(3): p. 299-303.
63. Pholnak, C., Sirisathikul, C., Suwanboon, S. and Harding, D. J., *Effects of Precursor Concentration and Reaction Time on Sonochemically Synthesized ZnO Nanoparticles*. Material Research, 2013.
64. Azadeh, A., Amin, A. M. and Ali, M. , *Sonochemically assisted synthesis of ZnO nanoparticles; A novel direct method*. Iran J. Chem. Chem. Eng. , 2011. **30**: p. 3.
65. Jung, S.-H., Oh, E., Lee, K.-H., Jeong, S.-H., Yang, Y. and Park, C. G. , *Fabrication of Diameter-tunable Well-aligned ZnO Nanorod Arrays via a Sonochemical Route*. Bulletin of the Korean Chemical Society, 2007. **28**(9): p. 1457.
66. Oh, E.a.J., S.-H. , *Sonochemical Method for Fabricating a High-performance ZnO Nanorod Sensor for CO Gas Detection*. Journal of the Korean physical society., 2011. **59**(1): p. 8-11. .
67. Vabbina, P.K., Nayyar, P., Nayak, A. P., Katzenmeyer, A.M., Logeeswaran V.J., Pala, N., Saif Islam, M. and Talin A.A. , *Synthesis of Crystalline ZnO*

- Nanostructures on Arbitrary Substrates at Ambient Conditions*. Proc. of SPIE 2010. **8106 81060H-1**.
68. Goswami, S.K., Lee, B. W., and Eunsoon, O., *Effect of Precursors on Optical and Structural Properties of ZnO Nanorods Synthesized by Sonochemical Method*. . Journal of the Korean Physical Society 2011. **59**(3): p. 2313-2317.
 69. Rusli, N., et al., *Growth of High-Density Zinc Oxide Nanorods on Porous Silicon by Thermal Evaporation*. Materials, 2012. **5**(12): p. 2817-2832.
 70. Das, S.N., Kar, J. P., Xiong, J. and Myoung, J-M., *Synthesis of ZnO Nanowire by MOCVD Technique: Effect of Substrate and Growth Parameter*. Nanotechnology and Nanomaterial, 2012.
 71. Liu, X., Wu, X., Cao, H. and Chang R. P. H., *Growth mechanism and properties of ZnO nanorods synthesized by plasma-enhanced chemical vapor depositio*. Journal of applied physics, 2004. **95**(6): p. 1341-1347.
 72. Bae, C.H., Park, S. M., Ahn, S. E., Oh, D-J., Kim, G. T. and Ha, J. S., *Sol-gel synthesis of sub-50 nm ZnO nanowires on pulse laser deposited ZnO thin films*. Applied Surface Science 2006. **253**: p. 1758-1761.
 73. Nayak, A.P., Katzenmeyer, A., and Gosho, Y., *Sonochemical Synthesis of Zinc Oxide Nanowire Arrays on Silicon and Glass Substrates*. . Proceedings of The National Conference On Undergraduate Research (NCUR) 2010.
 74. Palumbo, M., Henley, S. J., Lutz, T., Stolojan, V. and Silva, S. R. P, *A fast sonochemical approach for the synthesis of solution processable ZnO rods*. JOURNAL OF APPLIED PHYSICS 2008. **104**: p. 074906.
 75. Zak, A.K., Majid, W. H., Wang, H.Z., Yousefi, R., Golsheikh, A. M. and Ren, Z.F. , *Sonochemical synthesis of hierarchical ZnO nanostructures*. Ultrasonics Sonochemistry, 2013. **20**: p. 395-400.
 76. wikipedia. *SEM*. [cited 2013 09 Dec].
 77. wikipedia. *EDX*. [cited 2014 05 Mar].
 78. wikipedia. *raman_spectroscopy*. [cited 2014 05 Mar].
 79. Kaper, J.B., Nataro, J. P. and Mobley, H. L., *Pathogenic Escherichia coli*. Nat Rev Microbiol, 2004. **2**(2): p. 123-40.
 80. W., R.A., *Nosocomial Infection Update*. . Emerging Infectious Diseases. , 1998. **4**(3): p. 416-420.
 81. wikipedia. *Escherichia coli*. [cited 2013 09 Dec].
 82. Oggioni, M.R., Pozzi, G., Valensin P. E., Galieni, P. and Bigazzi, C., *Recurrent septicemia in an immunocompromised patient due to probiotic strains of Bacillus subtilis*. Journal of Clinical Microbiology., 1998. **36**(1): p. 325-326.
 83. Samarakoon, K., Senvirathne, M., Lee, W-W., Kim, Y-Y., Ou, M.-C. and Jeon Y-J., *Antibacterial effect of citrus press-cakes dried by high speed and far infrared radiation drying method*. Nutr. Res. Pract., 2012. **6**(3): p. 187-194.
 84. Samanta, P.K., Patra, S. K., Ghosh, A. and Chaudhuri, P. R. , *Visible Emission from ZnO Nanorods Synthesized by a Simple Wet Chemical Method*. International Journal of NanoScience and Nanotechnology, 2009. **1**(1-2): p. 81-90.
 85. Calizo, I., Alim, K. A., Fonoberov, V. A., Krishnakumar, S., Shamsa, M., Balandin, A. A. and Kurtz, R., *Micro-Raman spectroscopic characterization of ZnO quantum dots, nanocrystals and nanowires*. Proc. of SPIE, 2007. **6481**: p. 1-8.
 86. Khan, A., *Raman Spectroscopic Study of the ZnO Nanostructures*. J. Pak. Mater. Soc., 2010. **4**(1): p. 4-9.
 87. Ye, J., Gu, S., Zhu, S., Chen, T., Liu, W., Qin, F., Hu, L., Zhang, R., Shi, Y. and Zheng, Y., *Raman and photoluminescence of ZnO films deposited on*

- Si(111)...using low-pressure metalorganic chemical vapor deposition. J. Vac. Sci. Technol., 2003. 21(4): p. 979-982.*
88. Srikaow, A.a.S., S. M., *Flower-Like ZnO Derived by a Sonochemical Method and its Photocatalytic Activity for Water Treatment. Journal of the Microscopy Society of Thailand, 2011. 4(1): p. 41-45.*
 89. Ridhuan, N.S., Abdul Razak K., Lockman, Z., and Abdul Aziz, A . *Structural and Morphology of ZnO Nanorods Synthesized Using ZnO Seeded Growth Hydrothermal Method and Its Properties as UV Sensing. PLoS One, 2012. 7(11): p. 50405.*
 90. Dong, J.J., Zhen, C. Y., Hao, H. Y., Xing, J., Zhang, Z. L., ZhengZ.Y. and Zhang,W. Z., *Controllable synthesis of ZnO nanostructures on the Si substrate by a hydrothermal route. Nanoscale Research Letters 2013. 8(1): p. 378.*
 91. Tam, K., Djuricic, A., Chan, C., Xi, Y., Tse, C., Leung, Y., Chan, W., Leung, F., Au, D. , *Antibacterial activity of ZnO nanorods prepared by a hydrothermal method. Thin Solid Films, 2008. 516(18): p. 6167-6174.*
 92. Sapkota, A., Anceno, A.J., Baruah, S., Shipin, V.O. and Dutta, J., *Zinc oxide nanorod mediated visible light photoinactivation of model microbes in water. Nanotechnology 2011. 22: p. 215703.*

CURRICULUM VITAE

Name Surname: Rukayya Kawu Bala

Place and Date of Birth: Kano State, Nigeria/11-11-1987

Address: No. 1A Hausawa Zoo road, Kano.Nigeria.

E-Mail: rukayyabala45@yahoo.com

B.Sc.: Applied Biology

Professional Experience and Rewards:

- 2012 -2014** Nanotechnology Master program. Gediz University, izmir. Turkey.
- 2010-2011** National Youth Service Corps (NYSC). Aminu Kano Teaching Hospital, Kano. Nigeria.
- 2006-2010** B.Sc. Applied Biology. Bayero University Kano. Nigeria.
- 2008-2009** Students Industrial Work Experience Scheme (SIWES). Muhammadu Abdullahi Wase Specialists Hospital, kano. Nigeria.

PRESENTATION ON THE THESIS

Tugba O. Okyay, **Rukayya K. Bala**, Ramazan Atalay, Yavuz Bayam and Debora F.Rodrigues. 2013. Fast Growth of ZnO Nanorods and Their Antimicrobial Properties. Proceedings of the 7th IEEE international conference on nano/molecular medicine and engineering. November 10-13, 2013, Phuket, Thailand.